UNIVERSITÀ DEGLI STUDI DI PADOVA

DIPARTIMENTO DI INGEGNERIA CIVILE, EDILE E AMBIENTALE
Department of Civil, Environmental and Architectural Engineering

Corso di Laurea Magistrale in

MATHEMATICAL ENGINEERING
Mathematical Modelling for Engineering and Science

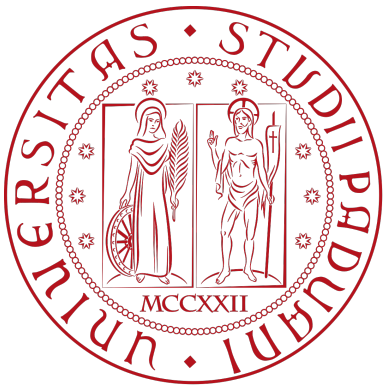

TESI DI LAUREA

Numerical Analysis of the Intrinsic Surface Finite Element Method for Linear Parabolic PDEs on Evolving Surfaces

Relatrice
Prof.ssa Elena Bachini
Correlatore
Prof. Mario Putti

Candidato
Lorenzo Massocco
Matricola 2139625

Academic Year 2025–2026

ABSTRACT

This thesis presents an intrinsic finite element framework for the approximation of linear parabolic partial differential equations posed on evolving surfaces. Starting from a conservation principle, the governing equation is derived using local parametrisations and induced metric tensors, with the surface evolution represented through a family of time-dependent diffeomorphisms.

Within the abstract framework of evolving Hilbert spaces, semi-discrete and fully discrete finite element formulations are introduced and analysed. Stability estimates and convergence results are established in the intrinsic geometric setting. For the fully discrete backward Euler scheme, optimal convergence rates of order $O(h^2)$ in the L^2 norm, $O(h)$ in the H^1 norm, and first-order accuracy in time are proved.

FEM matrices are computed by using only the tangent planes at the mesh nodes through suitable element parametrisations. Three strategies are considered: exact parametrisations, tangent vector reconstructions, and flat triangle approximations. The first two preserve the exact surface geometry by using intrinsic quantities, and for this reason they characterise the Evolving Intrinsic Surface Finite Element Method (E-ISFEM), which constitutes an intrinsic counterpart of the classical Evolving Surface Finite Element Method (ESFEM).

The proposed methodology is validated through numerical experiments on several evolving surfaces, including paraboloids, oscillating surfaces, spheres, and ellipsoids. The results confirm the theoretical convergence rates and exact mass conservation. Comparisons with the classical Evolving Surface Finite Element Method show that the intrinsic formulation achieves comparable accuracy.

Contents

Chapter 1

Introduction

Surface Partial Differential Equations are a class of partial differential equations posed on manifolds that naturally emerge in the mathematical modelling of phenomena occurring on curved geometries, such as heat diffusion and fluid interfaces [6]. Although their practical relevance has grown substantially in recent years, the theoretical framework underpinning these equations is not yet fully established. Well posedness and regularity results are reasonably well understood for problems posed on fixed surfaces, but their extension to time-dependent geometries remains only partially complete. Despite these limitations, numerical methods for both stationary and evolving surface PDEs are increasingly employed in applied contexts.

For problems posed on static surfaces, a variety of Finite Element-based approaches have been developed. A central role is played by the Surface Finite Element Method (SFEM), originally introduced by Dziuk [14] and subsequently extended by Dziuk and Elliott [18]. This methodology follows an embedded viewpoint: differential operators on the surface are formulated by extending functions to a tubular neighbourhood of the surface and then restricting the resulting quantities through projection along normal directions. In contrast, the Intrinsic Surface Finite Element Method (ISFEM), proposed more recently in [5, 7, 8, 9], adopts a fundamentally different perspective by expressing the governing equations entirely in terms of quantities defined on the surface itself, using local parametrisations and the associated metric tensor. This intrinsic formulation avoids projection or extension steps and ensures that both the solution and its derivatives remain naturally confined to the surface. One of the main peculiarity of the ISFEM construction is that it can work with the exact surface geometry through the local tangent vectors, with discretisation entering the method only at the level of numerical quadrature. Another key advantage of the intrinsic approach is its ability to extend to vector and tensor valued differential problems with a contained additional geometric complication [4].

When the surface evolves over time, additional complications arise. In particular, the bilinear forms that appear in the weak formulation become time dependent, and the evolution of surface integrals must be carefully tracked through transport identities [19, 26]. This requires the introduction of material derivatives for functions defined on moving geometries. The embedded extension of SFEM to this setting, known as the Evolving Surface Finite Element Method (ESFEM), is currently the most established framework [15, 16, 17]. Its intrinsic counterpart, which may be referred to as the Evolving Intrinsic Surface Finite Element Method (E-ISFEM), is still under active development, and several aspects ranging from analytical properties to computational performance remain to be clarified.

The present work analyses the E-ISFEM framework for linear parabolic PDEs posed on evolving surfaces. Building upon the formulation introduced in [27], where equivalence with the corresponding embedded approach was established, the thesis strengthens the analytical foundations of the Evolving Intrinsic Surface Finite Element Method (E-ISFEM), takes a closer look at numerical

aspects of the method, and presents a series of numerical experiments on evolving geometries of increasing complexity. As regards the numerical analysis, which constitutes one of the main objectives of this work, stability and convergence properties, previously established for the ES-FEM in [15, 16, 17] and within the abstract evolving space framework in [21], are here adapted to the intrinsic geometric setting. The analysis reveals the explicit dependence of the stability constants on intrinsic geometric quantities such as the metric tensor G_t and the surface measure factor λ. Optimal convergence rates of order $O(h^2)$ in the L^2 norm and $O(h)$ in the H^1 norm, and first-order accuracy in time, are established for the fully discrete backward Euler scheme. From a computational perspective, it is shown that the knowledge of the tangent planes at the mesh nodes is sufficient to compute the local FEM matrices through the introduction of an *ad hoc* parametrisation of each surface element. This approach constitutes one of three distinct strategies for matrix computation considered in this work, with the choice of method depending on the geometric information available: the exact surface parametrisation, the tangent vectors at the mesh nodes, or a flat-triangle approximation. The first strategy, based on the exact parametrisation, is often impractical in applications, as surfaces are typically known only through their mesh nodes. The second strategy, which is the method proposed in this thesis, requires only the tangent vectors at the nodes and is therefore particularly attractive in applications where such information is available. The third strategy coincides with the classical ESFEM approach and consists of approximating the surface by a polyhedral interpolant.

The thesis is organised as follows. The geometric and functional analytic prerequisites for the analysis, including the abstract framework of evolving Hilbert spaces and Bochner spaces developed in [2, 3], are presented in Chapter 2. The governing equation is derived in Chapter 3 from a conservation principle on an evolving surface, using the intrinsic formulation based on local parametrisations and the induced metric tensors. One can note that, in this case, the surface velocity field is not introduced explicitly: the geometric evolution is encoded entirely in a (purely scalar) reaction term where the coefficient contains the time dependence of the parametrisation through a family of diffeomorphisms $\{\hat{\alpha}_t\}_{t\in[0,T]}$. Chapter 4 is devoted to the introduction of the semi-discrete and fully discrete Finite Element formulations, together with the numerical implementation. The formulation is validated in Chapter 5 through several numerical experiments on surfaces of increasing geometric complexity: a collapsing paraboloid, a time-oscillating surface, an enlarging paraboloid, an enlarging perforated sphere, an enlarging sphere parametrised by two stereographic charts, and a deforming ellipsoid. All numerical experiments confirm the theoretically predicted optimal convergence rates and exact conservation of mass.

Chapter 2

Preliminary Mathematical Tools

In this chapter, all the definitions and results concerning partial differential equations on surfaces that will be used throughout the thesis are presented and subsequently referenced in the following chapters. The discussion begins with the introduction of the fundamental notions related to surfaces, formulated within the language of differential geometry, mainly following [1] and [25]. This geometric framework is essential for the intrinsic formulation of PDEs on surfaces and provides the necessary tools for the developments carried out in the thesis.

At the same time, since the well-established theory of surface finite element methods developed in [18] treats surfaces as embedded manifolds in $\mathbb{R}^3$, the corresponding embedded framework is also introduced. Presenting both perspectives allows for a direct comparison between the intrinsic and embedded approaches and clarifies the relation between the two formulations.

Once the geometric setting has been established, the focus shifts to the analytical framework required for the study of PDEs on surfaces. In particular, the functional analytic tools and results needed for the variational formulation and analysis of the problems considered in the thesis are introduced, with primary reference to [11, 23] and [2, 3].

2.1 Geometry of surfaces

This section presents both the embedded and intrinsic perspectives from which the formulation of PDEs on surfaces can be developed. In particular, both the intrinsic viewpoint, based on the differential geometry of manifolds, and the extrinsic viewpoint, where surfaces are regarded as embedded in the ambient space $\mathbb{R}^3$, will be discussed. Introducing these two complementary approaches is fundamental for establishing the connections between the classical embedded formulation and the intrinsic formulation presented in this thesis.

2.1.1 Intrinsic framework

Definition 2.1. Let $k \in \mathbb{N} \cup \{\infty\}$. A connected subset $\Gamma \subset \mathbb{R}^3$ is a C^k *regular surface* if for each $\mathbf{x} \in \Gamma$ there exists a map $\phi : \Xi \to \mathbb{R}^3$ of class C^k, where $\Xi \subseteq \mathbb{R}^2$ is open, such that:

i) $\phi(\Xi) \subseteq \Gamma$ is an open neighbourhood of $\mathbf{x} \in \Gamma$;

ii) ϕ is an homeomorphism with its image;

iii) the differential $d\phi_{\boldsymbol{\xi}} : \mathbb{R}^2 \to \mathbb{R}^3$ is injective for all $\boldsymbol{\xi} \in \Xi$.

Moreover, the map $\phi = \phi(\boldsymbol{\xi})$ is called *local parametrisation* of Γ in $\mathbf{x}$, and its inverse *local chart*. The neighbourhood $\phi(\Xi)$ of $\mathbf{x} \in \Gamma$ is called *coordinate neighbourhood* and the coordinates $\boldsymbol{\xi} = \phi^{-1}(\mathbf{x})$ are called *local coordinates* of $\mathbf{x}$.

In the following chapters, the existence of a single global parametrisation ϕ of the surface Γ will often be assumed in order to simplify both the exposition and the analytical arguments. However, it is not strictly required for the developments presented in this thesis. In the general setting, a surface must be described locally through a collection of compatible parametrisations rather than by a single global chart.

Definition 2.2. An *atlas* for a regular surface $\Gamma \subset \mathbb{R}^3$ is a collection $\mathcal{A} = \{(\Xi_i, \phi_i)\}_{i \in I}$ such that $\phi_i : \Xi_i \to \mathbb{R}^3$ is a local parametrisation for every $i \in I$ and $\Gamma = \bigcup_{i \in I} \phi_i(\Xi_i)$.

When dealing with a surface Γ, the utility of introducing a parametrisation ϕ relies on the fact that locally it is possible to look at Γ as a subset of $\mathbb{R}^2$ (just by considering the pre-image of ϕ). Therefore, for any function f defined on Γ, it is possible to define the notion of differentiability owing to the action of ϕ.

Definition 2.3. Let $k \in \mathbb{N} \cup \{\infty\}$, $\Gamma \subset \mathbb{R}^3$ be a regular surface and $\mathbf{x} \in \Gamma$. A function $f : \Gamma \to \mathbb{R}$ is *of class* C^k at $\mathbf{x}$ if there exists a local parametrisation $\phi : \Xi \to \Gamma$ at $\mathbf{x}$ such that $f \circ \phi : \Xi \to \mathbb{R}$ is of class C^k in a neighbourhood of $\phi^{-1}(\mathbf{x})$. The function f is *of class* C^k if it is so at every $\mathbf{x} \in \Gamma$.

Note that the differentiability of $f : \Gamma \to \mathbb{R}$ is defined by the differentiability (in the classical sense, from $\mathbb{R}^2$ to $\mathbb{R}$) of the function $f \circ \phi : \Xi \to \mathbb{R}$. In the theory of partial differential equations on surfaces, differential operators are defined on the tangent plane of the surface. Given a parametrisation of the surface, the tangent space can be characterised in a natural and straightforward manner.

Definition 2.4. Let $\Gamma \subset \mathbb{R}^3$ be a regular surface, and $\mathbf{x} \in \Gamma$. If $\phi : \Xi \to \Gamma$ is a local parametrisation centered in $\mathbf{x}$, the *tangent space* of Γ at $\mathbf{x} = \phi(\boldsymbol{\xi})$ is defined as:

$$T_{\mathbf{x}}\Gamma = \operatorname{span}\left\{ \frac{\partial \phi}{\partial \xi_1}(\boldsymbol{\xi}), \frac{\partial \phi}{\partial \xi_2}(\boldsymbol{\xi}) \right\}$$

The tangent space introduced in Definition 2.4 is independent of the particular choice of parametrisation. Nevertheless, the coordinates of a vector in $T_{\mathbf{x}}\Gamma$ with respect to the associated basis vectors do depend on the chosen parametrisation ϕ. The notion of tangent space plays a fundamental role in the intrinsic treatment of differential operators on surfaces, since it provides the natural setting in which derivatives and vector fields can be defined using only local coordinates.

Another fundamental object is the metric tensor, which can be defined as follows.

Definition 2.5. Let $\Gamma \subset \mathbb{R}^3$ be a regular surface. For every $\mathbf{x} \in \Gamma$, let ϕ be a local parametrisation at $\mathbf{x}$. The *metric tensor* G at $\mathbf{x} = \phi(\boldsymbol{\xi})$ is defined by:

$$G_{ij}(\boldsymbol{\xi}) = \left\langle \frac{\partial \phi}{\partial \xi_i}(\boldsymbol{\xi}), \frac{\partial \phi}{\partial \xi_j}(\boldsymbol{\xi}) \right\rangle$$

where $\langle \cdot, \cdot \rangle$ denotes the scalar product in $\mathbb{R}^3$.

This tensor encodes the geometric information of the surface and it is essential for measuring lengths of tangent vectors, defining scalar products between tangent fields, and performing integration on the surface.

Definition 2.6. Let $E \subseteq \Gamma$ be a regular region of a regular surface Γ and let $\phi : \Xi \to \Gamma$ be a local parametrisation such that $E \subseteq \phi(\Xi)$. Moreover let G be the metric defined in Definition 2.5 for all $\mathbf{x} \in E$. Then, for every continuous function $f : E \to \mathbb{R}$, the *integral of* f *on* E is defined as:

$$\int_E f = \int_{\phi^{-1}(E)} (f \circ \phi)(\boldsymbol{\xi}) \sqrt{\det G(\boldsymbol{\xi})}\, d\boldsymbol{\xi}$$

As Definition 2.5 suggests, the metric tensor is linked to the choice of the parametrisation ϕ. Nevertheless, it is not difficult to prove that Definition 2.6 is independent of the parametrisation [1].

Finally, the following definitions provide the fundamental tools through which a generic PDE can be formulated in intrinsic coordinates, expressing the problem entirely in terms of local variables and thereby reducing the analysis and computations to a two-dimensional setting.

Definition 2.7. Let Γ be a regular surface and let $f : \Gamma \to \mathbb{R}$ be a scalar function of class C^1. Given a parametrisation $\phi : \Xi \to \Gamma$ such that $\mathbf{x} \in \phi(\Xi)$, define $F := f \circ \phi$. The *intrinsic gradient* of f at $\mathbf{x} = \phi(\boldsymbol{\xi})$ is a vector of $T_{\mathbf{x}}\Gamma$ defined as:

$$\nabla_G f = G^{-1} \nabla F \tag{2.1}$$

where G is the metric tensor induced by ϕ, and $\nabla F = \left(\partial_{\xi_1} F, \partial_{\xi_2} F\right)^T$.
Let $\mathbf{q} : \Gamma \to \mathbb{R}^2$ be a vector field of class C^1 and define $\mathbf{Q} := \mathbf{q} \circ \phi$. The *intrinsic divergence* of $\mathbf{q}$ at $\mathbf{x} = \phi(\boldsymbol{\xi})$ is defined as:

$$\nabla_G \cdot \mathbf{q} = \frac{1}{\sqrt{\det G(\boldsymbol{\xi})}} \nabla \cdot \left(\sqrt{\det G(\boldsymbol{\xi})} \mathbf{Q} \right) \tag{2.2}$$

where $\nabla \cdot (\cdot)$ is the usual divergence in $\mathbb{R}^2$.
Finally, combining the two, the *intrinsic Laplace-Beltrami* operator for the scalar function of class C^2 $f : \Gamma \to \mathbb{R}$ is defined as:

$$\Delta_G f = \nabla_G \cdot \nabla_G f = \frac{1}{\sqrt{\det G(\boldsymbol{\xi})}} \nabla \cdot \left(\sqrt{\det G(\boldsymbol{\xi})} G^{-1} \nabla F \right) \tag{2.3}$$

Finally it is possible to state the Intrinsic Green Lemma, crucial for the development of weak theory for PDEs on surfaces.

Lemma 2.8. *Let Γ be a regular surface with smooth boundary $\partial\Gamma$ and let $f, g : \overline{\Gamma} \to \mathbb{R}$ be of class C^1. Then:*

$$\int_\Gamma \langle \nabla_G f, \nabla_G g \rangle = - \int_\Gamma f \Delta_G g + \int_{\partial\Gamma} f \, \langle \nabla_G g, \boldsymbol{\mu} \rangle_G \tag{2.4}$$

Where $\boldsymbol{\mu}$ denotes the co-normal vector which is normal to $\partial\Gamma$ and tangent to Γ, and the second term of the right-hand side is the integral on the regular curve $\partial\Gamma$ [1].

2.1.2 Embedded framework

Following the approach developed in [18], it is also possible to regard the surface Γ as a manifold embedded in the ambient space $\mathbb{R}^3$. Within this extrinsic framework, the geometric objects previously introduced can be reformulated in terms of Euclidean quantities defined in the surrounding space. This perspective is particularly useful in the context of surface finite element methods, where the geometry of the surface is often represented through embedded triangulations in $\mathbb{R}^3$. Adopting this point of view allows for a direct comparison between intrinsic and embedded formulations and clarifies the relation between the two approaches.

Definition 2.9. Let $k \in \mathbb{N} \cup \{\infty\}$. $\Gamma \subset \mathbb{R}^3$ is called a C^k *regular surface* if, for each $\mathbf{x} \in \Gamma$, there exists an open set $U \subset \mathbb{R}^3$ containing $\mathbf{x}$ and a function $\omega \in C^k(U)$ such that $\nabla\omega \neq 0$ on $U \cap \Gamma$ and such that $U \cap \Gamma = \{\mathbf{x} \in U : \omega(\mathbf{x}) = 0\}$.

A regular surface $\Gamma \subset \mathbb{R}^3$ admits a tangent plane at every point $\mathbf{x} \in \Gamma$. The tangent vectors at $\mathbf{x}$ are therefore the vectors in $\mathbb{R}^3$ lying in this plane. While the tangent space can be characterised locally through a parametrisation of the surface, it is also possible to provide an equivalent and fully geometric definition that does not rely on coordinates. More precisely, by exploiting the notion of a smooth curve on the surface passing through the point $\mathbf{x}$, tangent vectors can be defined intrinsically as velocities of such curves at the given point. This characterisation is independent of the choice of parametrisation and provides a natural geometric interpretation of tangent vectors directly in the ambient space.

Definition 2.10. Given $n \geq 2$, a *parametrised curve of class* C^∞ (or *smooth*) is a map $\boldsymbol{\gamma} : I \to \mathbb{R}^n$ of class C^∞, where $I \in \mathbb{R}$ is an interval. The image $\boldsymbol{\gamma}(I)$ is called *support* of the curve.

Definition 2.11. Let $\Gamma \subset \mathbb{R}^3$ be a regular surface, and $\mathbf{x} \in \Gamma$. A *tangent vector* to Γ at $\mathbf{x}$ is a vector of the form $\boldsymbol{\gamma}'(0)$ where $\boldsymbol{\gamma} : (-\varepsilon, \varepsilon) \to \Gamma$ is a curve of class C^∞ whose support lies in Γ and such that $\boldsymbol{\gamma}(0) = \mathbf{x}$. The set of all tangent vectors of Γ at $\mathbf{x}$ is called *tangent space* and it is denoted by $T_{\mathbf{x}}\Gamma$.

Note that, unlike Definition 2.4, Definition 2.11 does not involve any parametrisation of the surface. The tangent space is instead characterised directly in terms of geometric objects in the ambient space $\mathbb{R}^3$, making the definition completely independent of local coordinates.

One of the main differences between the intrinsic and the embedded approaches lies in the role played by the normal vector to the surface. Indeed, such a notion can only be introduced when the surface is regarded as embedded in $\mathbb{R}^3$, since the normal is itself a vector of the ambient Euclidean space.

Definition 2.12. Let $\Gamma \in \mathbb{R}^3$ be a C^k regular surface and let $\mathbf{x} \in \Gamma$. A vector $\boldsymbol{\nu}(\mathbf{x}) \in \mathbb{R}^3$ is called *normal unit vector* at $\mathbf{x} \in \Gamma$ if $\boldsymbol{\nu}(\mathbf{x}) \perp T_{\mathbf{x}}\Gamma$ and $|\boldsymbol{\nu}(\mathbf{x})| = 1$.

Definition 2.13. A C^1 regular surface is called *orientable* if there exists a continuous vector field $\boldsymbol{\nu} : \Gamma \to \mathbb{R}^3$ such that $\boldsymbol{\nu}(\mathbf{x})$ is a unit normal vector to Γ for all $\mathbf{x} \in \Gamma$.

Once the unit normal to the surface has been introduced, all the ingredients are available to define the embedded tangential gradient of a differentiable function on the surface. Unlike the intrinsic framework, where differentiability is defined through the parametrisation, the embedded approach requires extending the function to the so called *tubular neighbourhood*, namely a three-dimensional neighbourhood of the surface. In this way, one can exploit the classical notion of differentiability in $\mathbb{R}^3$. The tangential gradient is then obtained by projecting the standard Euclidean gradient onto the tangent plane of the surface.

Definition 2.14. Let $\Gamma \subset \mathbb{R}^3$ be a C^1 regular surface and let $f : \Gamma \to \mathbb{R}$ be differentiable at $\mathbf{x} \in \Gamma$. The *tangential gradient* of f at $\mathbf{x} \in \Gamma$ is defined by:

$$\nabla_\Gamma f(\mathbf{x}) = \nabla \overline{f}(\mathbf{x}) - \left\langle \nabla \overline{f}(\mathbf{x}), \boldsymbol{\nu}(\mathbf{x}) \right\rangle \boldsymbol{\nu}(\mathbf{x}) = P(\mathbf{x}) \nabla \overline{f}(\mathbf{x}) \tag{2.5}$$

where $P(\mathbf{x})_{ij} = \delta_{ij} - \nu_i(\mathbf{x})\nu_j(\mathbf{x})$ with $i, j = 1, 2, 3$, and $\overline{f}$ is a smooth extension of $f : \Gamma \to \mathbb{R}$ to a three-dimensional neighbourhood U of the surface Γ, in such a way $\overline{f}|_\Gamma = f$. ∇ denotes the usual gradient in $\mathbb{R}^3$.
Denoting with $D_i f = (\nabla_\Gamma f)_i$, the *tangential Laplace-Beltrami* operator is defined as:

$$\Delta_\Gamma f = \sum_{i=1}^{3} D_i D_i f \tag{2.6}$$

Definition 2.14 has the drawback of requiring a smooth extension of f to a tubular neighbourhood of Γ. However, unlike Definition 2.1, it does not depend on the choice of parametrisation of the surface, since it is formulated entirely in terms of quantities in the ambient space $\mathbb{R}^3$.

Proposition 2.15. *Let $f : \Gamma \to \mathbb{R}$ be a function of class C^1. Then the intrinsic gradient and the tangential gradient of f are equivalent.*

Proof. First note that $\nabla_\Gamma f$ is orthogonal to the unit normal $\boldsymbol{\nu}(\mathbf{x})$ for all $\mathbf{x} \in \Gamma$:

$$\langle \nabla_\Gamma f(\mathbf{x}), \boldsymbol{\nu}(\mathbf{x}) \rangle = \left\langle \nabla \overline{f}(\mathbf{x}), \boldsymbol{\nu}(\mathbf{x}) \right\rangle - \left\langle \nabla \overline{f}(\mathbf{x}), \boldsymbol{\nu}(\mathbf{x}) \right\rangle \langle \boldsymbol{\nu}(\mathbf{x}), \boldsymbol{\nu}(\mathbf{x}) \rangle = 0$$

Therefore $\nabla_\Gamma f(\mathbf{x}) \in T_{\mathbf{x}}\Gamma$. This means that, letting ϕ be a parametrisation of Γ at $\mathbf{x}$, and recalling Definition 2.4, there exist two scalars α_1, α_2 such that:

$$\nabla_\Gamma f(\phi(\boldsymbol{\xi})) = \sum_{i=1}^{2} \alpha_i \frac{\partial \phi}{\partial \xi_i}(\boldsymbol{\xi})$$

Setting $F(\boldsymbol{\xi}) := f(\phi(\boldsymbol{\xi}))$, the chain rule gives:

$$\frac{\partial F}{\partial \xi_k}(\boldsymbol{\xi}) = \left\langle \nabla_\Gamma F(\boldsymbol{\xi}), \frac{\partial \phi}{\partial \xi_k}(\boldsymbol{\xi}) \right\rangle = \sum_{i=1}^{2} \alpha_i \left\langle \frac{\partial \phi}{\partial \xi_i}(\boldsymbol{\xi}), \frac{\partial \phi}{\partial \xi_k}(\boldsymbol{\xi}) \right\rangle$$

Letting $\boldsymbol{\alpha} = (\alpha_1, \alpha_2)^T$, and recalling Definition 2.5, the previous is equivalent to:

$$\nabla F(\boldsymbol{\xi}) = G\boldsymbol{\alpha}$$

From which follows that α_1, α_2 are the coordinates of the vector $G^{-1}\nabla F = \nabla_G f$ with respect to the basis vectors of the tangent space induced by the parametrisation ϕ. □

In other words, once a parametrisation is fixed, the tangential gradient can be expressed as a linear combination of the two basis vectors of the tangent plane induced by that parametrisation, with coefficients given by the components of the intrinsic gradient computed in the same coordinates. However, as stated in the following lemma [18], the tangential gradient is in fact well-defined independently of the choice of parametrisation.

Lemma 2.16. *Let Γ be a C^k regular hypersurface and let $\mathbf{x} \in \Gamma$. The tangential gradient of a C^1 function $f : \Gamma \to \mathbb{R}$ only depends on the values of f on $\Gamma \cap U$, where $U \subset \mathbb{R}$ is a neighbourhood of $\mathbf{x}$.*

The curvature of a surface Γ at a point $\mathbf{x}$ can be interpreted as the *variation* of the tangent plane in a small neighbourhood of $\mathbf{x} \in \Gamma$. Instead of directly analysing how the tangent plane changes from point to point, it is possible to quantify curvature through the tangential gradient of the unit normal at $\mathbf{x}$. This is possible since the unit normal uniquely determines the tangent plane, and therefore its variation encodes the local geometric bending of the surface.

Definition 2.17. Let Γ be a C^2 regular surface. The *extended Weingarten map* is defined as:

$$\mathcal{H}_{ij} = D_i \nu_j \tag{2.7}$$

The restriction of $\mathcal{H}$ to the tangent space is called *Weingarten map*.
For $\mathbf{x} \in \Gamma$, the *mean curvature* of Γ at $\mathbf{x}$ is defined as:

$$H(\mathbf{x}) = \operatorname{tr}(\mathcal{H}(\mathbf{x})) = \sum_{i=1}^{3} \mathcal{H}_{ii}(\mathbf{x}) \tag{2.8}$$

The following theorem, proved in [18], establishes the integration by parts formula for functions defined on a regular surface Γ. The corresponding corollary is the embedded counterpart of the intrinsic Green Lemma stated previously (Lemma 2.8).

Theorem 2.18. *Let Γ be a regular surface with smooth boundary $\partial\Gamma$ and let $f : \overline{\Gamma} \to \mathbb{R}$ be of class C^1. Then:*

$$\int_\Gamma \nabla_\Gamma f \, d\boldsymbol{\sigma} = \int_\Gamma f H \boldsymbol{\nu} \, d\boldsymbol{\sigma} + \int_{\partial\Gamma} f \boldsymbol{\mu} \, d\boldsymbol{\gamma} \tag{2.9}$$

where $\boldsymbol{\mu}$ denotes the co-normal vector which is normal to $\partial\Gamma$ and tangent to Γ. $d\boldsymbol{\sigma}$ denotes the two dimensional surface measure and $d\boldsymbol{\gamma}$ denotes the one dimensional surface measure.

Corollary 2.19. *Let Γ be a regular surface with smooth boundary $\partial\Gamma$ and let $f, g : \overline{\Gamma} \to \mathbb{R}$ be of class C^1. Then:*

$$\int_\Gamma \langle \nabla_\Gamma f, \nabla_\Gamma g \rangle \, d\boldsymbol{\sigma} = -\int_\Gamma f \Delta_\Gamma g \, d\boldsymbol{\sigma} + \int_{\partial\Gamma} f \, \langle \nabla_\Gamma g, \boldsymbol{\mu} \rangle \, d\boldsymbol{\gamma} \tag{2.10}$$

As a final remark, it is worth noting that, unlike the embedded approach, the intrinsic framework does not require the introduction of the surface curvature in order to establish Green Lemma.

2.2 Preliminaries on Functional Analysis

The theory of partial differential equations is deeply rooted in functional analysis [11, 23]. In order to develop a consistent numerical method, the first step is to ensure the well posedness of the underlying mathematical problem. The following section introduces the analytical framework, based in particular on the notions of weak derivatives and Sobolev spaces, in which, under suitable assumptions, it is possible to prove existence and uniqueness results for a given class of PDEs.

When evolving surfaces are considered, one is naturally led to deal with time-dependent function spaces. This issue has been addressed in [2] through the formalism of Bochner spaces, which provides a rigorous way to handle functions defined on evolving geometries. This abstract framework serves as the foundation on which the differential problem studied in this thesis is formulated.

2.2.1 Sobolev spaces

Classical solutions to partial differential equations do not always exist. For this reason, weak derivatives and Sobolev spaces provide the appropriate analytical framework in which to formulate a well-posed differential problem. Establishing well posedness at this level is a necessary prerequisite for the construction of a stable and reliable numerical solver.
The following definitions introduce the concept of L^p spaces and Banach spaces.

Definition 2.20. Let $\Gamma \subset \mathbb{R}^3$ be a regular surface. For $p \in [1, \infty]$ the functions space $L^p(\Gamma)$ is defined as:

$$L^p(\Gamma) = \left\{ f : \Gamma \to \mathbb{R} \text{ measurable} : \int_\Gamma |f|^p < \infty \right\}$$

Proposition 2.21. *The space $L^p(\Gamma)$ is a Banach space equipped with the following norm:*

$$\|f\|_{L^p(\Gamma)} = \int_\Gamma |f|^p$$

The space of smooth, compactly supported functions and the concept of weak derivative are essential in the definition of Sobolev spaces. Therefore, the following definitions are introduced.

Definition 2.22. Let $\Gamma \subset \mathbb{R}^3$ be a regular surface. For any $f : \Gamma \to \mathbb{R}$, let supp($f$)=$\{\mathbf{x} \in \Gamma : f(\mathbf{x}) \neq 0\}$. The space $C_c^\infty(\Gamma)$ is defined as:

$$C_c^\infty(\Gamma) = \{f \in C^\infty(\Gamma) : \text{ supp}(f) \subset \Gamma \text{ and supp } (f) \text{ is compact}\}$$

Definition 2.23. Let $\Gamma \subset \mathbb{R}^3$ be a regular surface. Let $f : \Gamma \to \mathbb{R}$ be in L^p. The function $\mathbf{g} : \Gamma \to \mathbb{R}^3$ is called *weak tangential gradient* of f (and it will be denoted by $\nabla_\Gamma f$) provided that, for all $i = 1, 2, 3$:

$$\int_\Gamma f D_i \varphi = -\int_\Gamma g_i \varphi \qquad \forall \varphi \in C_c^\infty(\Gamma)$$

The necessity to weaken the regularity of the function space in which to look for a solution of a partial differential equation, combined with Corollary 2.8, suggests the following definition.

Definition 2.24. Let $\Gamma \subset \mathbb{R}^3$ be a regular surface. The *Sobolev space* $W^{1,p}(\Gamma)$ is defined as:

$$W^{1,p}(\Gamma) = \{f \in L^p(\Gamma) : \nabla_\Gamma f \in L^p(\Gamma)\}$$

If $p = 2$, $W^{1,p}(\Gamma)$ is usually denoted as $H^1(\Gamma)$.

Proposition 2.25. *The space $H^1(\Gamma)$ is an Hilbert space equipped with the following scalar product:*

$$(f, g)_{H^1(\Gamma)} = \int_\Gamma fg + \int_\Gamma \langle \nabla_\Gamma f, \nabla_\Gamma g \rangle$$

Proposition 2.26. *The space $H^1(\Gamma)$ is the closure of $C^\infty(\Gamma)$ with respect to the norm of $H^1(\Gamma)$. Moreover, the space $H_0^1(\Gamma) = \left\{f \in H^1(\Gamma) : f|_{\partial\Gamma} = 0\right\}$ is the closure of $C_c^\infty(\Gamma)$ with respect to the norm of $H^1(\Gamma)$.*

Proposition 2.26 states that $C_c^\infty(\Gamma)$ and $C^\infty(\Gamma)$ are dense in $H_0^1(\Gamma)$ and $H^1(\Gamma)$, respectively. This result is fundamental for the development of finite element methods, as it guarantees that smooth functions can approximate Sobolev functions arbitrarily well in the $H^1(\Gamma)$ norm. In particular, it justifies the use of finite-dimensional subspaces of continuous functions to approximate $H_0^1(\Gamma)$ and $H^1(\Gamma)$ in the $H^1(\Gamma)$ sense, providing a consistent variational framework for numerical discretisation.

The following lemma goes under the name of Poincarè Lemma. It states the equivalence between the $L^2(\Gamma)$ norm of $\nabla_\Gamma f$ and the $H^1(\Gamma)$ norm of f for any $f \in H_0^1$.

Lemma 2.27. *Let $p \in [1, \infty)$ and let $\Gamma \subset \mathbb{R}^3$ be a regular surface. Then for every $f \in H_0^1(\Gamma)$ there exists $C_\Gamma \in \mathbb{R}$ such that:*

$$\|f\|_{L^p(\Gamma)} \leq C_\Gamma \|\nabla_\Gamma f\|_{L^p(\Gamma)} \tag{2.11}$$

If $f \in H^1(\Gamma)$ the left-hand side of Lemma 2.27 must be replaced with: $\|f - f_\Gamma\|_{L^p(\Gamma)}$, where f_Γ is the integral mean value of f over the regular surface Γ.

Proposition 2.25 furnishes the norm to put on $H^1(\Gamma)$ to make it a Banach space. Applying Definition 2.6 to Proposition 2.25, it is straightforward to see that the norm on $H^1(\Gamma)$ (as well as the scalar product) can be equivalently expressed in terms of the intrinsic gradient and the metric tensor. Therefore, Lemma 2.27 is valid for the intrinsic gradient and with the same constant C_Γ.

Usually, the existence of a solution to a PDE is first established in the space $u \in H_0^1$, which naturally incorporates homogeneous Dirichlet boundary conditions. The following proposition makes it possible to extend these existence results to the case of non homogeneous Dirichlet boundary conditions [23], by reducing the problem to a suitable reformulation in which the boundary data are incorporated into the functional setting.

Proposition 2.28. *Let $\Gamma \subset \mathbb{R}^3$ be a regular surface such that $\partial\Gamma \neq \emptyset$ and regular. Then for $p \in [1, \infty)$ there exists a linear continuous operator $T : W^{1,p}(\Gamma) \to L^p(\Gamma)$ such that $Tu = u$ in $\partial\Gamma$.*

Proposition 2.29. *Let $\Gamma \subset \mathbb{R}^3$ be a regular surface with $\partial\Gamma \neq \emptyset$ and regular. Then for $p \in [1, \infty)$:*

$$f \in W_0^{1,p}(\Gamma) \iff Tf = 0$$

The abstract framework presented in [2] allows the PDE to be formulated in a setting that also accommodates forcing terms belonging to dual spaces. This generality is particularly useful in order to treat lower regularity data in a rigorous way. For this reason, it is convenient to introduce the following definition.

Definition 2.30. Let X be a Banach space. The *dual space* X' of X is defined as the set of all linear and continuous functionals on X. Moreover X' is a Banach space equipped with the norm:

$$\|f\|_{X'} = \sup_{u \in X} f(u) \qquad \forall f \in X' \tag{2.12}$$

2.2.2 Evolving Bochner spaces

Bochner spaces provide the natural functional-analytic framework for the study of parabolic partial differential equations on fixed domains [23]. When the problem is posed on a moving surface, however, it becomes necessary to introduce a suitable notion of evolving spaces in order to describe functions that are defined on different geometries at different times.

The following pages summarize this abstract framework in the context of evolving surfaces, following the approach developed by Alphonse, Elliott, and Stinner [2, 3].

Definition 2.31. Let $\mathcal{V}$ be a Hilbert space and let $T \in (0, \infty)$. The associated *Bochner spaces* are defined by

$$L^2(0,T;\mathcal{V}) = \left\{ u : [0,T] \to \mathcal{V} \ \text{ measurable} : \int_0^T \|u(t)\|_{\mathcal{V}}^2 \, dt < \infty \right\} \tag{2.13}$$

$$L^2(0,T;\mathcal{V}') = \left\{ f : [0,T] \to \mathcal{V}' \ \text{ measurable} : \int_0^T \|f(t)\|_{\mathcal{V}'}^2 \, dt < \infty \right\} \tag{2.14}$$

With an appropriate definition of measurability; see [2, 29] for details. Bochner spaces possess several fundamental properties that make them particularly well-suited for the variational formulation of parabolic problems. Since these results are classical, they will only be recalled when needed throughout the thesis.

The first step in the construction of evolving spaces is to properly characterise the evolution of the underlying geometry. This is done through the following notion of compatibility.

Definition 2.32. Let $\{\mathcal{V}_t\}_{t\in[0,T]}$ be a family of Hilbert spaces and let $\{\alpha_t\}_{t\in[0,T]}$ be a family of maps such that $\alpha_t : \mathcal{V}_0 \to \mathcal{V}_t$ for all $t \in [0,T]$. The pair $\{(\mathcal{V}_t, \alpha_t)\}_{t\in[0,T]}$ is said to be *compatible* if the following conditions hold.

i) For every $t \in [0,T]$, $\mathcal{V}_t$ is a separable Hilbert space and the map $\alpha_t : \mathcal{V}_0 \to \mathcal{V}_t$ is a linear homeomorphism, with α_0 equal to the identity.

ii) Denoting by $\alpha_{-t} : \mathcal{V}_t \to \mathcal{V}_0$ the inverse of α_t, there exists a constant $C_{\mathcal{V}} > 0$, independent of t, such that

$$\begin{aligned} \|\alpha_t u\|_{\mathcal{V}_t} &\leq C_{\mathcal{V}} \|u\|_{\mathcal{V}_0} \qquad \forall u \in \mathcal{V}_0 \\ \|\alpha_{-t} u\|_{\mathcal{V}_0} &\leq C_{\mathcal{V}} \|u\|_{\mathcal{V}_t} \qquad \forall u \in \mathcal{V}_t \end{aligned} \tag{2.15}$$

iii) For every $u \in \mathcal{V}_0$, the map $t \mapsto \|\alpha_t u\|_{\mathcal{V}_t}$ is continuous on $[0,T]$.

The maps α_t are usually referred to as *pushforward operators*, while their inverses α_{-t} are called *pullback operators*. Intuitively, they allow one to identify functions defined on the evolving spaces $\mathcal{V}_t$ with functions defined on the fixed reference space $\mathcal{V}_0$.

A direct consequence of the above assumptions is that the dual operator $\alpha_t' : \mathcal{V}_t' \to \mathcal{V}_0'$ is itself a linear homeomorphism, whose inverse is denoted by $\alpha_{-t}' : \mathcal{V}_0' \to \mathcal{V}_t'$. Moreover, they satisfy the bounds

$$\begin{aligned} \|\alpha_t' f\|_{\mathcal{V}_0'} &\leq C_{\mathcal{V}} \|f\|_{\mathcal{V}_t'} \qquad \forall f \in \mathcal{V}_t' \\ \|\alpha_{-t}' f\|_{\mathcal{V}_t'} &\leq C_{\mathcal{V}} \|f\|_{\mathcal{V}_0'} \qquad \forall f \in \mathcal{V}_0' \end{aligned} \tag{2.16}$$

It is now possible to define the evolving Bochner spaces in which linear parabolic PDEs on evolving surfaces are formulated.

Definition 2.33. Let $\{(\mathcal{V}_t, \alpha_t)\}_{t\in[0,T]}$ be a compatible pair. The associated *evolving Bochner spaces* are defined by

$$\begin{aligned} L^2_{\mathcal{V}} &= \left\{ u : [0,T] \to \bigcup_{t\in[0,T]} \mathcal{V}_t \times \{t\}, \quad t \mapsto (\overline{u}(t), t) : \alpha_{-t}\overline{u}(t) \in L^2(0,T;\mathcal{V}_0) \right\} \\ L^2_{\mathcal{V}'} &= \left\{ f : [0,T] \to \bigcup_{t\in[0,T]} \mathcal{V}_t' \times \{t\}, \quad t \mapsto (\overline{f}(t), t) : \alpha_t'\overline{f}(t) \in L^2(0,T;\mathcal{V}_0') \right\} \end{aligned} \tag{2.17}$$

When no ambiguity may arise, the functions $\overline{u}$ and $\overline{f}$ will simply be denoted by u and f, respectively.
The following result is proved in [2].

Theorem 2.34. *The spaces $L^2_{\mathcal{V}}$ and $L^2_{\mathcal{V}'}$ are separable Hilbert spaces, endowed with the scalar products*

$$\begin{aligned} (u,v)_{L^2_{\mathcal{V}}} &= \int_0^T (u(t), v(t))_{\mathcal{V}_t}\, dt \\ (f,g)_{L^2_{\mathcal{V}'}} &= \int_0^T (f(t), g(t))_{\mathcal{V}_t'}\, dt \end{aligned} \tag{2.18}$$

As in the classical Bochner setting, one can prove that $(L^2_{\mathcal{V}})'$ and $L^2_{\mathcal{V}'}$ are isometrically isomorphic, and therefore they can be identified. For $u \in L^2_{\mathcal{V}}$ and $f \in L^2_{\mathcal{V}'}$, the duality pairing is given by

$$(f,u)_{L^2_{\mathcal{V}'}\times L^2_{\mathcal{V}}} = \int_0^T (f(t), u(t))_{\mathcal{V}_t'\times\mathcal{V}_t}\, dt \tag{2.19}$$

Up to this point, evolving spaces have been introduced through a compatible pair $\{(\mathcal{V}_t, \alpha_t)\}_{t\in[0,T]}$. In order to formulate parabolic PDEs, one additionally considers another compatible pair $\{(\mathcal{H}_t, \alpha_t)\}_{t\in[0,T]}$ such that $\mathcal{V}_0 \subset \mathcal{H}_0$ is a continuous and dense embedding. By identifying $\mathcal{H}_0$ with its dual $\mathcal{H}_0'$, it follows that $\mathcal{H}_0 \subset \mathcal{V}_0'$ is also continuous and dense. Hence

$$\mathcal{V}_0 \subset \mathcal{H}_0 \subset \mathcal{V}_0'$$

forms a Gelfand triple, which constitutes the natural variational framework for linear parabolic equations.

One of the most delicate aspects in the analysis of PDEs on moving surfaces is the definition of the time derivative. Indeed, time dependent functions defined on evolving domains cannot be

treated as functions on a fixed Euclidean domain. A classical approach consists in introducing a tubular neighbourhood of the evolving surface and decomposing the velocity field into tangential and normal components, as done for example in [13] and subsequently in [15, 16, 17, 18]. Within the abstract framework of evolving spaces, however, it is possible to define the material derivative directly through the pushforward and pullback operators, both in the strong and weak sense. This approach characterises the intrinsic formulation of the differential equation with consequences on the definition of the FEM problem.

Definition 2.35. For $k \in \mathbb{N} \cup \{\infty\}$, the space of *pushforward continuously differentiable functions* is defined by

$$\begin{aligned} C^k_{\mathcal{V}} &= \left\{u \in L^2_{\mathcal{V}} : \alpha_{-t}u(t) \in C^k(0,T;\mathcal{V}_0)\right\} \\ \mathcal{D}_{\mathcal{V}}(0,T) &= \left\{u \in L^2_{\mathcal{V}} : \alpha_{-t}u(t) \in \mathcal{D}(0,T;\mathcal{V}_0)\right\} \end{aligned} \tag{2.20}$$

where $\mathcal{D}(0,T;\mathcal{V}_0)$ is the Bochner space of infinitely differentiable functions with compact support.

Definition 2.36. Let $u \in C^1_{\mathcal{V}}$. Its *strong material derivative* $\dot{u} \in C^0_{\mathcal{V}}$ is defined by

$$\dot{u}(t) = \alpha_t\left(\frac{d}{dt}\left(\alpha_{-t}u(t)\right)\right) \tag{2.21}$$

This definition has a clear interpretation: one first pulls the function back to the fixed reference space $\mathcal{V}_0$, where the classical time derivative is well defined, and then pushes the result forward to the evolving space $\mathcal{V}_t$.

As in the classical theory, the weak derivative is characterised through an integration by parts formula. In the present setting, however, the time dependence of the spaces themselves must also be taken into account [2].

Definition 2.37. Let $u \in L^2_{\mathcal{V}}$. A function $v \in L^2_{\mathcal{V}'}$ is called the *weak material derivative* of u if for every $\varphi \in \mathcal{D}_{\mathcal{V}}(0,T)$ the following identity holds:

$$\int_0^T (v(t),\varphi(t))_{\mathcal{V}_t'\times\mathcal{V}_t}\,dt = -\int_0^T (u(t),\dot{\varphi}(t))_{\mathcal{H}_t}\,dt - \int_0^T \frac{d}{dt}\,(\alpha_t u(0),\alpha_t\varphi(0))_{\mathcal{H}_t}\,dt \tag{2.22}$$

It is straightforward to prove that, whenever it exists, the weak material derivative is unique. Moreover, every strong material derivative is also a weak material derivative. This fact allows to denote the weak material derivative of u by $\dot{u}$, without ambiguity.

It is finally possible to define the function space in which look for the solution of linear parabolic PDEs on evolving domains. This space is made of $L^2_{\mathcal{V}}$ functions with weak material derivative in $L^2_{\mathcal{V}'}$.

$$\mathcal{W}(\mathcal{V},\mathcal{V}') := \left\{u \in L^2_{\mathcal{V}} : \dot{u} \in L^2_{\mathcal{V}'}\right\} \tag{2.23}$$

endowed with the inner product

$$(u,v)_{\mathcal{W}(\mathcal{V},\mathcal{V}')} := \int_0^T (u(t),v(t))_{\mathcal{V}_t}\,dt + \int_0^T (\dot{u}(t),\dot{v}(t))_{\mathcal{V}_t'}\,dt \tag{2.24}$$

Theorem 2.38. *The space $\mathcal{W}(\mathcal{V},\mathcal{V}')$ in an Hilbert space.*

The following proposition makes possible to specify initial conditions of solutions to PDEs.

Proposition 2.39. *The embedding $\mathcal{W}(\mathcal{V},\mathcal{V}') \subset C^0_{\mathcal{H}}$ holds, hence for any $u \in \mathcal{W}(\mathcal{V},\mathcal{V}')$ the evaluation $t \mapsto u(t)$ is well defined for all $t \in [0,T]$. Furthermore the following inequality holds:*

$$\max_{t\in[0,T]} \|u(t)\|_{\mathcal{H}_t} \le C\|u\|_{\mathcal{W}(\mathcal{V},\mathcal{V}')} \qquad \forall u \in \mathcal{W}(\mathcal{V},\mathcal{V}') \tag{2.25}$$

In many applications, the source term f belongs to a more regular space. This additional regularity has important consequences for the regularity of the solution, as discussed in Section 3.2. In order to capture this situation, it is convenient to introduce the following evolving space, which is continuously embedded in $\mathcal{W}(\mathcal{V}, \mathcal{V}')$:

$$\mathcal{W}(\mathcal{V}, \mathcal{H}) := \left\{ u \in L^2_{\mathcal{V}} : \dot{u} \in L^2_{\mathcal{H}} \right\} \tag{2.26}$$

Chapter 3

Linear parabolic PDEs on evolving surfaces

Combining together the geometric framework and abstract setting of evolving Hilbert spaces, the following chapter will present the formulation of linear parabolic PDEs on evolving surfaces within the context of compatible pairs and evolving Bochner spaces.

Let $\{\Gamma_t\}_{t\in[0,T]}$ be a family of oriented compact regular surfaces. Assume that for every $t \in [0,T]$ there exists a smooth diffeomorphism

$$\hat{\alpha}_t : \Gamma_0 \to \Gamma_t \tag{3.1}$$

with $\hat{\alpha}_0$ equal to the identity. The family $\{\hat{\alpha}_t\}_{t\in[0,T]}$ describes the evolution of the surface and naturally induces the maps defining the evolution of the corresponding function spaces.

In this analytical and geometrical context the Sobolev spaces $H^1(\Gamma_t)$ and $L^2(\Gamma_t)$ play the roles of the spaces $\mathcal{V}_t$ and $\mathcal{H}_t$ of Section 2.2.2. Notice that the former are Hilbert spaces and form a Gelfand triple, hence all properties stated in Section 2.2.2 hold also for such spaces. For every $u : \Gamma_0 \to \mathbb{R}$, define the pushforward operator

$$\alpha_t u := u \circ \hat{\alpha}_{-t} \tag{3.2}$$

which maps functions defined on Γ_0 to functions defined on Γ_t. Analogously, the pullback operator is defined by

$$\alpha_{-t} v := v \circ \hat{\alpha}_t \tag{3.3}$$

for every $v : \Gamma_t \to \mathbb{R}$. Under suitable regularity assumptions on $\hat{\alpha}_t$, the pairs

$$\{(L^2(\Gamma_t), \alpha_t)\}_{t\in[0,T]} \qquad \{(H^1(\Gamma_t), \alpha_t)\}_{t\in[0,T]} \tag{3.4}$$

are compatible pairs in the sense of Definition 2.32. Consequently, the evolving Bochner spaces introduced previously are well defined.

Let now $\tilde{\phi} : \Xi \subset \mathbb{R}^2 \to \Gamma_0$ be a local parametrisation of the reference surface Γ_0. The evolution map $\hat{\alpha}_t$ induces, for every $t \in [0,T]$, a parametrisation of the evolving surface Γ_t through the composition

$$\phi_t := \hat{\alpha}_t \circ \tilde{\phi} : \Xi \to \Gamma_t \tag{3.5}$$

Hence, for every $\boldsymbol{\xi} \in \Xi$,

$$\mathbf{x} = \phi_t(\boldsymbol{\xi}) \in \Gamma_t \tag{3.6}$$

In the non restrictive assumption that the reference surface admits a global parametrisation, the family $\{\phi_t\}_{t\in[0,T]}$ completely characterises the evolution of the surface. In particular, the

geometric evolution is entirely encoded in the time dependence of the parametrisation, and no additional notion of surface velocity is required. This is one of the main difference with respect to the embedded approach in which classical ESFEM theory is formulated.

Let now $u \in L^2_{\mathcal{V}}$ be a scalar function defined on the evolving surfaces. Its pullback to the reference configuration is the function

$$U(\boldsymbol{\xi}, t) := (\alpha_{-t} u(t))(\tilde{\phi}(\boldsymbol{\xi})) = u(\phi_t(\boldsymbol{\xi}), t) \tag{3.7}$$

The function U is defined on the fixed reference domain $\Xi \times [0, T]$, and the material derivative introduced in Definition 2.36 corresponds precisely to differentiation with respect to time at fixed reference coordinates $\boldsymbol{\xi}$:

$$\dot{u} = \alpha_t \left(\frac{d}{dt} (\alpha_{-t} u) \right) \tag{3.8}$$

Equivalently, if

$$U(\boldsymbol{\xi}, t) = u(\phi_t(\boldsymbol{\xi}), t) \tag{3.9}$$

then

$$\dot{u}(\phi_t(\boldsymbol{\xi}), t) = \frac{\partial U}{\partial t}(\boldsymbol{\xi}, t) \tag{3.10}$$

Therefore, the evolving space framework allows one to separate the temporal evolution from the spatial geometry by transporting all quantities to the fixed reference surface Γ_0. In this setting, the parametrisation ϕ_t and the induced operators α_t encode both the evolution of the manifold and the evolution of the associated function spaces.

All the geometric notions introduced in Chapter 2 for static surfaces extend naturally to the evolving setting by considering their dependence on time. In particular, metric tensors, tangential gradients, surface measures and the Laplace-Beltrami operator are defined on each surface Γ_t through the parametrisation ϕ_t, and their time dependence will be denoted either explicitly or through the subscript t.

3.1 Model problem

The aim of this section is to derive the partial differential equation considered throughout this thesis. The equation arises from a conservation principle posed on an evolving surface and naturally fits into the framework of evolving Bochner spaces introduced in the previous chapter.

As already presented in a slightly different form in [27], the derivation will be carried out entirely in the intrinsic setting. In particular, the evolution of the geometry will be encoded through the family of diffeomorphisms $\{\hat{\alpha}_t\}_{t\in[0,T]}$ and through the induced parametrisations $\phi_t = \hat{\alpha}_t \circ \tilde{\phi}$.

Again, this approach allows one to avoid explicitly introducing a velocity field for the evolving surface, since the geometric evolution is already contained in the time dependence of the parametrisation itself, together with the notation introduced in [13] for time derivatives.
The resulting equation will be a linear second-order parabolic PDE on the evolving manifold Γ_t.

3.1.1 Conservation law

Let $\{\Gamma_t\}_{t\in[0,T]}$ be a family of oriented, compact, regular surfaces. Time-dependent functions defined on evolving surfaces are typically introduced by means of the so called space-time manifold (see, e.g., [18]):

$$\mathcal{G}_T = \bigcup_{t\in(0,T)} \Gamma_t \times \{t\} \tag{3.11}$$

The notation $\Gamma_t \times (0, T)$ is not accurate, since the surface Γ_t itself depends on time and there is no genuine Cartesian product structure. The introduction of the space-time manifold $\mathcal{G}_T$ avoids

this misleading abuse of notation and provides a precise setting for defining functions on evolving geometries.

Let $u : \mathcal{G}_T \to \mathbb{R}$ be the conserved quantity on the evolving manifold. The function u may represent, for example, a concentration, a temperature, or a surface density. Let moreover $f : \mathcal{G}_T \to \mathbb{R}$ be a source term and let $\mathbf{q} : \mathcal{G}_T \to T\Gamma_t$ be a tangential flux vector field.

For every sufficiently regular evolving subsurface $T_t \subset \Gamma_t$, the conservation of the quantity u is expressed by the balance law

$$\frac{d}{dt}\int_{T_t} u(\mathbf{x},t)\,d\boldsymbol{\sigma} = \int_{T_t} f(\mathbf{x},t)\,d\boldsymbol{\sigma} - \int_{\partial T_t} \langle \mathbf{q}(\mathbf{x},t), \boldsymbol{\mu}\rangle\,d\boldsymbol{\gamma} \tag{3.12}$$

where $\boldsymbol{\mu}$ denotes the outer conormal vector to ∂T_t tangent to the surface Γ_t.

The first term represents the rate of change of the total quantity contained in the evolving region T_t, while the second and third terms describe respectively production and diffusive transport through the boundary.

In this thesis only diffusive transport mechanisms are considered. The flux is therefore assumed to satisfy a surface version of Fick's law:

$$\mathbf{q}(\mathbf{x},t) = K(\mathbf{x},t)\nabla_{\Gamma_t} u(\mathbf{x},t) \tag{3.13}$$

where

$$K(\mathbf{x},t) : T_{\mathbf{x}}\Gamma_t \to T_{\mathbf{x}}\Gamma_t \tag{3.14}$$

is a symmetric positive definite diffusion tensor acting on the tangent space. Applying the surface divergence theorem gives

$$\int_{\partial T_t} \langle \mathbf{q}, \boldsymbol{\mu}\rangle\,d\boldsymbol{\gamma} = \int_{T_t} \nabla_{\Gamma_t}\cdot \mathbf{q}\,d\boldsymbol{\sigma} = -\int_{T_t} \nabla_{\Gamma_t}\cdot\left(K\nabla_{\Gamma_t} u\right)\,d\boldsymbol{\sigma} \tag{3.15}$$

Substituting (3.15) into (3.12) yields

$$\frac{d}{dt}\int_{T_t} u\,d\boldsymbol{\sigma} = \int_{T_t} \left(f + \nabla_{\Gamma_t}\cdot(K\nabla_{\Gamma_t} u)\right)d\boldsymbol{\sigma} \tag{3.16}$$

The remaining task is to compute the time derivative of the integral over the evolving domain T_t.

Let $\tilde{\phi} : \Xi \subset \mathbb{R}^2 \to \Gamma_0$ be a parametrisation of the reference surface and let $\phi_t = \hat{\alpha}_t \circ \tilde{\phi}$ be the induced parametrisation of Γ_t through the action of $\hat{\alpha}_t$. Denote by $G_t(\boldsymbol{\xi})$ the metric tensor induced by ϕ_t and define the pullback of u to the reference coordinates by

$$U(\boldsymbol{\xi},t) := u(\phi_t(\boldsymbol{\xi}),t) \tag{3.17}$$

Using Definition 2.6, the integral over T_t can be rewritten as

$$\int_{T_t} u(\mathbf{x},t)\,d\boldsymbol{\sigma} = \int_{\phi_t^{-1}(T_t)} U(\boldsymbol{\xi},t)\sqrt{\det G_t(\boldsymbol{\xi})}\,d\boldsymbol{\xi} \tag{3.18}$$

Since the reference domain $\phi_t^{-1}(T_t)$ is independent of time, differentiation under the integral sign gives

$$\begin{aligned}\frac{d}{dt}\int_{T_t} u(\mathbf{x},t)\,d\boldsymbol{\sigma} &= \int_{\phi_t^{-1}(T_t)} \frac{\partial}{\partial t}\left(U(\boldsymbol{\xi},t)\sqrt{\det G_t(\boldsymbol{\xi})}\right)d\boldsymbol{\xi}\\ &= \int_{\phi_t^{-1}(T_t)} \left(\frac{\partial U}{\partial t} + U\frac{1}{\sqrt{\det G_t}}\frac{\partial}{\partial t}\sqrt{\det G_t}\right)\sqrt{\det G_t}\,d\boldsymbol{\xi}\end{aligned} \tag{3.19}$$

The quantity

$$\Lambda(\boldsymbol{\xi}, t) := \frac{1}{\sqrt{\det G_t(\boldsymbol{\xi})}} \frac{\partial}{\partial t} \sqrt{\det G_t(\boldsymbol{\xi})} \tag{3.20}$$

measures the local variation of the surface measure induced by the evolution of the geometry. Returning to spatial coordinates it is possible to define

$$\lambda(\mathbf{x}, t) := \Lambda(\phi_t^{-1}(\mathbf{x}), t) \tag{3.21}$$

Using the definition of material derivative introduced in Definition 2.36, as already shown in (3.10)

$$\dot{u}(\phi_t(\boldsymbol{\xi}), t) = \frac{\partial U}{\partial t}(\boldsymbol{\xi}, t) \tag{3.22}$$

Thus restoring spatial coordinates, equation (3.19) becomes

$$\frac{d}{dt} \int_{T_t} u \, d\boldsymbol{\sigma} = \int_{T_t} (\dot{u} + \lambda u) \, d\boldsymbol{\sigma} \tag{3.23}$$

Substituting (3.23) into (3.16) yields

$$\int_{T_t} \left(\dot{u} + \lambda u - \nabla_{\Gamma_t} \cdot (K \nabla_{\Gamma_t} u) - f \right) d\boldsymbol{\sigma} = 0 \tag{3.24}$$

Since the subsurface $T_t \subset \Gamma_t$ is arbitrary, localisation implies the pointwise equation

$$\dot{u} + \lambda u - \nabla_{\Gamma_t} \cdot (K \nabla_{\Gamma_t} u) = f \qquad \text{in } \mathcal{G}_T \tag{3.25}$$

Equation (3.25) is the strong form of the diffusion equation on the evolving surface.

The term $\dot{u}$ represents the material derivative of the transported quantity, while the geometric term λu appears because the surface measure varies in time. If the surface is stationary, then $\lambda \equiv 0$ and the classical diffusion equation on a fixed manifold is recovered. Finally notice that boundary conditions must be prescribed whenever $\partial\Gamma_t \neq \emptyset$.

Using the equivalence between tangential and intrinsic differential operators discussed in Chapter 2, equation (3.25) can be rewritten in local coordinates. Denoting by G_t the metric tensor associated with the parametrisation ϕ_t, the intrinsic divergence form reads

$$\dot{u} + \lambda u - \nabla_{G_t} \cdot (K \nabla_{G_t} u) = f \qquad \text{in } \mathcal{G}_T \tag{3.26}$$

Pulling back all quantities to the reference domain Ξ gives the purely local formulation. Defining

$$F(\boldsymbol{\xi}, t) = f(\phi_t(\boldsymbol{\xi}), t) \tag{3.27}$$

the governing equation becomes

$$\frac{\partial U}{\partial t} + \Lambda U - \frac{1}{\sqrt{\det G_t}} \nabla \cdot \left(\sqrt{\det G_t} K G_t^{-1} \nabla U \right) = F \qquad \text{in } \Xi \times (0, T) \tag{3.28}$$

Equation (3.28) is a linear second-order parabolic PDE posed on the fixed reference domain Ξ. All geometric effects induced by the evolution of the surface are contained in the metric tensor G_t and in the geometric coefficient Λ.

3.1.2 Weak formulation

The strong formulation (3.26) has been derived from purely geometric and conservation principles. In order to study well posedness and subsequently construct finite element approximations, it is necessary to introduce a suitable variational setting.

As already discussed in Section 2.2.2, the main difficulty lies in the fact that the solution at different times belongs to different function spaces, since the underlying surface itself evolves in time. Classical Bochner spaces are therefore not sufficient and must be replaced by evolving Bochner spaces.

For every $t \in [0,T]$ define $\mathcal{H}_t = L^2(\Gamma_t)$ and $\mathcal{V}_t = H^1(\Gamma_t)$. When homogeneous Dirichlet boundary conditions are prescribed on $\partial\Gamma_t$, one replaces $\mathcal{V}_t$ by $H_0^1(\Gamma_t)$. As already pointed out, they form a compatible pairs with the pushforward operators $\{\alpha_t\}_{t\in[0,T]}$ defined in (3.2), induced by the surface evolution encoded by the family $\{\hat{\alpha}_t\}_{t\in[0,T]}$. The natural functional setting for the solution is therefore the evolving Bochner space $L^2_{\mathcal{V}}$ of Definition 2.33.

For $f \in L^2_{\mathcal{V}'}$ equation (3.26) has to be intended in the distributional sense. Therefore the weak formulation is obtained by applying the strong equation on a generic test function $\varphi \in \mathcal{D}_{\mathcal{V}}(0,T)$, according to the duality pairing defined in (2.19). As remarked in [2], an equivalent weak formulation is obtained by fixing the time and looking at (3.26) in $\mathcal{V}_t'$, and asking to the duality pairing to hold for almost every $t \in (0,T)$. In this way the test function is just $\varphi(t) \in \mathcal{V}_t$ for $t \in (0,T)$. This equivalent formulation turns out to be more suited for the finite element procedure, since the finite element approximation of the test function space $\mathcal{V}_t$ is easier than the one of $L^2_{\mathcal{V}}$. Finally, note that the material derivative of a test function $\varphi(t) \in \mathcal{V}_t$ is well defined by taking the material time derivative of its representative $\varphi \in L^2_{\mathcal{V}}$.

The diffusion term requires an integration by parts on Γ_t. Assuming for simplicity homogeneous Dirichlet boundary conditions, the boundary contribution vanishes and Green's formula (Lemma 2.8) yields

$$-\int_{\Gamma_t} \nabla_{G_t} \cdot (K\nabla_{G_t} u)\varphi \, d\boldsymbol{\sigma} = \int_{\Gamma_t} \left\langle K\nabla_{G_t} u, \nabla_{G_t}\varphi \right\rangle_{G_t} d\boldsymbol{\sigma} \tag{3.29}$$

The treatment of the material derivative is more delicate. In the evolving spaces framework, the material derivative is understood in the weak sense introduced in Definition 2.36. More precisely, if $u \in L^2_{\mathcal{V}}$ admits weak material derivative $\dot{u} \in L^2_{\mathcal{V}'}$ then, by definition,

$$\int_0^T (\dot{u}(t), \varphi(t))_{\mathcal{V}_t'\times\mathcal{V}_t} \, dt = -\int_0^T (u(t), \dot{\varphi}(t))_{\mathcal{H}_t} \, dt - \int_0^T \frac{d}{dt} (\alpha_t u(0), \alpha_t \varphi(0))_{\mathcal{H}_t} \, dt \tag{3.30}$$

This identity plays the role of the classical integration by parts formula in time. The additional term involving the time derivative of the scalar product appears because the underlying Hilbert spaces evolve in time.
Using the transport identity derived in Section 3.1.1,

$$\frac{d}{dt}\int_{\Gamma_t} u\varphi \, d\boldsymbol{\sigma} = \int_{\Gamma_t} (\dot{u}\varphi + u\dot{\varphi} + \lambda u\varphi) \, d\boldsymbol{\sigma} \tag{3.31}$$

it follows that

$$\int_{\Gamma_t} \dot{u}\varphi \, d\boldsymbol{\sigma} + \int_{\Gamma_t} \lambda u\varphi \, d\boldsymbol{\sigma} = \frac{d}{dt}\int_{\Gamma_t} u\varphi \, d\boldsymbol{\sigma} - \int_{\Gamma_t} u\dot{\varphi} \, d\boldsymbol{\sigma} \tag{3.32}$$

Therefore the geometric contribution λu naturally compensates the variation of the surface measure induced by the evolving geometry.

It is now possible to formulate the weak problem. The test function $\varphi(t) \in \mathcal{V}_t$ will be denoted with φ to lighten the notation.

Problem 3.1. Let $f \in L^2_{\mathcal{V}'}$ and $u_0 \in \mathcal{H}_0$. The *weak formulation* of (3.26) reads: find $u \in \mathcal{W}(\mathcal{V}, \mathcal{V}')$ such that $u(0) = u_0$ and such that for every test function $\varphi \in \mathcal{V}_t$ and for almost every $t \in (0, T)$:

$$(\dot{u}(t), \varphi)_{\mathcal{V}_t' \times \mathcal{V}_t} + \int_{\Gamma_t} \left\langle K \nabla_{G_t} u(t), \nabla_{G_t} \varphi \right\rangle_{G_t} d\boldsymbol{\sigma} + \int_{\Gamma_t} \lambda u(t) \varphi \, d\boldsymbol{\sigma} = (f(t), \varphi)_{\mathcal{V}_t' \times \mathcal{V}_t} \tag{3.33}$$

Note that the weak formulation is defined directly on the evolving surface Γ_t and no reference configuration appears explicitly in the final formulation.

Nevertheless, from both theoretical and numerical viewpoints, it is often convenient to pull all quantities back to the fixed reference manifold Γ_0, or equivalently to the local coordinate domain Ξ. In this way the problem is transformed into a parabolic equation posed on a fixed domain, while all geometric effects are encoded into time-dependent coefficients.

Similarly to what has been done in Section 2.2.2, it is possible to define the space where to look for weak solutions of (3.28):

$$\mathcal{W}(H^1(\Xi), H^{-1}(\Xi)) := \left\{ U \in L^2(0, T; H^1(\Xi)) : \frac{\partial U}{\partial t} \in L^2(0, T; H^{-1}(\Xi)) \right\} \tag{3.34}$$

Letting $\Phi(\boldsymbol{\xi}, t) = \varphi(\phi_t(\boldsymbol{\xi}), t)$ and using the transformation formula for surface integrals (Definition 2.6), the local weak formulation reads as follows.

Problem 3.2. Let $F \in L^2(0, T; H^{-1}(\Xi))$ and $U_0 \in L^2(\Xi)$. The local weak formulation of (3.26) reads: find $U \in \mathcal{W}(H^1(\Xi), H^{-1}(\Xi))$ such that $U(0) = U_0$ and such that for every $\Phi \in H^1(\Xi)$ and for almost every $t \in (0, T)$:

$$\begin{aligned} \left(\frac{\partial U}{\partial t}, \Phi \sqrt{\det G_t} \right)_{H^{-1}(\Xi) \times H^1(\Xi)} &+ \int_\Xi \left\langle K G_t^{-1} \nabla U, \nabla \Phi \right\rangle \sqrt{\det G_t} \, d\boldsymbol{\xi} \\ &+ \int_\Xi \Lambda U \Phi \sqrt{\det G_t} \, d\boldsymbol{\xi} = \left(F(t), \Phi \sqrt{\det G_t} \right)_{H^{-1}(\Xi) \times H^1(\Xi)} \end{aligned} \tag{3.35}$$

Both Problem 3.1 and Problem 3.2 must be complemented with suitable boundary conditions. In the case of Neumann boundary conditions, the boundary contribution produced by Green's formula does not vanish and must be included in the right-hand side. In case of $\Gamma_t = \emptyset$, there are no boundary conditions.

In most applications, a parametrisation of the surface is not available, and the available information concerns the surface as embedded in the ambient Euclidean space. For this reason, Problem 3.1 is taken as the model problem. Nevertheless, as discussed in Section 4.1.4, the numerical implementation of the solver exploits suitably constructed local parametrisations, by identifying the weak formulation of Problem 3.2.

3.2 Well posedness

This section briefly summarizes the main results concerning the well posedness of Problem 3.1.

The existence and uniqueness of solutions for the embedded formulation of (3.26), together with corresponding a priori estimates for the solution norm, were first established in [15]. This analysis is carried out within a specific functional-analytic framework and, in its original form, does not include a forcing term.

A more general setting is considered in [2], where well posedness is established for abstract evolving spaces and for forcing terms $f \in L^2_{\mathcal{V}'}$. Within this framework, an a priori estimate in the

$\mathcal{W}(\mathcal{V},\mathcal{V}')$ norm of the solution is also derived, allowing one to treat a broader class of problems on evolving geometries in a unified way. The theorems reported below correspond to this general setting and will be used as the main analytical reference for the subsequent developments.

Finally, in [21], similar stability estimates to those in [15] are recovered within the abstract framework, although again in the absence of a forcing term.

Theorem 3.3. *There exists a unique solution $u \in \mathcal{W}(\mathcal{V},\mathcal{V}')$ of Problem 3.1. Moreover the solution satisfies the bound:*

$$\|u\|_{\mathcal{W}(\mathcal{V},\mathcal{V}')} \leq C \left(\|u_0\|_{\mathcal{H}_0} + \|f\|_{L^2_{\mathcal{V}'}} \right) \tag{3.36}$$

The following theorem shows that, under suitable regularity assumptions on the data of the problem, the solution inherits additional regularity properties. In particular, improved regularity of the forcing terms and initial data leads to enhanced regularity of the solution within the evolving space framework.

Theorem 3.4. *Under the assumption of $f \in L^2_{\mathcal{H}}$ and $u \in \mathcal{V}_0$, the unique solution of Problem 3.1 satisfies the regularity $u \in \mathcal{W}(\mathcal{V},\mathcal{H})$ and the estimate*

$$\|u\|_{\mathcal{W}(\mathcal{V},\mathcal{H})} \leq C \left(\|u_0\|_{\mathcal{H}_0} + \|f\|_{L^2_{\mathcal{H}}} \right) \tag{3.37}$$

Chapter 4

Intrinsic FEM on evolving surfaces

4.1 Finite Element formulation

The Finite Element Method requires the introduction of a finite-dimensional subspace of the function space used in the weak formulation. In this setting, a finite basis can be constructed, allowing every function in the discrete space to be represented as a linear combination of basis functions. As a consequence, the variational formulation, originally expressed as an integral equation, is transformed into a finite-dimensional algebraic linear system, where the unknowns are the coefficients of the basis expansion of the discrete solution.

This construction is justified by approximation properties of Sobolev spaces. In particular, any function in H^1 can be approximated (in the H^1 sense) by sequences of continuous functions, which supports the use of conforming finite element spaces consisting of continuous functions as natural choices for the discretisation [28].

4.1.1 Semi-discrete FEM

Assume Γ_t to be a regular surface admitting a single parametrisation $\phi_t : \Xi \to \Gamma_t$ for all $t \in [0, T]$. In numerical applications, the surface is typically represented as a discrete set of points $\{\mathbf{x}_i\}_i$ (the mesh nodes). Each node is mapped back to the reference domain through the inverse parametrisation, i.e. $\boldsymbol{\xi}_i = \phi_t^{-1}(\mathbf{x}_i)$.

This allows the construction of a triangulation $\mathcal{T}_h(\Xi)$ of the reference domain Ξ, based on the set of nodes $\{\boldsymbol{\xi}_i\}_i$. The triangulation consists of a collection of non overlapping triangles whose union equals Ξ, with the property that no node lies in the interior of any triangle. The parameter h denotes the maximal edge length of the triangulation and is commonly referred to as the *mesh size*. The corresponding conforming finite element space is then defined accordingly.

$$\mathcal{V}_h(\Xi) = \left\{\Phi \in C^0(\Xi, \mathbb{R}) : \Phi\big|_{\hat{T}_h} \in \mathcal{P}_1(\hat{T}_h), \forall \hat{T}_h \in \mathcal{T}_h(\Xi)\right\} \tag{4.1}$$

Here, $\mathcal{P}_1(\hat{T}_h)$ denotes the space of first-order polynomials on $\hat{T}_h$. The triangulation $\mathcal{T}_h(\Gamma_t)$ of the surface Γ_t is obtained by mapping each element $\hat{T}_h \in \mathcal{T}_h(\Xi)$ onto Γ_t through the parametrisation ϕ_t.

The index h is kept in both triangulations with a slight abuse of notation, since the actual geometry of the mesh on Γ_t is affected by the mapping ϕ_t and, in particular, the edge lengths are generally distorted by it. The definition of the finite element space on the surface at time t is then naturally obtained from (4.1).

$$\mathcal{V}_h(\Gamma_t) = \left\{\varphi : \Gamma_t \to \mathbb{R} : \exists \Phi \in \mathcal{V}_h(\Xi) : \varphi = \Phi \circ \phi_t^{-1}\right\} \tag{4.2}$$

Trivially, $\mathcal{V}_h(\Xi)$ and $\mathcal{V}_h(\Gamma_t)$ are finite dimensional subspaces of $H^1(\Xi)$ and $H^1(\Gamma_t)$ respectively, for all $t \in [0,T]$. The basis of $\mathcal{V}_h(\Xi)$ is simply the set $\{\Phi_i\}_i$ of elementwise linear functions such that $\Phi_i(\boldsymbol{\xi}_j) = \delta_{ij}$, where $\{\boldsymbol{\xi}_j\}_j$ are the nodes of the triangulation and $\delta_{ij} = 1$ if $i = j$ and $\delta_{ij} = 0$ otherwise. The key property of such basis functions is based on the nice property mentioned in (3.10), which implies:

$$\frac{d\varphi_i(\mathbf{x})}{dt}\Big|_{\mathbf{x}=\phi_t(\boldsymbol{\xi})} = \frac{\partial \Phi_i(\boldsymbol{\xi})}{\partial t} = 0 \tag{4.3}$$

Note that $\varphi_i = \Phi_i \circ \phi_t^{-1}$ is non linear (as long as the parametrisation is non linear). The generic function $U_h : \Xi \times [0,T] \to \mathbb{R}$ such that $U_h(\cdot,t) \in \mathcal{V}_h(\Xi)$ for all $t \in [0,T]$ can be therefore expressed as a linear combination of basis functions, for every fixed time instant:

$$U_h(\boldsymbol{\xi},t) = \sum_{j=1}^{n} U_j(t)\Phi_j(\boldsymbol{\xi}) \tag{4.4}$$

In other words, instead of defining a finite dimensional subspace of $H^1(\Xi \times [0,T])$, it suffices to define a time-independent basis of a finite dimensional subset of $H^1(\Xi)$, leaving the time dependence on the coefficients of the linear combination.
Clearly, the generic $u_h(\cdot,t) \in \mathcal{V}_h(\Gamma_t)$, can be expressed as:

$$u_h(\mathbf{x},t) = \sum_{j=1}^{n} u_j(t)\varphi_j(\mathbf{x}) \tag{4.5}$$

with $\mathbf{x} \in \Gamma_t$. The semi-discrete weak formulation is obtained by stating Problem 3.1 confining the functions inside the finite element space, and applying the transport identity (3.23).

Problem 4.1. The *semi-discrete finite element formulation* of (3.1) reads: find $u_h \in L^2_{\mathcal{V}_h}$ such that for all $\varphi_h \in \mathcal{V}_h(\Gamma_t)$ and for almost every $t \in (0,T)$:

$$\frac{d}{dt}\int_{\Gamma_t} u_h\varphi_h - \int_{\Gamma_t} u_h\dot{\varphi}_h + \int_{\Gamma_t} \left\langle \nabla_{G_t} u_h, \nabla_{G_t}\varphi_h \right\rangle_{G_t} = (f,\varphi_h)_{\mathcal{V}_t'\times\mathcal{V}_t} \tag{4.6}$$

With an abuse of notation, in (4.6) u_h actually denotes $u_h(t)$ (its representative at time t), and the same for f. Conversely, the material derivative of the test function is obtained by pulling it back, applying the derivation, and pushing forward, as mentioned in Definition 2.36.

Expanding the functions $\varphi_h \in \mathcal{V}_h(\Gamma_t)$ in the linear combination of n basis functions, (4.6) must hold for $\varphi_h = \varphi_i$ for all $i = 1,...,n$ and for all $t \in [0,T]$, where $\{\varphi_i\}_i$ are the basis functions of $\mathcal{V}_h(\Gamma_t)$. Hence (4.6) leads to n equations. Following what has been done in Section 3.1 and taking advantage of (4.3), (4.6) is equivalent to:

$$\frac{d}{dt}\int_{\Gamma_t} u_h\varphi_i + \int_{\Gamma_t} \left\langle \nabla_{G_t} u_h, \nabla_{G_t}\varphi_i \right\rangle_{G_t} = (f,\varphi_i)_{\mathcal{V}_t'\times\mathcal{V}_t} \quad \forall i = 1,...,n \ \ \forall t \in (0,T) \tag{4.7}$$

Following this derivation, it turns out that the material derivative of the basis functions is zero, as the pull back of these functions in independent of time. This is in agreement with the formulation proposed in [18].

As is standard in the finite element framework, u_h can also be expressed as a linear combination of basis functions, as in (4.5).

$$\frac{d}{dt}\int_{\Gamma_t} \sum_{j=1}^{n} u_j(t)\varphi_j\varphi_i + \int_{\Gamma_t} \left\langle \nabla_{G_t}\left(\sum_{j=1}^{n} u_j(t)\varphi_i\right), \nabla_{G_t}\varphi_i \right\rangle_{G_t} = (f,\varphi_i)_{\mathcal{V}_t'\times\mathcal{V}_t} \quad \forall i, \ \forall t \in (0,T) \tag{4.8}$$

$$\frac{d}{dt}\left(\sum_{j=1}^{n} u_j(t)\int_{\Gamma_t}\varphi_i\varphi_j\right)+\sum_{j=1}^{n} u_j(t)\int_{\Gamma_t}\left\langle\nabla_{G_t}\varphi_i,\nabla_{G_t}\varphi_j\right\rangle_{G_t}=(f,\varphi_i)_{\mathcal{V}_t'\times\mathcal{V}_t}\quad\forall i,\ \forall t\in(0,T) \tag{4.9}$$

It is straightforward to observe that (4.9) can be rewritten as a system of ordinary differential equations indexed by i and j, whose unknowns are the coefficients appearing in (4.5). In this way, it is natural to introduce the matrices and vectors associated with the system, which encode the finite element discretisation in algebraic form.

$$\begin{aligned}\mathrm{M}(t)_{ij}&=\int_{\Gamma_t}\varphi_i\varphi_j\\ \mathrm{A}(t)_{ij}&=\int_{\Gamma_t}\left\langle\nabla_{G_t}\varphi_i,\nabla_{G_t}\varphi_j\right\rangle_{G_t}\\ \mathbf{f}(t)_i&=(f,\varphi_i)_{\mathcal{V}_t'\times\mathcal{V}_t}\\ \mathbf{u}(t)_i&=u_i(t)\end{aligned} \tag{4.10}$$

Therefore the semi-discrete finite element formulation is equivalent to the following system of first order differential equations, of dimension n:

$$\frac{d}{dt}\left(\mathrm{M}(t)\mathbf{u}(t)\right)+\mathrm{A}(t)\mathbf{u}(t)=\mathbf{f}(t) \tag{4.11}$$

4.1.2 Well posedness of semi-discrete FEM

The following two lemmas are stated in [15] for the analysis of Problem 3.1, where they are used to establish existence and uniqueness of the solution. In this thesis, they are adapted to the study of Problem 4.1, and are therefore reformulated in a way that is consistent with the present intrinsic framework.

Another difference with respect to the original formulation lies in the explicit appearance of intrinsic geometric quantities, such as the metric tensor G and the term λ, which play a central role in the intrinsic representation of the finite element formulation.

Lemma 4.2. *Let u_h be the solution of Problem 4.1. Then:*

$$\frac{1}{2}\frac{d}{dt}\int_{\Gamma_t}u_h^2+\int_{\Gamma_t}\left|\nabla_{G_t}u_h\right|_{G_t}^2+\frac{1}{2}\int_{\Gamma_t}\lambda u_h^2=(f,u_h)_{\mathcal{V}_t'\times\mathcal{V}_t}$$

Proof. Since $u_h(\cdot,t)\in\mathcal{V}_h(\Gamma_t)$ for all $t\in(0,T)$, by choosing $\varphi_h=u_h(\cdot,t)$ it follows that:

$$\frac{d}{dt}\int_{\Gamma_t}u_h^2+\int_{\Gamma_t}\left|\nabla_{G_t}u_h\right|_{G_t}^2=\int_{\Gamma_t}u_h\dot{u}_h+(f,u_h)_{\mathcal{V}_t'\times\mathcal{V}_t} \tag{4.12}$$

Moreover:

$$\int_{\Gamma_t}u_h\dot{u}_h=\int_{\Gamma_t}\frac{1}{2}\frac{d}{dt}u_h^2=\frac{1}{2}\frac{d}{dt}\int_{\Gamma_t}u_h^2-\frac{1}{2}\int_{\Gamma_t}\lambda u_h^2 \tag{4.13}$$

Finally combining (4.12) and (4.13) the proof is complete. □

Lemma 4.3. *Let u_h be the solution of Problem 4.1 such that $\dot{u}_h\in L^2_{\mathcal{V}}$. Moreover let $\dot{G}_t$ (the componentwise time derivative of the metric G_t) be well defined. Then:*

$$\begin{aligned}\int_{\Gamma_t}\dot{u}_h^2+\frac{1}{2}\frac{d}{dt}\int_{\Gamma_t}\left|\nabla_{G_t}u_h\right|_{G_t}^2&=(f,\dot{u}_h)_{\mathcal{V}_t'\times\mathcal{V}_t}+\frac{1}{2}\int_{\Gamma_t}\lambda\left|\nabla_{G_t}u_h\right|_{G_t}^2\\ &\quad-\frac{1}{2}\int_{\Gamma_t}\left\langle\dot{G}_t\nabla_{G_t}u_h,\nabla_{G_t}u_h\right\rangle-\int_{\Gamma_t}\lambda u_h\dot{u}_h\end{aligned} \tag{4.14}$$

Proof. By putting $\varphi_h = \dot{u}_h$ in (4.6), it follows that:

$$\int_{\Gamma_t} \dot{u}_h^2 + \int_{\Gamma_t} \lambda u_h \dot{u}_h + \int_{\Gamma_t} \left\langle \nabla_{G_t} u_h, \nabla_{G_t} \dot{u}_h \right\rangle_{G_t} = (f, \dot{u}_h)_{\mathcal{V}_t' \times \mathcal{V}_t} \tag{4.15}$$

The third term of the right-hand side can be managed as follows:

$$\begin{aligned}
\frac{1}{2}\frac{d}{dt}\int_{\Gamma_t} \left|\nabla_{G_t} u_h\right|^2_{G_t} &= \frac{1}{2}\sum_{i,j=1}^{2} \int_{\phi^{-1}(G_t)} \frac{d}{dt}\left(\left(G_t^{-1}\right)_{ij} \frac{\partial U_h}{\partial \xi_i}\frac{\partial U_h}{\partial \xi_j}\sqrt{\det G_t}\right) d\boldsymbol{\xi} \\
&= \frac{1}{2}\sum_{i,j=1}^{2} \int_{\phi^{-1}(G_t)} \frac{d}{dt}\left(G_t^{-1}\right)_{ij} \frac{\partial U_h}{\partial \xi_i}\frac{\partial U_h}{\partial \xi_j}\sqrt{\det G_t} \\
&\quad + 2\left(G_t^{-1}\right)_{ij} \frac{\partial U_h}{\partial \xi_i}\frac{d}{dt}\left(\frac{\partial U_h}{\partial \xi_j}\right)\sqrt{\det G_t} + \left(G_t^{-1}\right)_{ij} \frac{\partial U_h}{\partial \xi_i}\frac{\partial U_h}{\partial \xi_j}\frac{d}{dt}\sqrt{\det G_t}\, d\boldsymbol{\xi}
\end{aligned} \tag{4.16}$$

Let I be the identity matrix. Note that:

$$0 = \frac{dI}{dt} = \frac{d}{dt}\left(G_t^{-1} G_t\right) \implies \frac{d}{dt}\left(G_t^{-1}\right) = -G_t^{-1}\dot{G}_t G_t^{-1}$$

In components:

$$\frac{d}{dt}\left(G_t^{-1}\right)_{ij} = -\left(G_t^{-1}\right)_{ik} \left(\dot{G}_t\right)_{kl} \left(G_t^{-1}\right)_{lj} \tag{4.17}$$

Thus the first term of the right-hand side of (4.16) reads:

$$\frac{d}{dt}\left(G_t^{-1}\right)_{ij} \frac{\partial U_h}{\partial \xi_i}\frac{\partial U_h}{\partial \xi_j}\sqrt{\det G_t} = -\left(\dot{G}_t\right)_{kl} \left(\nabla_{G_t} u_h\right)_k \left(\nabla_{G_t} u_h\right)_l \sqrt{\det G_t} \tag{4.18}$$

Hence it is possible to go back to the compact notation, and recognise:

$$\begin{aligned}
\frac{1}{2}\frac{d}{dt}\int_{\Gamma_t} \left|\nabla_{G_t} u_h\right|^2_{G_t} &= -\frac{1}{2}\int_{\Gamma_t} \left\langle \dot{G}_t \nabla_{G_t} u_h, \nabla_{G_t} u_h \right\rangle \\
&\quad + \int_{\Gamma_t} \left\langle \nabla_{G_t} u_h, \nabla_{G_t} \dot{u}_h \right\rangle_{G_t} + \frac{1}{2}\int_{\Gamma_t} \lambda \left|\nabla_{G_t} u_h\right|^2_{G_t}
\end{aligned} \tag{4.19}$$

Substituting (4.19) inside (4.15), the thesis is proved. □

The following lemma is known as Grönwall inequality and will be used repeatedly in the following pages. It is one of the main analytical tools for deriving a priori bounds on time-dependent quantities, in particular for controlling the evolution of the $L^2(\Gamma_t)$ norm of a function.

Lemma 4.4. *Let $I = [0, T] \subset \mathbb{R}$ be an interval, b and c continuous functions defined in I. If u is differentiable in $(0, T)$ and it is such that:*

$$u'(t) \leq b(t)u(t) + c(t) \quad \forall t \in I$$

Then u is bounded by the solution of the equation $y'(t) = b(t)u(t) + c(t)$ in I, namely:

$$u(t) \leq u(0)e^{\int_0^t b(s)\, ds} + \int_0^t c(s)e^{\int_s^t b(r)dr} ds \quad \forall t \in I$$

In [15], existence and uniqueness of the solution to the weak problem were established, together with corresponding bounds on the solution norm. Subsequently, well posedness was extended to a more general abstract setting in [2]. The following theorem establishes the well posedness of the semi-discrete problem (Problem 4.1) following standard arguments in the literature. The main emphasis here is placed on the stability constants and, in particular, the original contribution relies on their dependence on intrinsic geometric properties of the surface. To this end, it is necessary to make the following observations.

Let $\left\|\dot{G}_t\right\|$ be the operator norm of $\dot{G}_t$, namely:

$$\|\dot{G}_t\| := \sup_{\mathbf{v}\in\mathbb{R}^2} \left\langle \dot{G}_t\mathbf{v}, \mathbf{v}\right\rangle \tag{4.20}$$

Since $\dot{G}_t$ is symmetric, its operator norm coincides with its largest absolute eigenvalue, which here will be called $\dot{g}_t^*$. At the same time, if $g_{*,t}$ is the smallest eigenvalue of G_t, it is possible to bound the $\mathbb{R}^2$-scalar product with the scalar product induced by G_t:

$$g_{*,t}\left\langle \mathbf{v}, \mathbf{v}\right\rangle \leq \left\langle \mathbf{v}, \mathbf{v}\right\rangle_{G_t} \qquad \forall \mathbf{v} \in \mathbb{R}^2 \tag{4.21}$$

Which implies:

$$|\mathbf{v}| \leq \frac{1}{\sqrt{g_{*,t}}} |\mathbf{v}|_{G_t} \qquad \forall \mathbf{v} \in \mathbb{R}^2 \tag{4.22}$$

The following theorem will make use of the quantity defined below.

$$c_g := \int_0^T \frac{\dot{g}_t^*}{g_{*,t}}\, dt = \left\| \frac{\dot{g}_t^*}{g_{*,t}} \right\|_{L^1(0,T)} \tag{4.23}$$

In [21], a result analogous to the one stated below is proved, but in the absence of a forcing term and without the estimate (4.25). The following theorem can therefore be seen as an adaptation of the corresponding result in [15] to the abstract evolving space framework, enriched with additional information on the dependence of the stability constants on intrinsic geometric quantities.

Theorem 4.5. *Let $u_{h0} \in \mathcal{V}_h(\Gamma_0)$ and $f \in L^2_{\mathcal{V}'}$. Assume that the space-time manifold is regular enough such that $\dot{G}_t$ is well defined, $\lambda \in L^1_{L^\infty}$ and $c_g < \infty$. Then there exists a unique solution $u_h \in L^2_{\mathcal{V}_h}$ with $\dot{u}_h \in L^2_{\mathcal{V}_h}$ of Problem 4.1 and the following energy estimates hold:*

$$\sup_{(0,T)} \|u_h\|^2_{\mathcal{H}_t} + \int_0^T \|\nabla_{G_t} u_h\|^2_{\mathcal{H}_t} \leq c_1 \|u_{h0}\|^2_{\mathcal{H}_0} + c_2 \|f\|^2_{L^2_{\mathcal{V}'}} \tag{4.24}$$

$$\int_0^T \|\dot{u}_h\|^2_{\mathcal{H}_t} + \sup_{(0,T)} \|\nabla_{G_t} u_h\|^2_{\mathcal{H}_t} \leq c_3 \|u_{h0}\|^2_{\mathcal{V}_0} + c_4 \|f\|^2_{L^2_{\mathcal{V}'}} \tag{4.25}$$

Where the constants c_1, c_2, c_3, c_4 depend on T and on the metric.

Proof. Let u_h be the Galerkin ansatz. Then, as discussed in Section 4.1.1, the semi-discrete formulation is equivalent to a system of ordinary differential equations in time, see (4.11). The regularity of the matrices and of the right-hand side with respect to time allows one to conclude, by standard ODE theory [10], that the system admits a unique solution for any initial datum $u_{h0} \in \mathcal{V}_h(\Gamma_0)$. Moreover, the components of the coefficient vector $\mathbf{u}$ are absolutely continuous functions of time with time derivatives belonging to $L^2(0,T)$ [2].

Therefore, denoting by $\{\varphi_j\}_j$ the finite-dimensional basis of $\mathcal{V}_h(\Gamma_t)$:

$$\begin{aligned} u_h(\cdot,t) &= \sum_{j=1}^n u_j(t)\varphi_j \qquad \in \mathcal{V}_h(\Gamma_t) \\ \dot{u}_h(\cdot,t) &= \sum_{j=1}^n \dot{u}_j(t)\varphi_j \qquad \in \mathcal{V}_h(\Gamma_t) \end{aligned} \tag{4.26}$$

In particular $u_h, \dot{u}_h \in L^2_{\mathcal{V}_h}$.

The next step is to establish the bound (4.24). To simplify the notation, the dependence of the functions on time t will be omitted: a Bochner function and its representative at time t will be denoted by the same symbol.

If u_h is the solution of Problem 4.1, the hypothesis of Lemma 4.2 are satisfied, hence:

$$\frac{1}{2}\frac{d}{dt}\|u_h\|^2_{\mathcal{H}_t} + \frac{1}{2}\|\nabla_{G_t} u_h\|^2_{\mathcal{H}_t} + \frac{1}{2}\int_{\Gamma_t} \lambda u_h^2 = (f, u_h)_{\mathcal{V}_t' \times \mathcal{V}_t} \tag{4.27}$$

Using the Poincarè lemma, Hölder inequality and the Young inequality, it is possible to write:

$$\frac{d}{dt}\|u_h\|^2_{\mathcal{H}_t} + \left(2 - \varepsilon(C^2_{\Gamma_t} + 1)\right)\|\nabla_{G_t} u_h\|^2_{\mathcal{H}_t} \leq \|\lambda\|_{L^\infty(\Gamma_t)}\|u_h\|^2_{\mathcal{H}_t} + C_\varepsilon \|f\|^2_{\mathcal{V}'} \tag{4.28}$$

Picking ε small enough, the second term of the left-hand side can be neglected. Therefore hypothesis of Lemma 4.4 are satisfied:

$$\begin{aligned} \|u_h\|^2_{\mathcal{H}_t} &\leq \|u_{h0}\|^2_{\mathcal{H}_0} e^{\int_0^t \|\lambda\|_{L^\infty(\Gamma_t)}} + \int_0^t C_\varepsilon \|f\|^2_{\mathcal{V}'} e^{\int_s^t \|\lambda\|_{L^\infty(\Gamma_t)}} \\ &\leq \|u_{h0}\|^2_{\mathcal{H}_0} e^{\overbrace{\|\lambda\|_{L^1(0,T;L^\infty(\Gamma_t))}}^{:=c_\lambda}} + C_\varepsilon e^{c_\lambda}\|f\|^2_{L^2_{\mathcal{V}'}} \end{aligned} \tag{4.29}$$

Note that (4.27) holds for all $t \in (0, T)$. In particular, taking the supremum on both sides over the interval $(0, T)$ preserves the inequality, yielding a bound with the same right-hand side.

Now, integrating (4.27) in $(0, T)$ and making use of the same tricks as above:

$$\begin{aligned} \int_0^T \|\nabla_{G_t} u_h\|^2_{\mathcal{H}_t} \leq \frac{1}{2}\|u_{h0}\|^2_{\mathcal{H}_0} &+ \int_0^T \|\lambda\|_{L^\infty(\Gamma_t)}\|u_h\|^2_{\mathcal{H}_t} \\ &+ C_\varepsilon \|f\|^2_{L^2_{\mathcal{V}'}} + \varepsilon \int_0^T \|\nabla_{G_t} u_h\|^2_{\mathcal{H}_t} + \varepsilon \int_0^T \|u_h\|^2_{\mathcal{H}_t} \end{aligned} \tag{4.30}$$

Finally exploiting (4.29) it follows:

$$\int_0^T \|\nabla_{G_t} u_h\|^2_{\mathcal{H}_t} \leq \tilde{c}_1 \|u_{h0}\|^2_{\mathcal{H}_0} + \tilde{c}_2 \|f\|^2_{L^2_{\mathcal{V}'}} \tag{4.31}$$

with constants:

$$\begin{aligned} \tilde{c}_1 &= \frac{1}{1-\varepsilon}\left(\frac{1}{2} + c_\lambda e^{c_\lambda} + \varepsilon T e^{c_\lambda}\right) \\ \tilde{c}_2 &= \frac{1}{1-\varepsilon}\left(c_\lambda C_\varepsilon e^{c_\lambda} + C_\varepsilon + \varepsilon C_\varepsilon e^{c_\lambda}\right) \end{aligned} \tag{4.32}$$

Summing up (4.29) and (4.30) the bound (4.24) is achieved for u_h, with constants:

$$c_1 = \tilde{c}_1 + e^{c_\lambda} \tag{4.33}$$

$$c_2 = \tilde{c}_2 + C_\varepsilon e^{c_\lambda} \tag{4.34}$$

Now focus on the bound (4.25). Since $\dot{u}_h \in L^2_{\mathcal{V}_h}$, as remarked in (4.26), the hypothesis of Lemma 4.3 are satisfied:

$$\begin{aligned} \int_{\Gamma_t} \dot{u}_h^2 + \frac{1}{2}\frac{d}{dt}\int_{\Gamma_t} \left|\nabla_{G_t} u_h\right|^2_{G_t} &= (f, \dot{u}_h)_{\mathcal{V}_t' \times \mathcal{V}_t} + \frac{1}{2}\int_{\Gamma_t} \lambda \left|\nabla_{G_t} u_h\right|^2_{G_t} \\ &\quad - \frac{1}{2}\int_{\Gamma_t} \left\langle \dot{G}_t \nabla_{G_t} u_h, \nabla_{G_t} u_h \right\rangle - \int_{\Gamma_t} \lambda u_h \dot{u}_h \end{aligned} \tag{4.35}$$

Using again Hölder and Young inequality and taking advantage of (4.22, 4.21):

$$\begin{aligned} 2(1-\gamma-\delta\|\lambda\|_{L^\infty(\Gamma_t)})\|\dot{u}_h\|^2_{\mathcal{H}_t} + \|\nabla_{G_t} u_h\|^2_{\mathcal{H}_t} \leq \frac{1}{2\gamma}\|f\|^2_{\mathcal{V}'} \\ + \frac{1}{2\delta}\|\lambda\|_{L^\infty(\Gamma_t)}\left(c_1\|u_{h0}\|^2_{\mathcal{H}_0} + c_2\|f\|^2_{L^2_{\mathcal{V}'}}\right) + \left(\|\lambda\|_{L^\infty(\Gamma_t)} + \frac{\dot{g}^*_t}{g_{*,t}}\right)\|\nabla_{G_t} u_h\|^2_{\mathcal{H}_t} \end{aligned} \tag{4.36}$$

where δ and γ are two positive constants chosen in such a way that the first term on the left-hand side remains positive, and can therefore be neglected in the inequality. By introducing (4.23), it is possible to apply Lemma 4.4 to the norm of the intrinsic gradient of u_h, obtaining:

$$\|\nabla_{G_t} u_h\|^2_{\mathcal{H}_t} \leq \|\nabla_{G_0} u_h\|^2_{\mathcal{H}_0} e^{c_g+c_\lambda} + \frac{c_\lambda c_1}{2\delta}\|u_{h0}\|^2_{\mathcal{H}_0} e^{c_g+c_\lambda} + \left(\frac{1}{2\gamma} + \frac{c_\lambda c_2}{2\delta}\right)\|f\|^2_{L^2_{\mathcal{V}'}} e^{c_\lambda+c_g} \tag{4.37}$$

Since (4.37) holds for all $t \in (0,T)$ it is possible to take the supremum both sides, and the right-hand side does not change.
Finally, in order to obtain the bound (4.25), it suffices to integrate in time (4.36)

$$\int_0^T \|\dot{u}_h\|_{\mathcal{H}_t} \leq \tilde{C}\left(\|\nabla_{G_0} u_{h0}\|^2_{\mathcal{H}_0} + c_1 c_\lambda \|u_{h0}\|^2_{\mathcal{H}_0} + (1 + c_\lambda c_2)\|f\|^2_{L^2_{\mathcal{V}'}} + (c_\lambda + c_g)\|\nabla_{G_t} u_h\|^2_{\mathcal{H}_t}\right) \tag{4.38}$$

and making use of (4.37):

$$\begin{aligned} \int_0^T \|\dot{u}_h\|_{\mathcal{H}_t} \leq \underbrace{\tilde{C}_1(1 + (c_g + c_\lambda)e^{c_g+c_\lambda})}_{:=\tilde{c}_3}\|\nabla_{G_0} u_{h0}\|^2_{\mathcal{H}_0} \\ + \underbrace{\tilde{C}_2\left((c_g + c_\lambda)(c_\lambda c_g)e^{c_g+c_\lambda} + c_1 c_\lambda\right)}_{:=\tilde{c}'_3}\|u_{h0}\|^2_{\mathcal{H}_0} \\ + \underbrace{\tilde{C}_3\left((c_\lambda + c_g)(1 + c_\lambda c_g)e^{c_\lambda+c_g} + 1 + c_\lambda c_g\right)}_{:=\tilde{c}_4}\|f\|^2_{L^2_{\mathcal{V}'}} \end{aligned} \tag{4.39}$$

where $\tilde{C}, \tilde{C}_1, \tilde{C}_2, \tilde{C}_3$ are positive constants depending on γ, δ. Finally Summing up (4.37,4.39) the desired bound is obtained with constants:

$$c_3 = \max\left\{\tilde{c}_3 + e^{c_g+c_\lambda}, \tilde{c}'_3 + \frac{c_\lambda c_1}{2\delta}e^{c_\lambda+c_g}\right\} \tag{4.40}$$

$$c_4 = \tilde{c}_4 + \left(\frac{1}{2\gamma} + \frac{c_\lambda c_2}{2\delta}\right)e^{c_\lambda+c_g} \tag{4.41}$$

where c_1 and c_2 are the constants of the bound (4.24). □

4.1.3 Fully discrete FEM

The solution of (4.11) corresponds to the solution of (4.1) and can be computed numerically by solving the fully discrete formulation, which is obtained by selecting one of the several available numerical schemes for systems of ordinary differential equations. In other words, the fully discrete formulation depends on the specific time discretisation method chosen to approximate the system of ODEs (4.11). A particularly suitable choice is the Backward Euler scheme, due to its well-known unconditional stability properties [12].

The time interval $[0, T]$ is partitioned into $m - 1$ non overlapping subintervals such that

$$[0, T] = \bigcup_{k=1}^{m} [t_k, t_{k-1}]$$

All the quantities introduced in (4.10) are evaluated at the current time level t_k. The symbol τ^k denotes the time step size between the time instants t_k and t_{k-1}. For simplicity, any dependence on the time level t^k will be indicated simply by the index k, thereby reducing the notational complexity.

Problem 4.6. The *fully discrete finite element formulation* of Problem 4.1 obtained with the Backward Euler scheme reads: find $u_h^k \in \mathcal{V}_h(\Gamma_k)$ such that for all $k = 1, ..., m$ and for all $\varphi_h^k \in \mathcal{V}_h(\Gamma_k)$:

$$\frac{1}{\tau^k}\left(\int_{\Gamma_{k+1}} u_h^{k+1}\varphi_h^{k+1} - \int_{\Gamma_k} u_h^k \varphi_h^k\right) + \int_{\Gamma_{k+1}} \left\langle \nabla_{G_{k+1}} u_h^{k+1}, \nabla_{G_{k+1}} \varphi_h^{k+1} \right\rangle_{G_{k+1}} = (f^{k+1}, \varphi_h^{k+1})_{\mathcal{V}'_{k+1} \times \mathcal{V}_{k+1}} \tag{4.42}$$

Which in matrix form, after expanding quantities over basis functions and introducing the matrices defined in (4.10), is equivalent to solve the following n dimensional linear system for $k = 1, ..., m$:

$$\left(\frac{\mathrm{M}^{k+1}}{\tau^k} + \mathrm{A}^{k+1}\right)\mathbf{u}^{k+1} = \frac{\mathrm{M}^k}{\tau^k}\mathbf{u}^k + \mathbf{f}^{k+1} \tag{4.43}$$

4.1.4 Numerical implementation

As shown in Section 4.1.3 the fully discrete FEM requires the computation of the system matrices (4.10) at each time step. As usually done in FEM codes, matrices are computed element by element (local matrices) and subsequently assembled in the global ones. The integrals involved in the computation of the local matrices need to be treated with appropriate quadrature rules. An important thing to note is that the argument of the integral is not polynomial, in general. This means that there is no quadrature rule which computes exactly the integral (unless the metric is constant, as will be discussed very soon). As a consequence, it is necessary to pick a second-order accurate quadrature rule in order to maintain the accuracy of the method (which will be proved to be quadratic in the L^2 norm in Section 4.2).

Usually, the minimal information available about the surface is the position of the nodes. For this reason, instead of a more accurate Gauss quadrature rule [30], it is meaningful to define the second-order accurate quadrature rule [24] on the vertices of the curved triangle T_h^k of the triangulated surface $\mathcal{T}_h(\Gamma_k)$:

$$\int_{T_h^k} f \overset{\text{(Def. 2.6)}}{=} \int_{\phi_k^{-1}(T_h^k)} F(\boldsymbol{\xi}, t^k)\sqrt{\det G_k(\boldsymbol{\xi})}\, d\boldsymbol{\xi} \simeq \frac{1}{3}\sum_{q=1}^{3} F(\boldsymbol{\xi}_q, t^k)\sqrt{\det G_k(\boldsymbol{\xi}_q)} \tag{4.44}$$

Where $\phi_t : \Xi \to \Gamma_k$ is a proper parametrisation such that $T_h^k = \phi_k(\hat{T}_h^k)$ with $\hat{T}_h^k \subset \Xi$. Once the integral has been reduced to an integral in $\mathbb{R}^2$, it suffices to introduce the reference triangle $T_{\text{ref}} = \{(\eta_1, \eta_2) \in \mathbb{R}^2 : 0 \le \eta_1 \le 1, 0 \le \eta_2 \le 1, \eta_1 + \eta_2 \le 1\}$ and the affine tranformation Ψ which maps the reference triangle onto $\hat{T}_h \subset \mathbb{R}^2$, leading to:

$$\int_{T_h^k} f \simeq \frac{1}{6}\sum_{q=1}^{3} |\det d\Psi|(F \circ \Psi)(\boldsymbol{\eta}_q, t^k)\sqrt{\det(G_k \circ \Psi)(\boldsymbol{\eta}_q)} \tag{4.45}$$

where $d\Psi$ is the Jacobian matrix of Ψ and the quadrature points are the vertices of T_{ref}, namely $(0,0), (1,0), (0,1)$. It follows that the generic basis function defined on $\hat{T}_h$ can be straightforwardly written in reference coordinates just by setting:

$$\Phi_i \circ \Psi(\boldsymbol{\eta}_j) = \begin{cases} 1 & i = j \\ 0 & i \neq j \end{cases} \tag{4.46}$$

and for the gradients:

$$\nabla_{\boldsymbol{\xi}} \Phi_i = (d\Psi)^{-T} \nabla_{\boldsymbol{\eta}} \Phi_i \tag{4.47}$$

where $\nabla_{\boldsymbol{\xi}} \Phi_i$ is the gradient of Φ_i in local coordinates, $\nabla_{\boldsymbol{\eta}} \Phi_i$ is the gradient of $\Phi_i \circ \Psi$ in the coordinates of the reference triangle. The power of using the reference triangle relies on the fact that $\nabla_{\boldsymbol{\eta}} \Phi_i$ is equal to $[-1,-1]^T, [1,0]^T, [0,1]^T$, dependently on the considered vertex, making the implementation of the quadrature rule straightforward.

The following three sections provide the practical quadrature rule dependently on how much information about the surface is known.

Knowledge of the parametrisation

If the parametrisation is known, it is always possible define the triangulation $\mathcal{T}_h(\Xi)$ and map $\hat{T}_h \subset \mathbb{R}^2$ onto $T_h^k = \phi_k(\hat{T}_h)$ (namely the mesh is defined on Ξ, thanks to the knowledge of the nodes of Γ_k, pulled back to the chart). Therefore, there are all the ingredients to define $\Psi : T_{\text{ref}} \to \hat{T}_h$. Moreover knowing ϕ_k, also the metric G_k is known at the vertices. Hence, the local mass and stiffness matrices at time t^k can be computed straightforwardly. For simplicity the composition of the metric with Ψ has been left implicit.

$$\mathrm{M}_{ij}^k = \frac{1}{6} \sum_{q=1}^{3} |\det d\Psi| (\Phi_i \circ \Psi)(\Phi_j \circ \Psi)(\boldsymbol{\eta}_q) \sqrt{\det G_k(\boldsymbol{\eta}_q)} \tag{4.48}$$

$$\begin{aligned} \mathrm{A}_{ij}^k &= \frac{1}{3} \sum_{q=1}^{3} \left\langle \nabla_{G_k} \Phi_i, \nabla_{G_k} \Phi_j \right\rangle_{G_k} (\boldsymbol{\xi}_q) \sqrt{\det G_k(\boldsymbol{\xi}_q)} \\ &= \frac{1}{3} \sum_{q=1}^{3} \left(G_k^{-1} \nabla_{\boldsymbol{\xi}} \Phi_i \right)^T G_k G_k^{-1} \nabla_{\boldsymbol{\xi}} \Phi_j(\boldsymbol{\xi}_q) \sqrt{\det G_k(\boldsymbol{\xi}_q)} \\ &= \frac{1}{6} \sum_{q=1}^{3} |\det d\Psi| (\nabla_{\boldsymbol{\eta}} \Phi_i)^T (d\Psi)^{-1} G_k^{-1} (d\Psi)^{-T} \nabla_{\boldsymbol{\eta}} \Phi_j(\boldsymbol{\eta}_q) \sqrt{\det G_k(\boldsymbol{\eta}_q)} \end{aligned} \tag{4.49}$$

Knowledge of nodes and tangent vectors

In many practical applications, the parametrisation of the surface is not explicitly available, making the construction of $\mathcal{T}_h(\Xi)$ impractical. Typically, the surface is described only through the position of the nodes and the tangent vectors associated with each node. Likewise, each curved element T_h^k is known only through the coordinates of its vertices, so constructing an exact parametrisation of the element is, in general, impossible.

This section shows that all the quantities required by the method can nevertheless be computed by defining suitable parametrisations of curved elements in the local coordinates of the reference triangle, at the cost of introducing an approximation in the computation of the element area. Provided that the corresponding error exhibits the correct dependence on the mesh size, the overall order of accuracy of the numerical scheme is preserved.

These parametrisations are constructed so that the tangent planes induced by the parametrised surface coincide with those prescribed at the nodes, which are assumed to be known as input. The following discussion presents two explicit element-wise procedures for building such a parametrisation. The first one projects the curved element onto the coordinate planes, the second one onto the flat-triangular interpolant of the vertices.

For sufficiently fine meshes, each curved triangle $T_h^k \in \mathcal{T}_h(\Gamma_k)$ can always be seen as the graph of an height function defined on its projection to a coordinate plane:

$$\begin{aligned} &\tilde{\phi}_k : \tilde{T}_h^k \to T_h^k \\ &\tilde{\phi}_k\,(\alpha_1, \alpha_2) = \begin{cases} (\alpha_1, \alpha_2, H_k(\alpha_1, \alpha_2)) & \text{if } \tilde{T}_h^k \in \{\mathbf{x} \in \mathbb{R}^3 : x_3 = 0\} \\ (H_k(\alpha_1, \alpha_2), \alpha_1, \alpha_2) & \text{if } \tilde{T}_h^k \in \{\mathbf{x} \in \mathbb{R}^3 : x_1 = 0\} \\ (\alpha_1, H_k(\alpha_1, \alpha_2), \alpha_2) & \text{if } \tilde{T}_h^k \in \{\mathbf{x} \in \mathbb{R}^3 : x_2 = 0\} \end{cases} \end{aligned} \tag{4.50}$$

The knowledge of the tangent vectors $\mathbf{t}_1^k, \mathbf{t}_2^k$ gives the knowledge of the tangent plane and the outer unit normal to the surface:

$$\mathbf{n}^k = \frac{\mathbf{t}_1^k \times \mathbf{t}_2^k}{|\mathbf{t}_1^k \times \mathbf{t}_2^k|} \tag{4.51}$$

Unfortunately $\mathbf{t}_1^k, \mathbf{t}_2^k$ are induced by an unknown parametrisation, therefore it is not possible to recover $\hat{T}_h$ and there are not enough data to compute (4.48) and (4.49). In other words, it is not possible to map T_{ref} onto $\hat{T}_h$ because the latter is unknown.

The idea is to deduce the parametrisation $\tilde{\phi}_k$ by imposing its tangent vectors to belong to the tangent plane spanned by $\mathbf{t}_1^k, \mathbf{t}_2^k$. In this way $\tilde{T}_h^k$ plays the role of the element on the chart and it is just the projection of the curved triangle T_h^t onto the correspondent plane.

Assume T_h^k to be such that it could be parametrised by an height function with respect to the xy plane. Therefore:

$$\begin{aligned} \tilde{\mathbf{t}}_1^k &= \left(1, 0, \partial_{\alpha_1} H_k\right)^T \\ \tilde{\mathbf{t}}_2^k &= \left(0, 1, \partial_{\alpha_2} H_k\right)^T \end{aligned} \tag{4.52}$$

where the third component can be computed just by imposing orthogonality with $\mathbf{n}^k$:

$$\begin{cases} \tilde{\mathbf{t}}_1^k \perp \mathbf{n}^k \\ \tilde{\mathbf{t}}_2^k \perp \mathbf{n}^k \end{cases} \implies \begin{cases} \partial_{\alpha_1} H_k = -n_1^k / n_3^k \\ \partial_{\alpha_2} H_k = -n_2^k / n_3^k \end{cases} \tag{4.53}$$

At this point the metric is computed with Definition 2.5:

$$\tilde{G}^k = \begin{pmatrix} \langle \tilde{\mathbf{t}}_1^k, \tilde{\mathbf{t}}_1^k \rangle & \langle \tilde{\mathbf{t}}_1^k, \tilde{\mathbf{t}}_2^k \rangle \\ \langle \tilde{\mathbf{t}}_2^k, \tilde{\mathbf{t}}_1^k \rangle & \langle \tilde{\mathbf{t}}_2^k, \tilde{\mathbf{t}}_2^k \rangle \end{pmatrix} \tag{4.54}$$

Finally, in order to map the reference triangle to $\tilde{T}_h^k$ with an affine function, it suffices to approximate $\tilde{T}_h^k$ with the triangle obtained by linking the vertexes of $\tilde{T}_h^k$ with straight lines, which is called $\tilde{T}_h^{*k}$ (and it is the projection of the flat triangle embedded in $\mathbb{R}^3$ which interpolates linearly the vertices of the geodesic triangle). In this way the numerical error regards only the mismatch between the area of $\tilde{T}_h^k$ and its interpolant triangle, and this mismatch goes quadratically to zero with respect to the mesh size [18], preserving the order of accuracy of the method. The knowledge of $\tilde{T}_h^{*k}$ allows to define the affine map $\tilde{\Psi}_k$:

$$\tilde{\Psi}_k : T_{\text{ref}} \to \tilde{T}_h^{*k} \tag{4.55}$$

Therefore, local mass and stiffness matrices at time instant t^k can be computed as follows:

$$\begin{aligned} \mathrm{M}_{ij}^k &= \frac{1}{6}\sum_{q=1}^{3} |\det d\tilde{\Psi}_k| (\tilde{\Phi}_i \circ \tilde{\Psi}_k)(\tilde{\Phi}_j \circ \tilde{\Psi}_k)(\boldsymbol{\eta}_q)\sqrt{\det \tilde{G}_k(\boldsymbol{\eta}_q)} \\ \mathrm{A}_{ij}^k &= \frac{1}{6}\sum_{q=1}^{3} |\det d\tilde{\Psi}_k| (\nabla_{\boldsymbol{\eta}}\tilde{\Phi}_i)^T (d\tilde{\Psi}_k)^{-1}\tilde{G}_k^{-1}(d\tilde{\Psi}_k)^{-T}\nabla_{\boldsymbol{\eta}}\tilde{\Phi}_j(\boldsymbol{\eta}_q)\sqrt{\det \tilde{G}_k(\boldsymbol{\eta}_q)} \end{aligned} \tag{4.56}$$

where $\tilde{\Phi}$ denotes the linear Lagrangian basis function defined on $\tilde{T}_h^k$. The key observation is that the FEM space is not, in fact, $\mathcal{V}_h(\Xi)$, since the set Ξ is not explicitly known. Instead, the procedure implicitly constructs suitable local charts on which the basis functions are defined, exploiting the fact that surface integrals are invariant under reparametrisation.

As a consequence, the optimal convergence properties established in Section 4.2 remain valid also for a FEM implementation in which mass and stiffness matrices are computed in this manner. The strength of this approach lies in its applicability to a wide class of surfaces, provided that tangent vectors at the nodal points are available, without requiring the surface to admit a single global parametrisation. This observation justifies that assuming surfaces parametrised by a single mapping ϕ_t does not entail any loss of generality.

Projecting each triangle onto one of the other coordinate planes leads to analogous constructions:

$$\begin{cases} \tilde{\mathbf{t}}_1^k = \left(1, \partial_{\alpha_1} H_k, 0\right)^T \\ \tilde{\mathbf{t}}_2^k = \left(0, \partial_{\alpha_2} H_k, 1\right)^T \\ \partial_{\alpha_1} H_k = -n_1^k/n_2^k \\ \partial_{\alpha_2} H_k = -n_3^k/n_2^k \end{cases} \qquad \begin{cases} \tilde{\mathbf{t}}_1^k = \left(\partial_{\alpha_1} H_k, 1, 0\right)^T \\ \tilde{\mathbf{t}}_2^k = \left(\partial_{\alpha_2} H_k, 0, 1\right)^T \\ \partial_{\alpha_1} H_k = -n_2^k/n_1^k \\ \partial_{\alpha_2} H_k = -n_3^k/n_1^k \end{cases} \tag{4.57}$$

Another possible way to exploit the knowledge of the tangent vectors is the following. Given the set of nodes together with their connectivity, it is always possible to construct a triangulation on Γ_k whose edges are geodesic curves with respect to the underlying surface metric. In this setting, the curved triangle T_h^k can be interpreted as the graph of a height function defined over a corresponding planar triangle T_h^{*k}, obtained by projecting T_h^k onto the plane spanned by its three vertices.

This viewpoint allows one to decouple the geometric complexity of the surface from a flat reference configuration, since all computations can be performed on the planar triangle while the surface geometry is recovered through the height representation. In particular, the mapping structure becomes significantly simpler and more amenable to standard finite element constructions.

In this framework, the affine map Ψ^* is defined from the reference triangle T_{ref} to the flat triangle T_h^{*k} embedded in $\mathbb{R}^3$:

$$\begin{aligned} \Psi_k^* &: T_{\mathrm{ref}} \to T_h^{*k} \\ \Psi_k^*(\eta_1, \eta_2) &= \mathbf{x}_1 + (\mathbf{x}_2 - \mathbf{x}_1)\eta_1 + (\mathbf{x}_3 - \mathbf{x}_1)\eta_2 \end{aligned} \tag{4.58}$$

where $\mathbf{x}_1, \mathbf{x}_2, \mathbf{x}_3$ are the nodes of the element. The Jacobian of the affine transformation is given by:

$$d\Psi_k^* = \left[\hat{\mathbf{t}}_1^{*k} \;\; \hat{\mathbf{t}}_1^{*k}\right] = \left[\mathbf{x}_2 - \mathbf{x}_1 \;\; \mathbf{x}_3 - \mathbf{x}_1\right] \tag{4.59}$$

and the unit outer normal $\hat{\mathbf{n}}^k$ is computed accordingly. The parametrisation of the surface element with respect to T_h^{*k} has the form:

$$\begin{aligned} \phi_k^* &: T_h^{*k} \to T_h^k \\ \phi_k^*(\mathbf{y}) &= \mathbf{y} + \hat{H}_k(\mathbf{y})\hat{\mathbf{n}}^{*k}(\mathbf{y}) \\ \phi_k^* \circ \Psi_k^*(\boldsymbol{\eta}) &= \Psi_k^*(\boldsymbol{\eta}) + H_k^*(\boldsymbol{\eta})\mathbf{n}^{*k}(\boldsymbol{\eta}) \end{aligned} \tag{4.60}$$

with obvious definitions for the composition of functions with the affine map Ψ^*. This is admissible since, at the end of the construction, it will be clear that all quantities are expressed solely on the reference triangle. The tangent vectors $\mathbf{t}_1^{*k}, \mathbf{t}_2^{*k}$ associated with the height function representation take the form:

$$\begin{cases} \mathbf{t}_1^{*k} = \hat{\mathbf{t}}_1^{*k} + \left(\partial_{\eta_1} H_k^*\right) \hat{\mathbf{n}}^{*k}(\boldsymbol{\eta}) \\ \mathbf{t}_2^{*k} = \hat{\mathbf{t}}_2^{*k} + \left(\partial_{\eta_2} H_k^*\right) \hat{\mathbf{n}}^{*k}(\boldsymbol{\eta}) \end{cases} \tag{4.61}$$

where it has been used the fact that $\hat{\mathbf{n}}^{*k}$ in constant over the element. Once again the input tangent vectors give the unit normal of the surface at the nodes (4.51). Thus imposing orthogonality it is possible to compute the needed coefficients:

$$\begin{cases} \partial_{\eta_1} H_k^* = -\dfrac{\left\langle \hat{\mathbf{t}}_1^{*k}, \mathbf{n}^k \right\rangle}{\left\langle \hat{\mathbf{n}}^{*k}, \mathbf{n}^k \right\rangle} \\ \partial_{\eta_2} H_k^* = -\dfrac{\left\langle \hat{\mathbf{t}}_2^{*k}, \mathbf{n}^k \right\rangle}{\left\langle \hat{\mathbf{n}}^{*k}, \mathbf{n}^k \right\rangle} \end{cases} \tag{4.62}$$

Therefore the metric can be computed node by node consistently:

$$G_k^* = \begin{pmatrix} \left\langle \mathbf{t}_1^{*k}, \mathbf{t}_1^{*k} \right\rangle & \left\langle \mathbf{t}_1^{*k}, \mathbf{t}_2^{*k} \right\rangle \\ \left\langle \mathbf{t}_2^{*k}, \mathbf{t}_1^{*k} \right\rangle & \left\langle \mathbf{t}_2^{*k}, \mathbf{t}_2^{*k} \right\rangle \end{pmatrix} \tag{4.63}$$

and finally the local mass and stiffness matrices can be computed as follows:

$$\begin{aligned} \mathrm{M}_{ij}^k &= \frac{1}{6} \sum_{q=1}^{3} \Phi_i^* \Phi_j^*(\boldsymbol{\eta}_q) \sqrt{\det G_k^*(\boldsymbol{\eta}_q)} \\ \mathrm{A}_{ij}^k &= \frac{1}{6} \sum_{q=1}^{3} (\nabla_{\boldsymbol{\eta}} \Phi_i^*)^T G_k^{*-1} \nabla_{\boldsymbol{\eta}} \Phi_j^*(\boldsymbol{\eta}_q) \sqrt{\det G_k^*(\boldsymbol{\eta}_q)} \end{aligned} \tag{4.64}$$

where Φ^* is the Lagrangian basis function defined on the reference triangle. This formulation is satisfactory since it guarantees that all integrals can be computed using only intrinsic quantities and independently of the chosen parametrisation. Compared with the previous approach, which relies on projections onto the coordinate planes, this strategy avoids the problem to choose to which plane project the triangle. In case of bad shaped elements, this feature makes the method more robust and stable.

The geometric approximations employed in the last two methods rely on the discrepancy between the flat triangle and the pre-image of the height function parametrisation. In the first case, this discrepancy arises between the projection of the flat interpolant triangle onto the reference plane and the projection of the curved triangle onto the same plane. In the second case, it arises between the flat interpolant triangle and the projection of the curved triangle onto the plane spanned by its three vertices.

In [18], it is shown that the area of the flat interpolant triangle converges to the area of the curved element with second-order accuracy. Therefore, the assumption that the proposed approximations are second-order accurate is reasonable. This assumption is further supported by the experimental results presented in Chapter 5. A rigorous proof, however, is beyond the scope of this thesis and is left for future work.

Knowledge of the nodes

The most general and, in a sense, least favorable situation arises when the surface is known only through the coordinates of its nodes. When tangent vectors are not available, it becomes necessary

to perform some approximation of the geometry of the surface itself, and the easiest option is to consider the piecewise linear interpolation based on flat triangles connecting the given nodes. In this setting, the geometric approximation enters the model at an earlier stage, since the surface is replaced by a discrete counterpart. On the other hand, this choice leads to a metric that is constant on each element, which in turn makes the quadrature rule exact for linear basis functions. The use of this strategy in approximating the geometric information makes the E-ISFEM approach coincide with ESFEM.

Let $\Gamma_{h,k}$ denote the interpolated surface and let $\mathcal{T}_h(\Gamma_{h,k})$ be the associated triangulation consisting of flat triangles. Let $\hat{T}_h^k \in \mathcal{T}_h(\Gamma_{h,k})$ be a generic element with nodes $\mathbf{x}_1, \mathbf{x}_2, \mathbf{x}_3$. In this geometric approximation setting, the parametrisation can be identified with an affine map $\hat{\Psi}_k$. As a consequence, there is no longer any need to introduce an explicit parametrisation (which is why this is referred to as an embedded approach), and the reference triangle T_{ref} can be mapped directly onto $\hat{T}_h^k$ via the affine mapping $\hat{\Psi}_k$:

$$\begin{aligned} \hat{\Psi}_k &: T_{\text{ref}} \to \hat{T}_h^k \\ \hat{\Psi}_k(\eta_1, \eta_2) &= \mathbf{x}_1 + (\mathbf{x}_2 - \mathbf{x}_1)\eta_1 + (\mathbf{x}_3 - \mathbf{x}_1)\eta_2 \end{aligned} \tag{4.65}$$

Therefore, the local mass and stiffness matrices can be computed exactly. Since each element is flat, the metric tensor is constant on $\hat{T}_h^k$, which implies that the standard three-point quadrature rule based on the vertices yields the exact value of the corresponding integrals.

The linear basis function $\hat{\varphi}$ is of Lagrangian type on $\hat{T}_h^k$ and can therefore be straightforwardly transported to the reference triangle through the affine mapping $\hat{\Psi}_k$.

$$\begin{aligned} \mathrm{M}_{ij}^k &= \frac{1}{6} \sum_{q=1}^{3} |\det d\hat{\Psi}_k| (\hat{\varphi}_i \circ \hat{\Psi}_k)(\hat{\varphi}_j \circ \hat{\Psi}_k) \\ \mathrm{A}_{ij}^k &= \frac{1}{6} \sum_{q=1}^{3} |\det d\hat{\Psi}_k| \nabla_{\boldsymbol{\eta}}^k \hat{\varphi}_i^T G_k^{-1} \nabla_{\boldsymbol{\eta}}^k \hat{\varphi}_j(\boldsymbol{\eta}_q) \end{aligned} \tag{4.66}$$

where $\nabla_{\boldsymbol{\eta}}^k \hat{\varphi} = \nabla_{\boldsymbol{\eta}}(\hat{\varphi} \circ \hat{\Psi}_k)$.

In other words, this method discretises the surface in such a way that the parametrisation of each $\hat{T}_h^k$ is explicitly known. This parametrisation acts from the reference triangle to $\hat{T}_h^k$, thereby providing a consistent set of local coordinates, which in this setting coincide with those of the reference element, on which the quadrature rule can be directly applied.

A final remark concerns the fact that the flat area associated with each element converges quadratically to the corresponding curved surface area with respect to the mesh size [18]. This property is essential in order to guarantee the preservation of optimal convergence rates of the numerical method.

4.2 Convergence Analysis

The Finite Element Method in the classical Euclidean setting is expected to converge with quadratic order in the L^2 norm and linear order in the H^1 norm when piecewise linear basis functions are employed [28]. The Surface Finite Element Method has been shown to achieve the same optimal convergence rates [18], and analogous results hold for the Evolving Surface Finite Element Method as well [15, 16, 17, 20].

In this section, and following in particular the analytical strategies developed in [16] and [17], will be established that the Intrinsic Evolving Surface Finite Element Method also attains these optimal convergence rates.

4.2.1 Convergence in space

Consider the semi-discrete finite element formulation of Problem 4.1. It is often useful to get rid of the notation that involves integrals. Hence, as commonly done in Finite Element theory, it is possible to introduce the following bilinear forms which allow to make the equations more readable.

$$\begin{aligned} m_t(u,v) &:= \int_{\Gamma_t} uv \\ a_t(u,v) &:= \int_{\Gamma_t} \left\langle \nabla_{G_t} u, \nabla_{G_t} v \right\rangle_{G_t} \end{aligned} \tag{4.67}$$

Lemma 4.7. *Let $a_t : H_0^1(\Gamma_t) \times H_0^1(\Gamma_t) \to \mathbb{R}$ be the bilinear form defined in(4.67). Then $a_t(\cdot,\cdot)$ is coercive, namely there exists $\beta_t \in \mathbb{R}$ such that:*

$$\beta_t \|u\|^2_{H^1(\Gamma_t)} \leq a_t(u,u) \quad \forall u \in H_0^1(\Gamma_t) \tag{4.68}$$

Proof. Let $u \in H^1(\Gamma_t)$.

$$\|u\|^2_{H^1(\Gamma_t)} = \|u\|^2_{L^2(\Gamma_t)} + \left\|\nabla_{G_t} u\right\|^2_{L^2(\Gamma_t)} \overset{(2.11)}{\leq} \left(1 + C^2_{\Gamma_t}\right) \left\|\nabla_{G_t} u\right\|^2_{L^2(\Gamma_t)} = \left(1 + C^2_{\Gamma_t}\right) a_t(u,u) \tag{4.69}$$

□

The following definition is crucial for the proof of convergence of the numerical scheme. From this perspective, the Ritz projection provides the appropriate representative (with respect to the present analysis) of a generic function $u \in H^1(\Gamma_t)$ within the discrete space $\mathcal{V}_h(\Gamma_t)$ [17].

Definition 4.8. For a given $f \in H^1(\Gamma_t)$ such that $\int_{\Gamma_t} f = 0$, there exists a unique Ritz projection $\mathcal{R}_h f \in \mathcal{V}_h(\Gamma_t)$ such that:

$$a_t(\mathcal{R}_h f, \varphi_h) = a_t(f, \varphi_h) \quad \forall \varphi_h \in \mathcal{V}_h(\Gamma_t)$$

and $\int_{\Gamma_t} \mathcal{R}_h f = 0$.

From now the function space will be denoted with their original names $H^1(\Gamma_t)$ and $L^2(\Gamma_t)$, instead of $\mathcal{V}_t$ and $\mathcal{H}_t$.

The following lemmas give the flavour of how the Ritz projection is the basis for proving optimal convergence of the FEM scheme.

Lemma 4.9. *Let $f \in H^2(\Gamma_t)$, and let $\mathcal{R}_h$ be the Ritz projector of Definition 4.8. Then the following interpolation bounds hold:*

$$\|f - \mathcal{R}_h f\|_{L^2(\Gamma_t)} \leq k_{1,t} h^2 \|f\|_{H^2(\Gamma_t)} \tag{4.70}$$

$$\|f - \mathcal{R}_h f\|_{H^1(\Gamma_t)} \leq k_{2,t} h \|f\|_{H^2(\Gamma_t)} \tag{4.71}$$

Lemma 4.10. *Let $f \in H^2(\Gamma_t)$ and $\dot{f} \in H^2(\Gamma_t)$ for all $t \in [0,T]$. The time derivative of the Ritz projection satisfies the bound:*

$$\|\dot{f} - \dot{\mathcal{R}_h f}\|_{L^2(\Gamma_t)} + h \|\nabla_{G_t} \left(\dot{f} - \dot{\mathcal{R}_h f}\right)\|_{L^2(\Gamma_t)} \leq k_{3,t} h^2 \left(\|f\|_{H^2(\Gamma_t)} + \|\dot{f}\|_{H^2(\Gamma_t)}\right) \tag{4.72}$$

It is now possible to state and prove the theorem concerning the convergence rate of the semi-discrete formulation (Problem 4.1). In [17], an analogous result is established for the ESFEM formulation. As already discussed, the ESFEM approach relies on an initial interpolation of the surface, which implies that the error analysis must compare the exact solution, defined on the true surface, with the numerical solution, defined on the interpolated geometry. This naturally leads to the additional difficulty of estimating the errors arising from the lifting of functions between the exact and discrete surfaces.

In contrast, the intrinsic formulation preserves the exact geometry of the evolving surface throughout the discretisation process, thereby avoiding the need to introduce lifting operators and eliminating the associated geometric approximation errors. This significantly simplifies the analytical framework, since no additional estimates related to the approximation of geometric quantities are required.

Theorem 4.11. *Let u be the weak solution of (3.26) and let u_h the semi-discrete solution of Problem 4.1 such that:*

$$\|\mathcal{R}_h u(\cdot,0) - u_h(\cdot,0)\|_{H^1(\Gamma_0)} \leq h^2 \tag{4.73}$$

Assume also $\lambda \in L^\infty(0,T;L^\infty(\Gamma_t))$. Then there exists $k_4, k_5 \in \mathbb{R}$ depending on u, T, G, λ such that the following error estimates hold:

$$\sup_{t\in(0,T)} \|u - u_h\|_{L^2(\Gamma_t)} \leq k_4 h^2 \tag{4.74}$$

$$\sup_{t\in(0,T)} \|u - u_h\|_{H^1(\Gamma_t)} \leq k_5 h + \hat{k}_5 h^2 \tag{4.75}$$

Proof. Since u solves the weak formulation, it solves also the semi-discrete weak formulation:

$$m_t(\dot{u}, \varphi_h) + a_t(u, \varphi_h) + m_t(\lambda u, \varphi_h) = (f, \varphi_h)_{H^{-1}\times H^1} \quad \forall \varphi_h \in \mathcal{V}_h(\Gamma_t), \forall t \in (0,T) \tag{4.76}$$

Therefore subtracting (4.6) to (4.76), the error equation reads:

$$m_t(\dot{u} - \dot{u}_h, \varphi_h) + a_t(u - u_h, \varphi_h) + m_t(\lambda u - \lambda u_h, \varphi_h) = 0 \quad \forall \varphi_h \in \mathcal{V}_h(\Gamma_t), \forall t \in (0,T) \tag{4.77}$$

The idea is to exploit the favourable properties of the Ritz projection (Definition 4.8) together with the interpolation estimates (4.70) and (4.71). In order to proceed in this direction, it is convenient to explicitly introduce the Ritz projection into the analysis:

$$u - u_h = \underbrace{u - \mathcal{R}_h u}_{:=\eta} + \underbrace{\mathcal{R}_h u - u_h}_{:=\zeta} \tag{4.78}$$

Note that Definition 4.8 specifies that the Ritz projection acts on $H^1(\Gamma_t)$, so (4.78) should be understood, with a slight abuse of notation, in this sense. However, since $\mathcal{R}_h f$ is well defined for every $f \in H^1(\Gamma_t)$ and for all $t \in (0,T)$, it is sufficient to interpret (4.78) as being applied to $u(\cdot,t) \in H^1(\Gamma_t)$. This abuse of notation will be maintained in the following pages for the sake of clarity and compactness of notation. Under this convention, equation (4.77) becomes:

$$m_t(\dot{\zeta}, \varphi_h) + a_t(\zeta, \varphi_h) + m_t(\lambda\zeta, \varphi_h) = -m_t(\dot{\eta}, \varphi_h) - m_t(\lambda\eta, \varphi_h) \quad \forall \varphi_h \in \mathcal{V}_h(\Gamma_t), \forall t \in (0,T) \tag{4.79}$$

where it has been used the nice property of Ritz projection:

$$a_t(\eta, \varphi_h) = a_t(u - \mathcal{R}_h u, \varphi_h) = 0 \quad \forall \varphi_h \in \mathcal{V}_h(\Gamma_t), \forall t \in (0,T)$$

Now it suffices to choose $\varphi_h = \zeta(\cdot, t)$ to get the approximation error equation:

$$m_t(\dot{\zeta}, \zeta) + a_t(\zeta, \zeta) + m_t(\lambda\zeta, \zeta) = -m_t(\dot{\eta}, \zeta) - m_t(\lambda\eta, \zeta) \quad \forall t \in (0, T) \tag{4.80}$$

Now note that:

$$m_t(\dot{\zeta}, \zeta) = \frac{1}{2}\frac{d}{dt}m_t(\zeta, \zeta) - \frac{1}{2}m_t(\lambda\zeta, \zeta) \tag{4.81}$$

and substituting (4.81) into (4.80):

$$\frac{1}{2}\frac{d}{dt}m_t(\zeta, \zeta) + a_t(\zeta, \zeta) = -m_t(\dot{\eta}, \zeta) - m_t(\lambda\eta, \zeta) - \frac{1}{2}m_t(\lambda\zeta, \zeta) \tag{4.82}$$

Setting $c := \sup_{t\in(0,T)} \|\lambda\|_{L^\infty(\Gamma_t)}$. By coercitivity of $a(\cdot, \cdot)$ (Lemma 4.7) it is possible to write:

$$\begin{aligned}
\frac{1}{2}\frac{d}{dt}\|\zeta\|^2_{L^2(\Gamma_t)} &\le \frac{1}{2}\frac{d}{dt}\|\zeta\|^2_{L^2(\Gamma_t)} + \beta_t \|\zeta\|^2_{H^1(\Gamma_t)} \le \frac{1}{2}\frac{d}{dt}\|\zeta\|^2_{L^2(\Gamma_t)} + a_t(\zeta, \zeta) \\
&= -m_t(\dot{\eta}, \zeta) - m_t(\lambda\eta, \zeta) - \frac{1}{2}m_t(\lambda\zeta, \zeta) \\
&\le \|\dot{\eta}\|_{L^2(\Gamma_t)}\|\zeta\|_{L^2(\Gamma_t)} + c\|\eta\|_{L^2(\Gamma_t)}\|\zeta\|_{L^2(\Gamma_t)} + \frac{c}{2}\|\zeta\|^2_{L^2(\Gamma_t)} \\
&\le \frac{1}{2}\|\dot{\eta}\|^2_{L^2(\Gamma_t)} + \frac{1}{2}\|\zeta\|^2_{L^2(\Gamma_t)} + \frac{c}{2}\|\eta\|^2_{L^2(\Gamma_t)} + \frac{c}{2}\|\zeta\|^2_{L^2(\Gamma_t)} + \frac{c}{2}\|\zeta\|^2_{L^2(\Gamma_t)} \\
&\le \underbrace{\frac{k_{3,t}^2}{2}h^4\left(\|u\|_{H^2(\Gamma_t)} + \|\dot{u}\|_{H^2(\Gamma_t)}\right)^2 + \frac{c}{2}k_{1,t}^2h^4\|u\|^2_{H^2(\Gamma_t)}}_{:=\tilde{k}_{1,t}h^4} + \underbrace{\left(\frac{1}{2} + c\right)}_{:=\tilde{k}_{2,t}}\|\zeta\|^2_{L^2(\Gamma_t)}
\end{aligned} \tag{4.83}$$

where (4.70),(4.71) and (4.72) have been used. Now it suffices to take $\tilde{k}_1 := \sup_t \tilde{k}_{1,t}$ and $\tilde{k}_2 := \sup_t \tilde{k}_{2,t}$, obtaining:

$$\frac{1}{2}\frac{d}{dt}\|\zeta\|^2_{L^2(\Gamma_t)} \le \tilde{k}_1h^4 + \tilde{k}_2\|\zeta\|^2_{L^2(\Gamma_t)} \tag{4.84}$$

The hypothesis of Lemma 4.4 are satisfied, therefore:

$$\|\zeta\|^2_{L^2(\Gamma_t)} \le \|\zeta(0)\|^2_{L^2(\Gamma_0)}e^{2\tilde{k}_2t} + \frac{\tilde{k}_1}{\tilde{k}_2}\left(e^{2\tilde{k}_2t} - 1\right)h^4 \tag{4.85}$$

Making use of hypothesis (4.73) and taking the supremum over $t \in (0, T)$ both sides:

$$\sup_{t\in(0,T)} \|\zeta\|^2_{L^2(\Gamma_t)} \le \underbrace{\left(e^{2\tilde{k}_2T} + \frac{\tilde{k}_1}{\tilde{k}_2}\left(e^{2\tilde{k}_2T} - 1\right)\right)}_{:=\tilde{k}_3}h^4 \tag{4.86}$$

Finally taking advantage of (4.70):

$$\begin{aligned}
\sup_{t\in(0,T)} \|u - u_h\|_{L^2(\Gamma_t)} &= \sup_{t\in(0,T)} \|\eta + \zeta\|_{L^2(\Gamma_t)} \le \sup_{t\in(0,T)} \|\eta\|_{L^2(\Gamma_t)} + \sup_{t\in(0,T)} \|\zeta\|_{L^2(\Gamma_t)} \\
&\le h^2 \sup_{t\in(0,T)} k_{1,t}\|u\|_{H^2(\Gamma_t)} + \sqrt{\tilde{k}_3}h^2 \\
&= \underbrace{\left(\sup_{t\in(0,T)} k_{1,t}\|u\|_{H^2(\Gamma_t)} + \sqrt{\tilde{k}_3}\right)}_{:=k_4}h^2 = k_4h^2
\end{aligned} \tag{4.87}$$

Hence L^2 optimal convergence is proved. To prove (4.75), it suffices to plug $\varphi_h = \dot{\zeta}(\cdot, t)$ in the approximation error equation (4.80) and apply Lemma 4.3:

$$\begin{aligned}
\|\dot{\zeta}\|^2_{L^2(\Gamma_t)} + \frac{1}{2}\frac{d}{dt}\left\|\nabla_{G_t}\zeta\right\|^2_{L^2(\Gamma_t)} &= -m_t(\lambda\zeta,\dot{\zeta}) + \frac{1}{2}\int_{\Gamma_t}\lambda\left|\nabla_{G_t}\zeta\right|^2_{G_t} - \frac{1}{2}\int_{\Gamma_t}\left\langle \dot{G}\nabla_{G_t}\zeta, \nabla_{G_t}\zeta\right\rangle \\
&\quad - m_t(\dot{\eta},\dot{\zeta}) - m_t(\lambda\eta,\dot{\zeta}) \\
&\leq c\|\zeta\|_{L^2(\Gamma_t)}\|\dot{\zeta}\|_{L^2(\Gamma_t)} + \frac{c}{2}\|\nabla_{G_t}\zeta\|^2_{L^2(\Gamma_t)} + \frac{\dot{g}^*_t}{2g_{*,t}}\|\nabla_{G_t}\zeta\|^2_{L^2(\Gamma_t)} \\
&\quad + \|\dot{\eta}\|_{L^2(\Gamma_t)}\|\dot{\zeta}\|_{L^2(\Gamma_t)} + c\|\eta\|_{L^2(\Gamma_t)}\|\dot{\zeta}\|_{L^2(\Gamma_t)} \\
&\leq \frac{c}{4\varepsilon}\|\zeta\|^2_{L^2(\Gamma_t)} + \varepsilon\|\dot{\zeta}\|^2_{L^2(\Gamma_t)} + \left(\frac{c}{2} + \frac{\dot{g}^*_t}{2g_{*,t}}\right)\|\nabla_{G_t}\zeta\|^2_{L^2(\Gamma_t)} \\
&\quad + \frac{1}{4\varepsilon}\|\dot{\eta}\|^2_{L^2(\Gamma_t)} + \varepsilon\|\dot{\zeta}\|^2_{L^2(\Gamma_t)} + \frac{c}{4\varepsilon}\|\eta\|^2_{L^2(\Gamma_t)} + \varepsilon\|\dot{\zeta}\|^2_{L^2(\Gamma_t)} \\
&\overset{(4.70,4.71)}{\leq} \frac{c}{4\varepsilon}\sup_{t\in(0,T)}\|\zeta\|^2_{L^2(\Gamma_t)} + \underbrace{\left(\frac{c}{2} + \frac{\dot{g}^*_t}{2g_{*,t}}\right)}_{:=\tilde{k}_{4,t}}\|\nabla_{G_t}\zeta\|^2_{L^2(\Gamma_t)} \\
&\quad + \frac{k^2_{3,t}}{4\varepsilon}h^4\left(\|u\|_{H^2(\Gamma_t)} + \|\dot{u}\|_{H^2(\Gamma_t)}\right)^2 + 3\varepsilon\|\dot{\zeta}\|^2_{L^2(\Gamma_t)} + \frac{ck_{1,t}}{4\varepsilon}h^4\|u\|^2_{H^2(\Gamma_t)}
\end{aligned} \tag{4.88}$$

Again it is possible to rewrite the inequality by replacing $\tilde{k}_{4,t}, k_{3,t}, k_{1,t}$ with their supremum over $t \in (0,T)$, namely $\tilde{k}_4, k_3, k_1$, and making use of the definition of $\tilde{k}_3$ made in (4.86).

$$\begin{aligned}
(1-3\varepsilon)\|\dot{\zeta}\|^2_{L^2(\Gamma_t)} &+ \frac{1}{2}\frac{d}{dt}\left\|\nabla_{G_t}\zeta\right\|^2_{L^2(\Gamma_t)} \\
&\leq \underbrace{\frac{1}{4\varepsilon}\left(c\tilde{k}_3 + k_3^2\left(\|u\|_{H^2(\Gamma_t)} + \|\dot{u}\|_{H^2(\Gamma_t)}\right)^2 + ck_1\|u\|^2_{H^2(\Gamma_t)}\right)}_{:=\tilde{k}_5}h^4 \\
&\quad + \tilde{k}_4\|\nabla_{G_t}\zeta\|^2_{L^2(\Gamma_t)}
\end{aligned} \tag{4.89}$$

By choosing ε sufficiently small in order to make $1 - 3\varepsilon > 0$, from (4.89) directly follows the bound:

$$\frac{d}{dt}\|\nabla_{G_t}\zeta\|^2_{L^2(\Gamma_t)} \leq 2\tilde{k}_4\|\nabla_{G_t}\zeta\|^2_{L^2(\Gamma_t)} + 2\tilde{k}_5h^4 \tag{4.90}$$

Again, by Lemma 4.4 and by hypothesis (4.73):

$$\begin{aligned}
\|\nabla_{G_t}\zeta\|^2_{L^2(\Gamma_t)} &\leq \|\nabla_{G_0}\zeta(0)\|^2_{L^2(\Gamma_0)}e^{2\tilde{k}_4t} + \frac{\tilde{k}_5}{\tilde{k}_4}\left(e^{2\tilde{k}_4t} - 1\right)h^4 \\
\sup_{t\in(0,T)}\|\nabla_{G_t}\zeta\|^2_{L^2(\Gamma_t)} &\leq \underbrace{\left(e^{2\tilde{k}_4T} + \frac{\tilde{k}_5}{\tilde{k}_4}\left(e^{2\tilde{k}_4T} - 1\right)\right)}_{:=\tilde{k}_6}h^4
\end{aligned} \tag{4.91}$$

Unfortunately, for the H^1 norm, the interpolation estimate is just linearly dependent on h:

$$\begin{aligned}\sup_{t\in(0,T)} \|u-u_h\|_{H^1(\Gamma_t)} &= \sup_{t\in(0,T)} \|\eta+\zeta\|_{H^1(\Gamma_t)} \leq \sup_{t\in(0,T)} \|\eta\|_{H^1(\Gamma_t)} + \sup_{t\in(0,T)} \|\zeta\|_{H^1(\Gamma_t)} \\ &\leq \sup_{t\in(0,T)} \|\eta\|_{H^1(\Gamma_t)} + \sup_{t\in(0,T)} \|\zeta\|_{L^2(\Gamma_t)} + \sup_{t\in(0,T)} \|\nabla_{G_t}\zeta\|_{L^2(\Gamma_t)} \\ &\leq \underbrace{h \sup_{t\in(0,T)} k_{2,t}\|u\|_{H^2(\Gamma_t)}}_{:=k_5} + \underbrace{\left(\sqrt{\tilde{k}_6}+\sqrt{\tilde{k}_3}\right)}_{:=\hat{k}_5} h^2 = k_5 h + \hat{k}_5 h^2\end{aligned} \tag{4.92}$$

which proves (4.75). □

Note that hypothesis (4.73) is without loss of generality. Indeed, the initial datum is assumed to be known, so it is always possible to enforce that the semi-discrete solution achieves the correct initial value, possibly up to a tolerance of order h^2. In other words, this is equivalent to assuming that the initial condition is available as a given datum and that one can construct a sufficiently accurate approximation of it up to machine precision, which is standard in practical computations.

4.2.2 Convergence in time

The convergence properties established in Section 4.2.1 hold for the semi-discrete formulation (4.6), i.e. under the assumption that the problem is solved exactly in time. As already discussed, the semi-discrete weak formulation is equivalent to a system of first-order ordinary differential equations, which in practice must be solved numerically, for instance by means of the backward Euler scheme (4.43). This additional numerical procedure introduces further errors due to time discretisation. In this section, we investigate the dependence of the L^2 and H^1 errors on the time step τ, which is assumed to be constant throughout the entire time interval.

In analogy with Section 4.2.1, the main analytical tool for deriving the corresponding error bounds is the Grönwall Lemma. The following result is a discrete version of Lemma 4.4, which is precisely the form required in the present analysis [22].

Lemma 4.12. *Let $(u_n)_{n\in\mathbb{N}}$, $(a_n)_{n\in\mathbb{N}}$ and $(b_n)_{n\in\mathbb{N}}$ be non negative sequences such that:*

$$u_{n+1} \leq a_{n+1}u_n + b_{n+1} \qquad \forall n \in \mathbb{N} \tag{4.93}$$

Then, $\forall n \in \mathbb{N}$:

$$u_n \leq u_0 \prod_{k=1}^{n} a_k + \sum_{k=1}^{n} b_k \prod_{i=k+1}^{n} a_i \tag{4.94}$$

Proof. The proof is simply by recursive argument:

$$\begin{aligned} u_{n+1} &\leq a_{n+1}u_n + b_{n+1} \\ &\leq a_{n+1}\left(a_n u_{n-1} + b_n\right) + b_{n+1} \\ &\leq a_{n+1}\left(a_n\left(a_{n-1}u_{n-2} + b_{n-1}\right) + b_n\right) + b_{n+1} \\ &\leq \dots \\ &\leq u_0 \prod_{k=1}^{n+1} a_k + b_{n+1} + b_n a_{n+1} + b_{n-1}a_n a_{n+1} + \dots \\ &\leq u_0 \prod_{k=1}^{n+1} a_k + \sum_{k=1}^{n+1} b_k \prod_{i=k+1}^{n+1} a_i \end{aligned} \tag{4.95}$$

□

The scheme introduced in Problem 4.6 is obtained by defining the discrete time derivative of a function f, as in (4.96). The pointwise error between the exact time derivative and its discrete counterpart is of order $O(\tau)$ in the absolute norm [12], a property that will play a crucial role in the derivation of the accuracy of the method.

$$\partial_\tau f^k = \frac{f\left(t^{k+1}\right) - f\left(t^k\right)}{\tau} \tag{4.96}$$

$$\left.\frac{df}{dt}\right|_{t^k} = \partial_\tau f^k + C_f^k \tau \tag{4.97}$$

From now on, the dependence of functions on t^k will be indicated by a superscript k, whereas the dependence of other quantities on t^k will be denoted by a subscript k, in order to distinguish clearly between the two notational conventions.

The numerical solution of the fully discrete formulation is represented through the coefficients of its expansion in terms of the finite element basis functions at each time step. In this context, however, the notion of a discrete time derivative is not immediately evident, since the solution is given in terms of nodal coefficients rather than an explicit time-dependent function. To overcome this difficulty, one introduces the following definition:

$$\partial_\tau^k u_h^k = \sum_{i=1}^{n} \frac{u_i^{k+1} - u_i^k}{\tau} \varphi_i^k \tag{4.98}$$

When working with discrete time derivatives, it may occur that a linear combination involves quantities evaluated at time level $k+1$ but expanded in a basis associated with time level k, as in (4.98). The following lemma provides an additional tool to handle such situations in a consistent manner.

Lemma 4.13. *Let Γ_k be a regular surface for all $k = 1, ..., m$, and let $f_h^k \in \mathcal{V}_h(\Gamma_k)$, with basis functions $\{\varphi_i^k\}_i$. Assume $\lambda \in L^\infty(0,T; L^\infty(\Gamma_t))$. Then there exist two constants C_G^k, D_G^k such that:*

$$\left| \int_{\Gamma_{k+1}} \sum_{i=1}^{n} f_i^k \varphi_i^{k+1} - \int_{\Gamma_k} f_h^k \right| \leq \tau C_G^k \left| \int_{\Gamma_k} f_h^k \right| \tag{4.99}$$

$$\left| \int_{\Gamma_{k+1}} \sum_{i=1}^{n} f_i^k \varphi_i^{k+1} \right| \leq D_G^k \left| \int_{\Gamma_k} f_h^k \right| \tag{4.100}$$

Proof. Once again, the idea is to take advantage of the time independence of basis functions when composed with the parametrisation $\phi : \Xi \times [0,T] \to \mathcal{G}_T$.

$$\begin{aligned}
\left| \int_{\Gamma_{k+1}} \sum_{i=1}^{n} f_i^k \varphi_i^{k+1} - \int_{\Gamma_k} \sum_{i=1}^{n} f_i^k \varphi_i^k \right| &= \left| \int_\Xi \sum_{i=1}^{n} F_i^k \Phi_i \sqrt{\det G_{k+1}} - \int_\Xi \sum_{i=1}^{n} F_i^k \Phi_i \sqrt{\det G_k} \right| \\
&= \left| \int_\Xi \sum_{i=1}^{n} F_i^k \Phi_i \left(\sqrt{\det G_{k+1}} - \sqrt{\det G_k} \right) \right| \\
&= \left| \tau \int_\Xi \sum_{i=1}^{n} F_i^k \Phi_i \left(\partial_\tau \sqrt{\det G_k} \right) \right| \\
&\leq \tau \left\| \partial_\tau \sqrt{\det G_k} \right\|_{L^\infty(\Xi)} \left| \int_\Xi \sum_{i=1}^{n} F_i^k \Phi_i \right|
\end{aligned} \tag{4.101}$$

$$
\begin{aligned}
&\leq \tau \underbrace{\left\|\sqrt{\det G_k}\right\|_{L^\infty(\Xi)} \|\Lambda\|_{L^\infty(\Xi\times[t^k,t^{k+1}])} \frac{1}{\inf_{\xi\in\Xi}\sqrt{\det G_k}}}_{:=C_G} \left|\int_\Xi \sum_{i=1}^n F_i^k \Phi_i \sqrt{\det G_k}\right| \\
&= \tau C_G^k \left|\int_{\Gamma_k} f_h^k\right|
\end{aligned}
\tag{4.102}
$$

which is (4.99). For (4.100) the procedure is the same:

$$
\begin{aligned}
\left|\int_{\Gamma_{k+1}} \sum_{i=1}^n f_i^k \varphi_i^{k+1}\right| &= \left|\int_\Xi \sum_{i=1}^n F_i^k \Phi_i \sqrt{\det G_{k+1}}\right| \\
&= \left|\int_\Xi \sum_{i=1}^n F_i^k \Phi_i \frac{\sqrt{\det G_{k+1}}}{\sqrt{\det G_k}} \sqrt{\det G_k}\right| \\
&\leq \underbrace{\left\|\frac{\sqrt{\det G_{k+1}}}{\sqrt{\det G_k}}\right\|_{L^\infty(\Xi)}}_{:=D_G^k} \left|\int_\Xi \sum_{i=1}^n F_i^k \Phi_i \sqrt{\det G_k}\right| \\
&= D_G^k \left|\int_{\Gamma_k} f_h^k\right|
\end{aligned}
\tag{4.103}
$$

and the proof is complete. □

Classical ESFEM results on stability and convergence require a careful discussion of the distinction between the velocity of the interpolated surface and that of the lifted surface. This discrepancy affects both the definition of time derivatives and the evaluation of the bilinear forms appearing in the weak formulation. In [16], several technical lemmas are introduced to handle these issues and to establish stability and convergence results for the embedded formulation.

In the present E-ISFEM framework, the geometric structure of the surface is preserved, and hence Lemma (4.13) can be used to bypass the technical complications that arise in the classical ESFEM theory. As a consequence, the stability and convergence analysis developed in the following sections follows the main ideas of [16], but is carried out entirely within the intrinsic setting.

The following stability result for the fully discrete scheme is the natural counterpart of the semi-discrete result stated in Theorem 4.5.

Proposition 4.14. *Let $u_h^k \in \mathcal{V}_h(\Gamma_k)$ be the fully discrete solution of Problem 4.6 for $k = 1, ..., m$, and $f \in L^2(0, T, L^2(\Gamma_t))$. Then the following a priori bounds hold for $\tau \leq \tau_0$, $\forall k = 1, ..., m$ and with constants independent of τ:*

$$
\left\|u_h^k\right\|^2_{L^2(\Gamma_k)} + \tau \sum_{i=1}^k \left\|\nabla_{G_i} u_h^i\right\|^2_{L^2(\Gamma_i)} \leq d_1 \left\|u_h^0\right\|^2_{L^2(\Gamma_0)} + d_2 \sum_{i=1}^k \left\|f_h^i\right\|^2_{L^2(\Gamma_i)} \tag{4.104}
$$

$$
\tau \sum_{i=1}^k \left\|\partial_\tau^i u_h^{i-1}\right\|^2_{L^2(\Gamma_i)} + d_3 \left\|\nabla_{G_k} u_h^k\right\|^2_{L^2(\Gamma_k)} \leq d_4 \left\|u_h^0\right\|^2_{H^1(\Gamma_0)} + d_5 \sum_{i=1}^k \left\|f_h^i\right\|^2_{L^2(\Gamma_i)} \tag{4.105}
$$

Proof. Since u_h^k solves the fully discrete scheme, it solves:

$$
\partial_\tau m_k\left(u_h^k, \varphi_h^k\right) + a_{k+1}\left(u_h^{k+1}, \varphi_h^{k+1}\right) = \left(f_h^{k+1}, \varphi_h^{k+1}\right)_{L^2(\Gamma_{k+1})} \qquad \forall \varphi_h^k \in \mathcal{V}_h(\Gamma_k) \tag{4.106}
$$

In (4.106) both φ_h^k and φ_h^{k+1} appear. The interpretation is that φ_h^{k+1} is the transported counterpart of φ_h^k on the surface Γ_{k+1}, obtained via the action of the parametrisation, as is standard in this setting. In other words, if $\varphi_h^k \circ \phi_k = \Phi_h$, then φ_h^{k+1} is given by $\varphi_h^{k+1} = \Phi_h \circ \phi_{k+1}^{-1}$.

Substituting $u_h^k = \varphi_h^k$ into (4.106) and employing the definitions of the bilinear forms in (4.67), one obtains:

$$\left\|u_h^{k+1}\right\|^2_{L^2(\Gamma_{k+1})} - \left\|u_h^k\right\|^2_{L^2(\Gamma_k)} + \tau \left\|\nabla_{G_{k+1}} u_h^{k+1}\right\|^2_{L^2(\Gamma_{k+1})} = \tau \left(f_h^{k+1}, u_h^{k+1}\right)_{L^2(\Gamma_{k+1})}$$

$$\left\|u_h^{k+1}\right\|^2_{L^2(\Gamma_{k+1})} \leq \left\|u_h^k\right\|^2_{L^2(\Gamma_k)} + \frac{\tau}{4\varepsilon} \left\|f_h^{k+1}\right\|^2_{L^2(\Gamma_{k+1})} + \varepsilon\tau \left\|u_h^{k+1}\right\|^2_{L^2(\Gamma_{k+1})}$$

For $\varepsilon > 0$ such that $\varepsilon \leq \frac{1}{\tau_0}$. This requirement on ε makes the quantity $1 - \varepsilon\tau$ always greater than zero.

$$\begin{aligned}(1-\varepsilon\tau)\left\|u_h^{k+1}\right\|^2_{L^2(\Gamma_{k+1})} &\leq \left\|u_h^k\right\|^2_{L^2(\Gamma_k)} + \frac{\tau}{4\varepsilon}\left\|f_h^{k+1}\right\|^2_{L^2(\Gamma_{k+1})} \\ \left\|u_h^{k+1}\right\|^2_{L^2(\Gamma_{k+1})} &\leq \frac{1}{1-\varepsilon\tau}\left\|u_h^k\right\|^2_{L^2(\Gamma_k)} + \frac{1}{1-\varepsilon\tau}\frac{\tau}{4\varepsilon}\left\|f_h^{k+1}\right\|^2_{L^2(\Gamma_{k+1})}\end{aligned} \tag{4.107}$$

Hypothesis of Lemma 4.12 are satisfied, hence from (4.107) follows that for all $k = 1, ..., m$:

$$\begin{aligned}\left\|u_h^k\right\|^2_{L^2(\Gamma_k)} &\leq \left(\frac{1}{1-\varepsilon\tau}\right)^k \left\|u_h^0\right\|^2_{L^2(\Gamma_0)} + \frac{1}{1-\varepsilon\tau}\frac{\tau}{4\varepsilon}\sum_{i=1}^k \left\|f_h^i\right\|^2_{L^2(\Gamma_k)} \prod_{j=i+1}^k \frac{1}{1-\varepsilon\tau} \\ &= \left(\frac{1}{1-\varepsilon\tau}\right)^k \left\|u_h^0\right\|^2_{L^2(\Gamma_0)} + \frac{1}{1-\varepsilon\tau}\frac{\tau}{4\varepsilon}\sum_{i=1}^k \left\|f_h^i\right\|^2_{L^2(\Gamma_k)} \left(\frac{1}{1-\varepsilon\tau}\right)^{k-i} \\ &\leq \left(\frac{1}{1-\varepsilon\tau}\right)^m \left\|u_h^0\right\|^2_{L^2(\Gamma_0)} + \frac{1}{1-\varepsilon\tau}\frac{\tau}{4\varepsilon}\sum_{i=1}^k \left\|f_h^i\right\|^2_{L^2(\Gamma_i)} \left(\frac{1}{1-\varepsilon\tau}\right)^m \\ &= \left(\frac{1}{1-\varepsilon\tau}\right)^m \left\|u_h^0\right\|^2_{L^2(\Gamma_0)} + \left(\frac{1}{1-\varepsilon\tau}\right)^{m+1} \frac{\tau}{4\varepsilon}\sum_{i=1}^k \left\|f_h^i\right\|^2_{L^2(\Gamma_i)}\end{aligned} \tag{4.108}$$

Note that the two coefficients at the first term of the last line of (4.108) is always greater than 1 and smaller than $e^{\varepsilon T}$ (monotonically increasing with τ):

$$\left(\frac{1}{1-\varepsilon\tau}\right)^m = \left(1 + \frac{1}{\frac{1-\varepsilon\tau}{\varepsilon\tau}}\right)^{\frac{T}{\tau}} = \left[\left(1 + \frac{1}{\frac{1-\varepsilon\tau}{\varepsilon\tau}}\right)^{\frac{1-\varepsilon\tau}{\varepsilon\tau}}\right]^{\frac{\varepsilon\tau}{1-\varepsilon\tau}\frac{T}{\tau}} \underset{\tau\to 0}{\to} e^{\varepsilon T} \tag{4.109}$$

Bounding (4.108) with (4.109), and letting $\tau < \tau_0$:

$$\begin{aligned}\left\|u_h^k\right\|^2_{L^2(\Gamma_k)} &\leq e^{\varepsilon T}\left\|u_h^0\right\|^2_{L^2(\Gamma_0)} + \frac{\tau_0 e^{\varepsilon T}}{4\varepsilon}\sum_{i=1}^k \|f_h^i\|^2_{L^2(\Gamma_i)} \\ &\leq e^{\frac{T}{\tau_0}}\left(\left\|u_h^0\right\|^2_{L^2(\Gamma_0)} + \frac{\tau_0^2}{4}\sum_{i=1}^k \left\|f_h^i\right\|^2_{L^2(\Gamma_i)}\right)\end{aligned} \tag{4.110}$$

which holds for all $k = 1, ..., m$ and for all $\tau \leq \tau_0$. This is the bound for the first term of the left-hand side of (4.104). For what concerns the gradient, denoting by C_Γ the supremum of the Poincarè constant (Lemma 2.27) over the whole time interval, and plugging again $u_h^i = \varphi_h^i$ inside (4.106):

$$\begin{aligned}\left\|u_h^{i+1}\right\|^2_{L^2(\Gamma_{i+1})} - \left\|u_h^i\right\|^2_{L^2(\Gamma_i)} + \tau\left\|\nabla_{G_{i+1}} u_h^{i+1}\right\|^2_{L^2(\Gamma_{i+1})} &= \tau\left(f_h^{i+1}, u_h^{i+1}\right)_{L^2(\Gamma_{k+1})} \\ &\leq \frac{\tau}{4\delta}\left\|f_h^{i+1}\right\|^2_{L^2(\Gamma_{i+1})} + \tau\delta\left\|u_h^{i+1}\right\|^2_{L^2(\Gamma_{i+1})} \\ &\leq \frac{\tau}{4\delta}\left\|f_h^{i+1}\right\|^2_{L^2(\Gamma_{i+1})} + \tau C_\Gamma\delta\left\|\nabla_{G_{i+1}} u_h^{i+1}\right\|^2_{L^2(\Gamma_{i+1})}\end{aligned} \tag{4.111}$$

with $\delta > 0$ small enough to make $1 - \delta C_\Gamma > 0$. Now it suffices to sum (4.111) for $i = 0, ..., k-1$ to obtain:

$$\sum_{i=0}^{k-1} \left(\left\| u_h^{i+1} \right\|^2_{L^2(\Gamma_{i+1})} - \left\| u_h^i \right\|^2_{L^2(\Gamma_i)} \right) + \tau(1 - \delta C_\Gamma) \sum_{i=0}^{k-1} \left\| \nabla_{G_{i+1}} u_h^{i+1} \right\|^2_{L^2(\Gamma_{i+1})} \leq \sum_{i=0}^{k-1} \frac{\tau}{4\delta} \left\| f_h^{i+1} \right\|^2_{L^2(\Gamma_{i+1})}$$

$$\left\| u_h^k \right\|^2_{L^2(\Gamma_k)} - \left\| u_h^0 \right\|^2_{L^2(\Gamma_0)} + \tau(1 - \delta C_\Gamma) \sum_{i=1}^{k} \left\| \nabla_{G_i} u_h^i \right\|^2_{L^2(\Gamma_i)} \leq \frac{\tau_0}{4\delta} \sum_{i=1}^{k} \left\| f_h^i \right\|^2_{L^2(\Gamma_i)}$$

As usual, the positive term on the left-hand side can be neglected, leading to the following bound for the gradient term:

$$\tau \sum_{i=1}^{k} \left\| \nabla_{G_i} u_h^i \right\|^2_{L^2(\Gamma_i)} \leq \frac{1}{1 - \delta C_\Gamma} \left(\frac{\tau_0}{4\delta} \sum_{i=1}^{k} \left\| f_h^i \right\|^2_{L^2(\Gamma_i)} + \left\| u_h^0 \right\|^2_{L^2(\Gamma_0)} \right) \tag{4.112}$$

which is the bound for the second term of the left-hand side of (4.104). Summing up (4.110) and (4.112) the bound (4.104) is proved with constants:

$$d_1 = e^{\frac{T}{\tau_0}} + \frac{1}{1 - \delta C_\Gamma} \tag{4.113}$$

$$d_2 = \frac{1}{1 - \delta C_\Gamma} \frac{\tau_0}{4\delta} + e^{\frac{T}{\tau_0}} \frac{\tau_0^2}{4} \tag{4.114}$$

In order to prove (4.105), it is useful to write the fully discrete formulation in matrix form (exploiting definitions (4.10), and apply the scalar product with the vector $\mathbf{u}^{k+1} - \mathbf{u}^k$:

$$\begin{aligned} \left\langle \mathrm{M}^{k+1} \mathbf{u}^{k+1}, \mathbf{u}^{k+1} - \mathbf{u}^k \right\rangle - \left\langle \mathrm{M}^k \mathbf{u}^k, \mathbf{u}^{k+1} - \mathbf{u}^k \right\rangle + \tau \left\langle \mathrm{A}^{k+1} \mathbf{u}^{k+1}, \mathbf{u}^{k+1} - \mathbf{u}^k \right\rangle \\ = \tau \left\langle \mathbf{f}^{k+1}, \mathbf{u}^{k+1} - \mathbf{u}^k \right\rangle \end{aligned} \tag{4.115}$$

It is useful to rewrite each term as follows:

$$\begin{aligned} \left\langle \mathrm{M}^{k+1} \mathbf{u}^{k+1}, \mathbf{u}^{k+1} - \mathbf{u}^k \right\rangle - \left\langle \mathrm{M}^k \mathbf{u}^k, \mathbf{u}^{k+1} - \mathbf{u}^k \right\rangle &= \left\langle \mathrm{M}^{k+1} \left(\mathbf{u}^{k+1} - \mathbf{u}^k \right), \mathbf{u}^{k+1} - \mathbf{u}^k \right\rangle \\ &+ \left\langle \mathrm{M}^{k+1} \mathbf{u}^k, \mathbf{u}^{k+1} - \mathbf{u}^k \right\rangle - \left\langle \mathrm{M}^k \mathbf{u}^k, \mathbf{u}^{k+1} - \mathbf{u}^k \right\rangle \\ &= \tau^2 \left\langle \mathrm{M}^{k+1} \partial_\tau \mathbf{u}^k, \partial_\tau \mathbf{u}^k \right\rangle + \tau \left\langle \left(\mathrm{M}^{k+1} - \mathrm{M}^k \right) \mathbf{u}^k, \partial_\tau \mathbf{u}^k \right\rangle \end{aligned} \tag{4.116}$$

$$\begin{aligned} \left\langle \mathrm{A}^{k+1} \mathbf{u}^{k+1}, \mathbf{u}^{k+1} - \mathbf{u}^k \right\rangle &= \frac{1}{2} \left\langle \mathrm{A}^{k+1} \left(\mathbf{u}^{k+1} - \mathbf{u}^k \right), \mathbf{u}^{k+1} - \mathbf{u}^k \right\rangle + \frac{1}{2} \left\langle \mathrm{A}^{k+1} \mathbf{u}^k, \mathbf{u}^{k+1} - \mathbf{u}^k \right\rangle \\ &+ \frac{1}{2} \left\langle \mathrm{A}^{k+1} \mathbf{u}^{k+1}, \mathbf{u}^{k+1} - \mathbf{u}^k \right\rangle \\ &= \frac{1}{2} \left\langle \mathrm{A}^{k+1} \left(\mathbf{u}^{k+1} - \mathbf{u}^k \right), \mathbf{u}^{k+1} - \mathbf{u}^k \right\rangle + \frac{1}{2} \left\langle \mathrm{A}^{k+1} \mathbf{u}^{k+1}, \mathbf{u}^{k+1} \right\rangle \\ &- \frac{1}{2} \left\langle \mathrm{A}^k \mathbf{u}^k, \mathbf{u}^k \right\rangle + \frac{1}{2} \left\langle \left(\mathrm{A}^k - \mathrm{A}^{k+1} \right) \mathbf{u}^k, \mathbf{u}^k \right\rangle \end{aligned} \tag{4.117}$$

Putting (4.116) and (4.117) into (4.115):

$$\begin{aligned} \tau^2 \left\langle \mathrm{M}^{k+1} \partial_\tau \mathbf{u}^k, \partial_\tau \mathbf{u}^k \right\rangle + \tau \left\langle \left(\mathrm{M}^{k+1} - \mathrm{M}^k \right) \mathbf{u}^k, \partial_\tau \mathbf{u}^k \right\rangle + \frac{\tau}{2} \left\langle \mathrm{A}^{k+1} \left(\mathbf{u}^{k+1} - \mathbf{u}^k \right), \mathbf{u}^{k+1} - \mathbf{u}^k \right\rangle \\ + \frac{\tau}{2} \left\langle \mathrm{A}^{k+1} \mathbf{u}^{k+1}, \mathbf{u}^{k+1} \right\rangle \\ = \frac{\tau}{2} \left\langle \mathrm{A}^k \mathbf{u}^k, \mathbf{u}^k \right\rangle + \frac{\tau}{2} \left\langle \left(\mathrm{A}^{k+1} - \mathrm{A}^k \right) \mathbf{u}^k, \mathbf{u}^k \right\rangle + \tau^2 \left\langle \mathbf{f}^{k+1}, \partial_\tau \mathbf{u}^k \right\rangle \end{aligned} \tag{4.118}$$

A bilinear form acting on elements of $\mathcal{V}_h(\Gamma_{k+1})$ requires both of its arguments to belong to this space. For this reason, whenever a function indexed with apex k appears as an argument of a bilinear form defined on Γ_{k+1}, it is implicitly understood that, in its expansion over the finite element basis, the coefficients are taken at time level k, while the basis functions are those associated with time level $k+1$. This interpretation is consistent with the framework of Lemma 4.13.
In this way, using (4.98), it is possible to rewrite the bilinear forms in a consistent notation:

$$\begin{aligned}\tau^2 m_{k+1}\left(\partial_\tau^{k+1}u_h^k, \partial_\tau^{k+1}u_h^k\right) + \frac{\tau}{2}a_{k+1}\left(u_h^{k+1}, u_h^{k+1}\right) - \frac{\tau}{2}a_k\left(u_h^k, u_h^k\right)\\ = \tau\left(m_k - m_{k+1}\right)\left(u_h^k, \partial_\tau^{k+1}u_h^k\right) - \frac{\tau^3}{2}a_{k+1}\left(\partial_\tau^{k+1}u_h^k, \partial_\tau^{k+1}u_h^k\right)\\ + \frac{\tau}{2}\left(a_{k+1} - a_k\right)\left(u_h^k, u_h^k\right) + \tau^2\left(f_h^{k+1}, \partial_\tau^{k+1}u_h^k\right)_{L^2(\Gamma_{k+1})}\end{aligned} \tag{4.119}$$

Using the definition of bilinear forms (4.67):

$$\begin{aligned}\tau\left\|\partial_\tau^{k+1}u_h^k\right\|^2_{L^2(\Gamma_{k+1})} + \frac{1}{2}\left(\left\|\nabla_{G_{k+1}}u_h^{k+1}\right\|^2_{L^2(\Gamma_{k+1})} - \left\|\nabla_{G_k}u_h^k\right\|^2_{L^2(\Gamma_k)}\right)\\ = \left(m_k - m_{k+1}\right)\left(u_h^k, \partial_\tau^{k+1}u_h^k\right) - \frac{\tau^2}{2}\left\|\nabla_{G_{k+1}}\partial_\tau^{k+1}u_h^k\right\|^2_{L^2(\Gamma_{k+1})}\\ + \frac{1}{2}\left(a_{k+1} - a_k\right)\left(u_h^k, u_h^k\right) + \tau\left(f_h^{k+1}, \partial_\tau^{k+1}u_h^k\right)_{L^2(\Gamma_{k+1})}\end{aligned} \tag{4.120}$$

The second term of the right-hand side of (4.120) is negative, hence the left-hand side can be bounded from above just by neglecting it. It it possible to bound each term of the right-hand side as follows:

$$\left(f_h^{k+1}, \partial_\tau^{k+1}u_h^k\right)_{L^2(\Gamma_{k+1})} \le \frac{1}{4\beta}\left\|f_h^{k+1}\right\|^2_{L^2(\Gamma_{k+1})} + \beta\left\|\partial_\tau^{k+1}u_h^k\right\|^2_{L^2(\Gamma_{k+1})} \tag{4.121}$$

Moreover thanks to Lemma 4.13:

$$\begin{aligned}\left(m_k - m_{k+1}\right)\left(u_h^k, \partial_\tau^{k+1}u_h^k\right) &\overset{(4.99)}{\le} \tau C_G^{k+1} m_{k+1}\left(u_h^k, \partial_\tau^{k+1}u_h^k\right)\\ &\le \tau C_G^{k+1}\left\|u_h^k\right\|_{L^2(\Gamma_{k+1})}\left\|\partial_\tau^{k+1}u_h^k\right\|_{L^2(\Gamma_{k+1})}\\ &\overset{(4.100)}{\le} \tau C_G^{k+1}\sqrt{D_G^k}\left\|u_h^k\right\|_{L^2(\Gamma_k)}\left\|\partial_\tau^{k+1}u_h^k\right\|_{L^2(\Gamma_{k+1})}\\ &\le \tau\underbrace{\frac{C_G^{k+1}D_G^k}{4\alpha}}_{:=\tilde{d}_1}\left\|u_h^k\right\|^2_{L^2(\Gamma_k)} + \tau\alpha C_G^{k+1}\left\|\partial_\tau^{k+1}u_h^k\right\|^2_{L^2(\Gamma_{k+1})}\end{aligned} \tag{4.122}$$

$$\left(a_{k+1} - a_k\right)\left(u_h^k, u_h^k\right) \overset{(4.99)}{\le} \tau C_G^{k+1} a_k\left(u_h^k, u_h^k\right) = \tau C_G^{k+1}\left\|\nabla_{G_k}u_h^k\right\|^2_{L^2(\Gamma_k)} \tag{4.123}$$

where α, β are two positive constant such that $1 - \alpha C_G - \beta > 0$, where $C_G := \max_k C_G^k$. Putting everything together the following bound holds for all $k = 0, ..., m-1$:

$$\begin{aligned}\tau\left(1 - \alpha C_G - \beta\right)\left\|\partial_\tau^{k+1}u_h^k\right\|^2_{L^2(\Gamma_{k+1})} + \frac{1}{2}\left(\left\|\nabla_{G_{k+1}}u_h^{k+1}\right\|^2_{L^2(\Gamma_{k+1})} - \left\|\nabla_{G_k}u_h^k\right\|^2_{L^2(\Gamma_k)}\right)\\ \le \tau\tilde{d}_1\left\|u_h^k\right\|^2_{L^2(\Gamma_k)} + \tau C_G\left\|\nabla_{G_k}u_h^k\right\|^2_{L^2(\Gamma_k)} + \frac{\tau}{4\beta}\left\|f_h^{k+1}\right\|^2_{L^2(\Gamma_{k+1})}\end{aligned} \tag{4.124}$$

Let $\hat{d}_1 = \max_k \tilde{d}_1$. Changing the dumb index k with i, summing for $i = 0, ..., k-1$ (and renaming

indexes for a cleaner notation, if necessary) and dividing by $1 - \alpha C_G - \beta$:

$$\begin{aligned}
&\tau \sum_{i=1}^{k} \left\|\partial_\tau^i u_h^{i-1}\right\|_{L^2(\Gamma_i)}^2 + \underbrace{\frac{1}{2(1-\alpha C_G-\beta)}}_{:=d_3} \left(\left\|\nabla_{G_k} u_h^k\right\|_{L^2(\Gamma_k)}^2 - \left\|\nabla_{G_0} u_h^0\right\|_{L^2(\Gamma_0)}^2\right) \\
&\quad \le 2\tau d_3 \hat{d}_1 \sum_{i=0}^{k-1} \left\|u_h^i\right\|_{L^2(\Gamma_i)}^2 + 2\tau d_3 C_G \sum_{i=0}^{k-1} \left\|\nabla_{G_i} u_h^i\right\|_{L^2(\Gamma_i)}^2 + \frac{2d_3\tau}{4\beta} \sum_{i=1}^{k} \left\|f_h^i\right\|_{L^2(\Gamma_i)}^2 \\
&\quad \overset{(4.104)}{\le} 2d_3 T d_1 \hat{d}_1 \left\|u_h^0\right\|_{L^2(\Gamma_0)}^2 + 2d_3 T d_2 \hat{d}_1 \sum_{i=1}^{k} \left\|f_h^i\right\|_{L^2(\Gamma_i)}^2 \\
&\quad + 2d_3 C_G d_1 \left\|u_h^0\right\|_{L^2(\Gamma_0)}^2 + 2d_3 C_G d_2 \sum_{i=1}^{k} \left\|f_h^i\right\|_{L^2(\Gamma_i)}^2 + \frac{2d_3\tau_0}{4\beta} \sum_{i=1}^{k} \left\|f_h^i\right\|_{L^2(\Gamma_i)}^2 \\
&\quad \le \underbrace{2d_3(T d_1 \hat{d}_1 + C_G d_1)}_{:=\tilde{d}_2} \left\|u_h^0\right\|_{L^2(\Gamma_0)}^2 + \underbrace{2d_3 \left(T d_2 \hat{d}_1 + C_G d_1 + \frac{\tau_0}{4\beta}\right)}_{:=d_5} \sum_{i=1}^{k} \left\|f_h^i\right\|_{L^2(\Gamma_i)}^2
\end{aligned} \tag{4.125}$$

and finally:

$$\begin{aligned}
\tau \sum_{i=1}^{k} \left\|\partial_\tau^i u_h^{i-1}\right\|_{L^2(\Gamma_i)}^2 + d_3 \left\|\nabla_{G_k} u_h^k\right\|_{L^2(\Gamma_k)}^2 &\le d_3 \left\|\nabla_{G_0} u_h^0\right\|_{L^2(\Gamma_0)}^2 + \tilde{d}_2 \left\|u_h^0\right\|_{L^2(\Gamma_0)}^2 + d_5 \sum_{i=1}^{k} \left\|f_h^i\right\|_{L^2(\Gamma_i)}^2 \\
&\le \underbrace{\max\left\{d_3, \tilde{d}_2\right\}}_{:=d_4} \left\|u_h^0\right\|_{H^1(\Gamma_0)}^2 + d_5 \sum_{i=1}^{k} \left\|f_h^i\right\|_{L^2(\Gamma_i)}^2
\end{aligned} \tag{4.126}$$

which is (4.105) and completes the proof. □

The following theorem gives the optimal error bound for the fully discrete formulation. All properties of the Ritz projection used in Section 4.2.1 naturally extends for sampled time instants.

Theorem 4.15. *Let $u_h^k \in \mathcal{V}_h(\Gamma_k)$ be the solution of the fully discrete formulation stated in Problem 4.6 and let u be the solution of Problem 3.1 such that:*

$$\left\|u(\cdot,0) - u_h^0\right\|_{L^2(\Gamma_0)}^2 \le h^2 \tag{4.127}$$

Then the numerical solution satisfies the following bounds:

$$\left\|u(\cdot,t^k) - u_h^k\right\|_{L^2(\Gamma_k)}^2 \le C_1 h^4 + C_2 \tau^2 \tag{4.128}$$

$$\tau \sum_{i=1}^{k} \left\|\nabla_{G_i} \left(u(\cdot,t^i) - u_h^i\right)\right\|_{L^2(\Gamma_i)}^2 \le C_3 h^2 + C_4 h^4 + C_5 \tau^2 \tag{4.129}$$

for all $k = 1, ..., m$ with constants depending on the data of the problem, but not on τ and h.

Proof. Since u solves the weak formulation, the following equality holds for all φ_j^i basis functions of $\mathcal{V}_h(\Gamma_i)$ and for all $i = 0, ..., m-1$.

$$\frac{d}{dt} m_i \left(u^i, \varphi_j^i\right) + a_i \left(u^i, \varphi_j^i\right) = \left(f_h^i, \varphi_j^i\right)_{H^{-1} \times H^1} \tag{4.130}$$

Thanks to property (4.97) of the backward discrete time derivative, it is possible to do the following for all $j = 1, ..., n$:

$$\frac{d}{dt} m_i \left(u^i, \varphi_j^i \right) = \partial_\tau m_i \left(u^i, \varphi_j^i \right) + \tau c \frac{d^2}{dt^2} m_i \left(u^i, \varphi_j^i \right) \tag{4.131}$$

Assuming that all the following quantities exist with the suitable regularity, it is possible to write:

$$\frac{d}{dt} \left(m_i \left(\dot{u}^i, \varphi_j^i \right) + m_i \left(\lambda u^i, \varphi_j^i \right) \right) = m_i \left(\underbrace{\ddot{u}^i + 2\lambda^i \dot{u}^i + \dot{\lambda}^i u^i + (\lambda^i)^2 u^i}_{:= \psi^i(u,\lambda)}, \varphi_j^i \right) \tag{4.132}$$

Then, up to renaming constants, thanks to Lemma 4.13, (4.130) can be rewritten as follows, for all $j = 1, ..., n$:

$$\partial_\tau m_i \left(u^i, \varphi_j^i \right) + a_i \left(u^{i+1}, \varphi_j^{i+1} \right) = \left(f_h^{i+1}, \varphi_j^{i+1} \right)_{H^{-1} \times H^1} + m_{i+1} \left(c\psi^{i+1}\tau, \varphi_j^{i+1} \right) \tag{4.133}$$

while the numerical solution u_h^i solves the following for all $i = 0, ..., m-1$:

$$\partial_\tau m_i \left(u_h^i, \varphi_j^i \right) + a_{i+1} \left(u_h^{i+1}, \varphi_j^{i+1} \right) = \left(f_h^{i+1}, \varphi_j^{i+1} \right)_{H^{-1} \times H^1} \tag{4.134}$$

As done in Theorem 4.11, it is possible to apply the decomposition of the error by using the Ritz projection of u on $\mathcal{V}_h(\Gamma_k)$. Subtracting (4.134) to (4.133), making use of the error decomposition (4.78), and taking advantage of Definition 4.8, it is possible to obtain the error equation:

$$\partial_\tau m_i \left(\zeta^i, \varphi_j^i \right) + a_{i+1} \left(\zeta^{i+1}, \varphi_j^{i+1} \right) = -m_i \left(\eta^i, \varphi_j^i \right) + m_{i+1} \left(c\psi^{i+1}\tau, \varphi_j^{i+1} \right) \tag{4.135}$$

At each time instant, ζ^i can be written as linear combination of basis functions φ_j^i. Therefore, by linearity:

$$\partial_\tau m_i \left(\zeta^i, \zeta^i \right) + a_{i+1} \left(\zeta^{i+1}, \zeta^{i+1} \right) = -m_i \left(\eta^i, \zeta^i \right) + m_{i+1} \left(c\psi^{i+1}\tau, \zeta^{i+1} \right) \tag{4.136}$$

Expliciting the definition of the bilinear forms (4.67) and the action of the discrete backward time derivative:

$$\begin{aligned} \left\| \zeta^{i+1} \right\|^2_{L^2(\Gamma_{i+1})} - \left\| \zeta^i \right\|^2_{L^2(\Gamma_i)} + \tau \left\| \nabla_{G_{i+1}} \zeta^{i+1} \right\|^2_{L^2(\Gamma_{i+1})} \\ = -m_{i+1} \left(\eta^{i+1}, \zeta^{i+1} \right) + m_i \left(\eta^i, \zeta^i \right) + \tau m_{i+1} \left(c\psi^{i+1}\tau, \zeta^{i+1} \right) \end{aligned} \tag{4.137}$$

for all $i = 0, ..., k-1$, for all $k \leq m$. Therefore summing over $i = 0, ..., k-1$ as done in Proposition

4.14:

$$\begin{aligned}
\left\|\zeta^k\right\|^2_{L^2(\Gamma_k)} - \left\|\zeta^0\right\|^2_{L^2(\Gamma_0)} + \tau \sum_{i=1}^{k} \left\|\nabla_{G_i}\zeta^i\right\|^2_{L^2(\Gamma_i)} & \\
&\leq -m_k\left(\eta^k, \zeta^k\right) + m_0\left(\eta^0, \zeta^0\right) + \tau^2 \sum_{i=1}^{k} m_i\left(c\psi^i, \zeta^i\right) \\
&\leq \frac{1}{4\gamma}\left\|\eta^k\right\|^2_{L^2(\Gamma_k)} + \gamma\left\|\zeta^k\right\|^2_{L^2(\Gamma_k)} + \frac{1}{2}\left\|\eta^0\right\|^2_{L^2(\Gamma_0)} + \frac{1}{2}\left\|\zeta^0\right\|^2_{L^2(\Gamma_0)} \\
&\quad + \tau^2 \sum_{i=1}^{k}\left(\frac{c\|\psi^i\|^2_{L^2(\Gamma_i)}}{4\omega} + \omega\left\|\zeta^i\right\|^2_{L^2(\Gamma_i)}\right) \\
&\overset{(4.70,4.127,2.11)}{\leq} \underbrace{\left(\frac{k_{1,k}^2\|u^k\|^2_{H^2(\Gamma_k)}}{4\gamma} + \frac{k_{1,0}^2\|u^0\|^2_{H^2(\Gamma_0)}}{2} + \frac{1}{2}\right)}_{:=\tilde{C}_1} h^4 \\
&\quad + \gamma\left\|\zeta^k\right\|^2_{L^2(\Gamma_k)} + \tau^2 \underbrace{\frac{c}{4\omega}\sum_{i=1}^{k}\|\psi^i\|^2_{L^2(\Gamma_i)}}_{:=\tilde{C}_2}\tau^2 + \tau^2\omega C_\Gamma^2 \sum_{i=1}^{k}\left\|\nabla_{G_i}\zeta^i\right\|^2_{L^2(\Gamma_i)}
\end{aligned} \tag{4.138}$$

with the following constraints on the constants γ, ω:

$$\begin{cases} \gamma, \omega > 0 \\ 1 - \tau\omega C_\Gamma^2 > 0 \\ 1 - \gamma < 1 - \tau\omega C_\Gamma^2 \end{cases} \tag{4.139}$$

Rearranging and making use of (4.139):

$$(1-\gamma)\left\|\zeta^k\right\|^2_{L^2(\Gamma_k)} + \tau\left(1 - \tau\omega C_\Gamma^2\right)\sum_{i=1}^{k}\left\|\nabla_{G_i}\zeta^i\right\|^2_{L^2(\Gamma_i)} \leq \tilde{C}_1 h^4 + \tilde{C}_2\tau^2 \tag{4.140}$$

$$\begin{aligned}
\left\|\zeta^k\right\|^2_{L^2(\Gamma_k)} + \tau\sum_{i=1}^{k}\left\|\nabla_{G_i}\zeta^i\right\|^2_{L^2(\Gamma_i)} &\leq \left\|\zeta^k\right\|^2_{L^2(\Gamma_k)} + \tau\frac{1-\tau\omega C_\Gamma^2}{1-\gamma}\sum_{i=1}^{k}\left\|\nabla_{G_i}\zeta^i\right\|^2_{L^2(\Gamma_i)} \\
&\leq \frac{1}{1-\gamma}\left(\tilde{C}_1 h^4 + \tilde{C}_2\tau^2\right)
\end{aligned} \tag{4.141}$$

Trivially both the terms of the left-hand side of (4.141) can be bounded by the right-hand side:

$$\begin{aligned}
\left\|u - u_h^k\right\|^2_{L^2(\Gamma_k)} = \left\|\eta^k + \zeta^k\right\|^2_{L^2(\Gamma_k)} &\leq 2\left\|\eta^k\right\|^2_{L^2(\Gamma_k)} + 2\left\|\zeta^k\right\|^2_{L^2(\Gamma_k)} \\
&\overset{(4.71,4.141)}{\leq} 2k_{1,k}^2\|u\|^2_{H^2(\Gamma_k)}h^4 + \frac{2}{1-\gamma}\left(\tilde{C}_1 h^4 + \tilde{C}_2\tau^2\right) \\
&= \underbrace{\left(2k_{1,k}^2\|u\|^2_{H^2(\Gamma_k)} + \frac{2\tilde{C}_1}{1-\gamma}\right)}_{:=C_1} h^4 + \underbrace{\frac{2\tilde{C}_2}{1-\gamma}}_{:=C_2}\tau^2 \\
&= C_1 h^4 + C_2\tau^2
\end{aligned} \tag{4.142}$$

and similarly for the gradient. This time the interpolation estimate (4.71) is weaker, therefore the convergence rate is weaker, as expected.

$$\begin{aligned}
\tau \sum_{i=1}^{k} \left\| \nabla_{G_i} \left(u - u_h^i \right) \right\|_{L^2(\Gamma_i)}^2 &= \tau \sum_{i=1}^{k} \left\| \nabla_{G_i} \left(\eta^i + \zeta^i \right) \right\|_{L^2(\Gamma_i)}^2 \\
&\leq \tau \sum_{i=1}^{k} 2 \left\| \nabla_{G_i} \eta^i \right\|_{L^2(\Gamma_i)}^2 + \tau \sum_{i=1}^{k} 2 \left\| \nabla_{G_i} \zeta^i \right\|_{L^2(\Gamma_i)}^2 \\
&\overset{(4.71,4.141)}{\leq} 2\tau \sum_{i=1}^{k} h^2 k_{2,i}^2 \left\| u \right\|_{H^2(\Gamma_i)}^2 + \frac{2}{1-\gamma} \left(\tilde{C}_1 h^4 + \tilde{C}_2 \tau^2 \right) \qquad (4.143) \\
&= \underbrace{2T \sup_{i \leq k} k_{2,i}^2 \left\| u \right\|_{H^2(\Gamma_i)}^2}_{:=C_3} h^2 + \underbrace{\frac{2\tilde{C}_1}{1-\gamma}}_{:=C_4} h^4 + C_2 \tau^2 \\
&= C_3 h^2 + C_4 h^4 + C_2 \tau^2
\end{aligned}$$

The bound (4.129) is proved with $C_5 = C_2$. □

Chapter 5

Experimental results

In the classical Finite Element Method, one expects second-order accuracy in the L^2 norm and first-order accuracy in the H^1 norm. As discussed in Section 4.2.1, for the Surface Finite Element Method the error analysis must also account for the evolution of the underlying surface over time. Consequently, the numerical experiments presented in this chapter are designed to validate the convergence estimates (4.74, 4.75) by computing of the following quantities:

$$\begin{aligned} \max_k \|e_h\|_{L^2(\Gamma_k)} &= \max_k \sqrt{\int_{\Gamma_k} (u_h - u)^2 dx} \\ \max_k \|e_h\|_{H^1(\Gamma_k)} &= \max_k \sqrt{\int_{\Gamma_k} (u_h - u)^2 dx + \int_{\Gamma_k} \left|\nabla_{G_k} u_h - \nabla_{G_k} u\right|^2_{G_k} dx} \end{aligned} \tag{5.1}$$

As usual, the experimental order of accuracy (EOC), is computed with the formula:

$$\text{EOC} = \frac{\log(\text{err}_1) - \log(\text{err}_2)}{\log(h_1) - \log(h_2)} \tag{5.2}$$

The optimal convergence of the numerical scheme is verified using the method of manufactured solutions. In [18], the convergence tables report only the maximum error norm. However, this quantity is influenced by the norm of the exact solution, so relatively large inaccuracies may be masked when the exact solution itself has a small norm. For this reason, in this chapter it is also analysed the maximum relative error norm, which provides additional insight into the actual effectiveness and accuracy of the numerical scheme.

$$\begin{aligned} \max_k \varepsilon_h^k(L^2) &= \max_k \frac{\|e_h\|_{L^2(\Gamma_k)}}{\|u\|_{L^2(\Gamma_k)}} \\ \max_k \varepsilon_h^k(H^1) &= \max_k \frac{\|e_h\|_{H^1(\Gamma_k)}}{\|u\|_{H^1(\Gamma_k)}} \end{aligned} \tag{5.3}$$

Nevertheless, the theoretical convergence rates available in the literature are established with respect to the absolute error norms defined in (5.1). Consequently, the Experimental Order of Convergence (EOC) computed using relative errors (5.3) should be interpreted only as an empirical indicator of the method's accuracy, since no corresponding theoretical convergence estimates are currently available for this measure.

Another way to assess the validity of the solver is to exploit the fact that the model problem (3.12) is a conservation law. In the absence of a forcing term, and starting from an initial condition $u(\mathbf{x}, 0) = u_0(\mathbf{x})$, the integral of the solution over the surface should remain constant at all times,

corresponding to conservation of mass.

$$\Delta_k M = \int_{\Gamma_k} u(\mathbf{x}, t^k) - \int_{\Gamma_0} u_0(\mathbf{x}) = 0 \quad \forall k = 1, ..., m \tag{5.4}$$

The relative loss of mass is obtained just by dividing the loss of mass by the initial mass:

$$\delta_k M = \Delta_k M \left(\int_{\Gamma_0} u_0(\mathbf{x}) \right)^{-1} \tag{5.5}$$

Both of these two benchmarks have been tested in all simulations.

The simulations are performed using those procedures described in Section 4.1.4 which do not require an explicit parametrisation of the surface. Particular attention is devoted to the methods that introduce a suitable element parametrisation in order to exploit the additional geometric information encoded in the tangent vectors (4.56, 4.64). To cover the general setting in which tangent vectors are unavailable as input, the method based on approximating the surface by its polyhedral interpolant is also employed (4.66).

From a geometric perspective, method (4.64) is more interesting to the author than method (4.66) because it can exploit the geometric information encoded in the tangent vectors whenever they are available. From a computational perspective, method (4.64) is also preferred due to its greater robustness, as discussed in Section 4.1.4. For these reasons, all figures and tables reporting mass conservation and relative errors are obtained using method (4.64).

To define the test cases considered in this work, the problem data (e.g. the surface geometry, forcing terms, and other model quantities) must be specified explicitly. For this purpose, each surface is described through a parametrisation, which is used solely to generate the required data and to provide a precise characterisation of the geometry. The parametrisation is reported in the following sections for completeness; however, it is not required by the numerical method. Indeed, the solver operates exclusively on the nodal coordinates and the associated tangent planes, reconstructing suitable local parametrisations on an element by element basis. Consequently, the method remains fully applicable in practical settings where a parametrisation of the surface is not available, as no stage of the numerical computation relies on such information (see Section 4.1.4).

The meshes are generated on the chart; therefore, the resulting triangles may become significantly distorted depending on the motion of the surface. Since the mesh size directly affects the error, as shown in Section 4.2, it is computed on the triangulated embedded surface. Nevertheless, evaluating the mesh size directly on the chart would not affect the observed order of accuracy.

The numerical experiments are organized according to a progressively increasing level of generality. The analysis begins with height function surfaces, namely a paraboloid, which exponentially flattens onto the xy-plane, and an oscillating cosine surface. The latter, owing to the strong spatio-temporal dependence of its metric and its oscillatory nature, constitutes a significantly more challenging benchmark than the paraboloid. The second stage of the analysis considers general single-chart surfaces, namely surfaces that cannot be represented as height functions. The first example is a generalization of the paraboloid considered previously: besides flattening onto the xy-plane, the surface also undergoes an isotropic expansion. Although this example still retains some characteristics of a height-function surface, the second test case considers an expanding perforated sphere. The final class of problems investigated in this thesis consists of multi-chart surfaces. The first test case is an expanding sphere, which demonstrates the natural extension of the proposed method to general surfaces. The second example is a deforming ellipsoid, whose solution was also considered in [18]. This benchmark enables a direct comparison between the E-ISFEM and ESFEM methods on the same problem.

Finally, the time step τ is always chosen proportional to h^2 in order to observe the optimal convergence rates.

5.1 Height function surfaces

The first class of problems considered in the numerical experiments is defined on surfaces parametrised by a height function. This property leads to significant simplifications in both the analytical computations and the numerical implementation.

5.1.1 Paraboloid collapsing in a plane

The first numerical experiment considers a paraboloid that collapses exponentially in a plane. The surface is defined over the spatial domain $[0,1]^2$ and evolves within the time interval $[0,1]$. Despite its relatively simple geometric description, this test case is already fairly general, since the induced metric depends on both space and time. As a consequence, it provides a meaningful benchmark for assessing the ability of the numerical scheme to accurately handle the evolution of geometrical quantities and their interaction with the underlying partial differential equation.

$$\begin{aligned} \phi_t : [0,1]^2 &\to \mathbb{R}^3 \\ (\xi_1, \xi_2) &\longmapsto \left(\xi_1, \xi_2, e^{-t}\left(\xi_1(1-\xi_1) + \xi_2(1-\xi_2)\right)\right) \end{aligned} \tag{5.6}$$

Manufactured solution

The convergence analysis is carried out by defining a manufactured solution:

$$u(x,y,z,t) = xyt \tag{5.7}$$

Which in local coordinates reads:

$$U(\xi_1, \xi_2, t) = \xi_1 \xi_2 t \tag{5.8}$$

The forcing term f is obtained by substituting the manufactured solution into the left-hand side of (3.26). The convergence results reported in Table 5.1, 5.2, 5.3, obtained using respectively the methods characterised by (4.56, 4.64, 4.66) confirm the expected second-order convergence in the L^2 norm and the first-order convergence in the H^1 norm. Table 5.4 reports the E-ISFEM relative errors obtained with (4.64), providing additional information on the experimental accuracy of the numerical approximation.

A graphical comparison between the numerical and exact solutions is presented in Figure 5.1, where both solutions are displayed at three different instants of time throughout the evolution.

Conservation of mass

Discontinuities in the initial datum provide a demanding benchmark for the numerical solver. Owing to the parabolic nature of the equation, the solution is expected to become immediately smooth for positive times, while preserving the conservative properties of the model. Therefore, a robust numerical scheme should correctly capture the smoothing effect without generating spurious oscillations or instabilities near the discontinuity. For this reason, the following discontinuous initial datum is considered:

$$u_0(\boldsymbol{\xi}) = \mathbf{1}_B \tag{5.9}$$

where $B = \left\{\boldsymbol{\xi} \in \mathbb{R}^2 : |\boldsymbol{\xi} - \mathbf{p}| \leq r\right\}$, with $\mathbf{p} = \left(\frac{1}{2}, \frac{1}{2}\right)$ and $r = 0.2$. Table 5.5 demonstrates the consistency of the numerical method with the conservation property expressed by (3.12), independently of the mesh size employed. The results show that the total mass is preserved throughout the simulation, confirming the conservative character of the discretisation.

Figure 5.2 illustrates the evolution of the initial datum under the combined effects of diffusion and surface motion. The solution is displayed at six different instants of time, highlighting both the progressive smoothing of the initial discontinuity and the influence of the evolving geometry.

h	τ	$\max_k \|e_h\|_{L^2(\Gamma_k)}$	EOC	$\max_k \|e_h\|_{H^1(\Gamma_k)}$	EOC
3.063631e-01	9.385833e-02	1.151223e-02	-	1.686160e-01	-
1.422194e-01	2.022636e-02	2.971497e-03	1.76	7.436354e-02	1.07
7.887586e-02	6.221401e-03	5.882882e-04	2.75	4.091085e-02	1.01
3.964382e-02	1.571633e-03	1.449178e-04	2.04	2.042437e-02	1.01

Table 5.1: Errors and experimental order of accuracy of the problem defined by the manufactured solution (5.7) on the paraboloid (5.6), obtained with method (4.56).

h	τ	$\max_k \|e_h\|_{L^2(\Gamma_k)}$	EOC	$\max_k \|e_h\|_{H^1(\Gamma_k)}$	EOC
3.063631e-01	9.385833e-02	1.166802e-02	-	1.686512e-01	-
1.422194e-01	2.022636e-02	2.936691e-03	1.80	7.436454e-02	1.07
7.887586e-02	6.221401e-03	5.998677-04	2.69	4.091149e-02	1.01
3.964382e-02	1.571633e-03	1.422672e-04	2.09	2.042440e-02	1.01

Table 5.2: Errors and experimental order of accuracy of the problem defined by the manufactured solution (5.7) on the paraboloid (5.6), obtained method (4.64).

h	τ	$\max_k \|e_h\|_{L^2(\Gamma_k)}$	EOC	$\max_k \|e_h\|_{H^1(\Gamma_k)}$	EOC
3.063631e-01	9.385833e-02	1.150962e-02	-	1.686150e-01	-
1.422194e-01	2.022636e-02	2.972175e-03	1.76	7.436344e-02	1.07
7.887586e-02	6.221401e-03	5.879901e-04	2.75	4.091082e-02	1.01
3.964382e-02	1.571633e-03	1.449723e-04	2.06	2.042437e-02	1.02

Table 5.3: Errors and experimental order of accuracy of the problem defined by the manufactured solution (5.7) on the paraboloid (5.6), obtained with method (4.66).

h	τ	$\max_k \varepsilon_h^k(L^2)$	EOC	$\max_k \varepsilon_h^k(H^1)$	EOC
3.063631e-01	9.385833e-02	3.287773e-02	-	4.032309e-02	-
1.422194e-01	2.022636e-02	8.575587e-03	1.75	8.405438e-03	2.04
7.887586e-02	6.221401e-03	1.885496e-03	2.57	2.558902e-03	2.02
3.964382e-02	1.571633e-03	7.542908e-04	1.33	6.398838e-04	2.01

Table 5.4: Relative errors of the problem defined by the manufactured solution (5.7) on the paraboloid (5.6), obtained with method (4.64).

h	τ	$\max_k \Delta_k M$	$\max_k \delta_k M$
3.795149e-01	1.440315e-01	1.526557e-16	2.171103e-15
1.731240e-01	2.997193e-02	4.163336e-16	2.634345e-15
8.298212e-02	6.886032e-03	7.771561e-16	6.112034e-15
4.065486e-02	1.652818e-03	1.915135e-15	1.458210e-14

Table 5.5: Loss of mass of the numerical solution starting from the discontinuous initial datum (5.9) on the paraboloid (5.6), obtained with method (4.66).

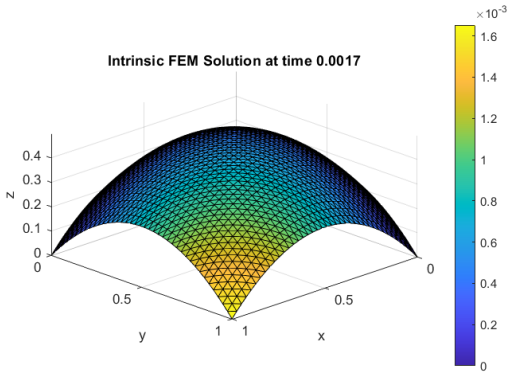

(a) Numerical solution at time $t = 0.0017$.

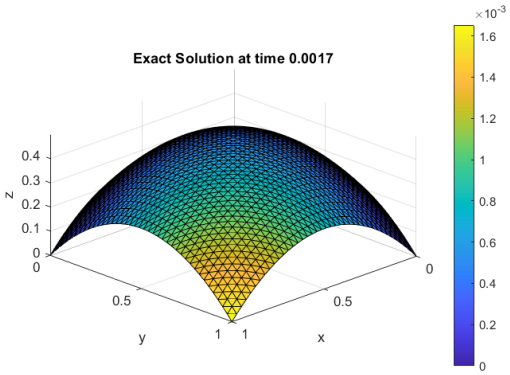

(b) Exact solution (5.7) at time $t = 0.0017$.

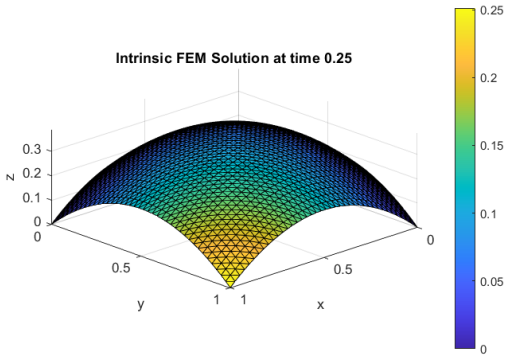

(c) Numerical solution at time $t = 0.25$.

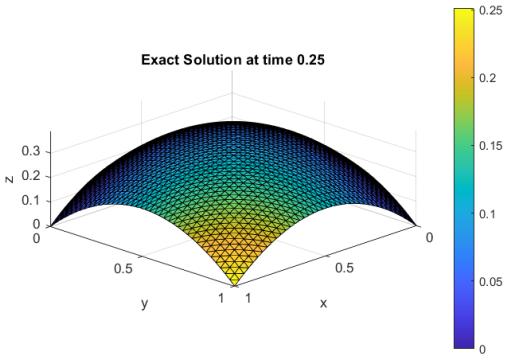

(d) Exact solution (5.7) at time $t = 0.25$.

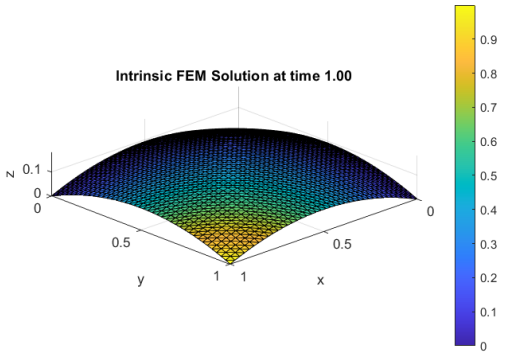

(e) Numerical solution at time $t = 1.0$.

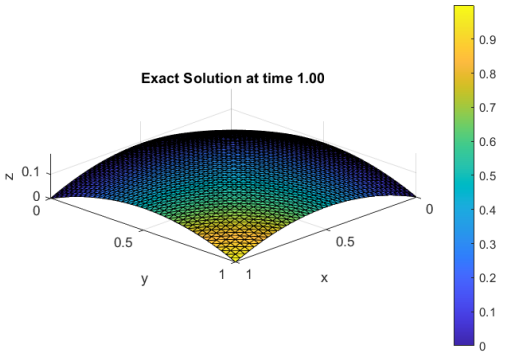

(f) Exact solution (5.7) at time $t = 1.0$.

Figure 5.1: Comparison between the numerical solution of the problem on the paraboloid (5.6) and the exact solution (5.7).

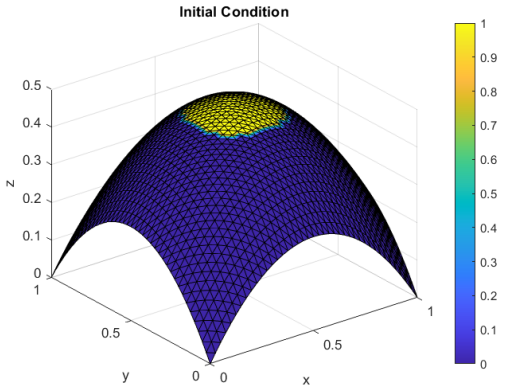

(a) Initial condition

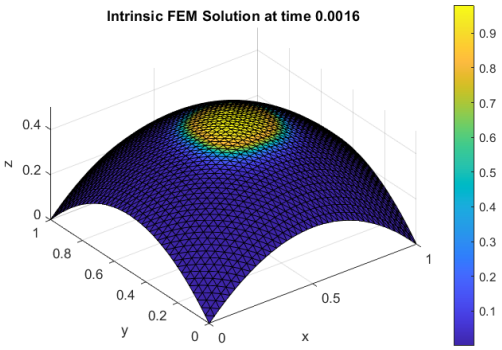

(b) Solution at time $t = 0.0016$.

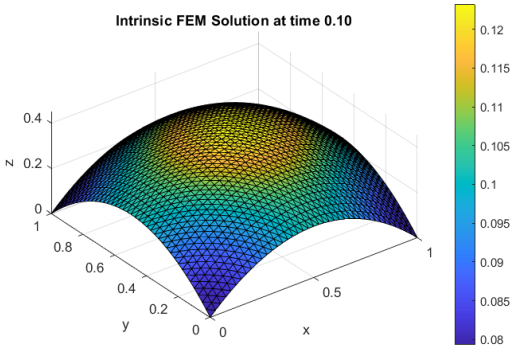

(c) $t = 0.10$.

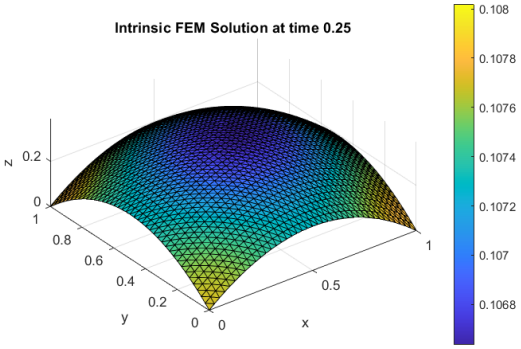

(d) Solution at time $t = 0.25$

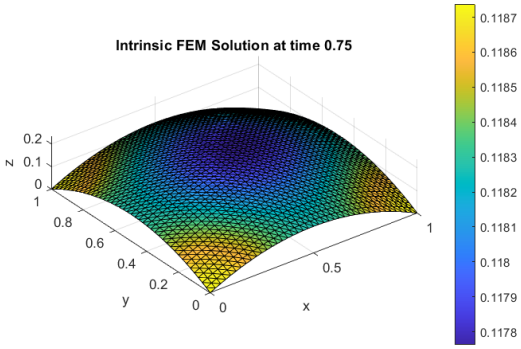

(e) Solution at time $t = 0.75$

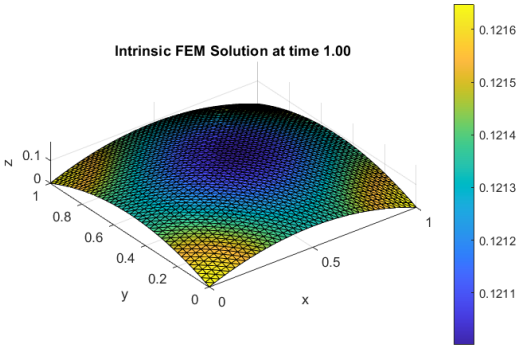

(f) $t = 1.00$.

Figure 5.2: Evolution of the discontinuous initial datum (5.9) through the motion of the paraboloid (5.6).

5.1.2 Oscillating cosine surface

One of the most general benchmarks used to test the solver is a surface oscillating in time, where the curvature depends on both space and time. The chosen parametrisation reads:

$$\begin{aligned} \phi_t : [0,1]^2 &\to \mathbb{R}^3 \\ (\xi_1, \xi_2) &\longmapsto (\xi_1, \xi_2, \cos(2\pi\xi_1)\cos(2\pi\xi_2)\cos(2t)) \end{aligned} \tag{5.10}$$

The time interval is chosen as $[0, 3]$ in order to allow the surface to undergo changes in concavity during the evolution. The oscillatory nature of the surface makes this test case more challenging and significantly stiffer than the previous example.

Manufactured solution

It has been chosen space and time dependent manufactured solution:

$$\begin{aligned} u(x, y, z, t) &= x^2 y^2 t \\ U(\xi_1, \xi_2, t) &= \xi_1^2 \xi_2^2 t \end{aligned} \tag{5.11}$$

The second spatial derivatives of (5.11) do not vanish, so all terms involved in the computation of the forcing term are nonzero. This feature is important in order to preserve the generality of the chosen benchmark problem.

Table 5.6, 5.7, 5.8 highlight the expected optimal convergence rates for all the considered methods, while Table 5.9 reports the relative errors. The results are in agreement with the theoretical predictions, indicating that the solver performs correctly also in the presence of strongly time-dependent dynamics, as in this case. Figure 5.3 compares graphically the numerical solution with the manufactured exact solution at three different instants of time.

Conservation of mass

As initial datum, the same discontinuous function used in the previous example (5.9) has been chosen. Table 5.10 shows that, once again, the total mass is conserved throughout the entire simulation time.

Figure 5.4 illustrates the evolution of the initial datum during the motion of the surface, at six different instants of time.

h	τ	$\max_k \|e_h\|_{L^2(\Gamma_k)}$	EOC	$\max_k \|e_h\|_{H^1(\Gamma_k)}$	EOC
6.017847e-01	3.621448e-01	7.997590e-02	-	7.144951e-01	-
3.050183e-01	9.303619e-02	2.317968e-02	1.82	2.659281e-01	1.45
1.543086e-01	2.381116e-02	7.184263e-03	1.72	1.179778e-01	1.19
1.030957e-01	1.062871e-02	3.042054e-03	2.13	7.434284e-02	1.15
7.738039e-02	5.987725e-03	1.805121e-03	1.82	5.520078e-02	1.04

Table 5.6: Errors and experimental order of accuracy of the problem defined by the manufactured solution (5.11) on the oscillating cosine surface (5.10), obtained with (4.56).

h	τ	$\max_k \|e_h\|_{L^2(\Gamma_k)}$	EOC	$\max_k \|e_h\|_{H^1(\Gamma_k)}$	EOC
6.017847e-01	3.621448e-01	1.811956e-01	-	1.567104e+00	-
3.050183e-01	9.303619e-02	2.900480e-02	2.70	3.296121e-01	2.29
1.543086e-01	2.381116e-02	7.103435e-03	2.06	1.306216e-01	1.36
1.030957e-01	1.062871e-02	3.307384e-03	1.93	7.820705e-02	1.30
7.738039e-02	5.987725e-03	1.832666e-03	2.06	5.651043e-02	1.13

Table 5.7: Errors and experimental order of accuracy of the problem defined by the manufactured solution (5.11) on the oscillating cosine surface (5.10), obtained with (4.64).

h	τ	$\max_k \|e_h\|_{L^2(\Gamma_k)}$	EOC	$\max_k \|e_h\|_{H^1(\Gamma_k)}$	EOC
6.017847e-01	3.621448e-01	8.695402e-02	-	8.600986e-01	-
3.050183e-01	9.303619e-02	2.256225e-02	1.99	2.644920e-01	1.74
1.543086e-01	2.381116e-02	7.078734e-03	1.70	1.164576e-01	1.20
1.030957e-01	1.062871e-02	3.003543e-03	2.13	7.370707e-02	1.13
7.738039e-02	5.987725e-03	1.756230e-03	1.87	5.434609e-02	1.06

Table 5.8: Errors and experimental order of accuracy of the problem defined by the manufactured solution (5.11) on the oscillating cosine surface (5.10), obtained with (4.66).

h	τ	$\max_k \varepsilon_h^k(L^2)$	EOC	$\max_k \varepsilon_h^k(H^1)$	EOC
6.017847e-01	3.621448e-01	1.741981e-01	-	1.177418e-01	-
3.050183e-01	9.303619e-02	4.079419e-02	2.14	1.162734e-02	3.41
1.543086e-01	2.381116e-02	1.473923e-02	1.48	2.284432e-03	2.36
1.030957e-01	1.062871e-02	6.167612e-03	2.20	9.083916e-04	2.33
7.738039e-02	5.987725e-03	3.800469e-03	1.69	4.909683e-04	2.14

Table 5.9: Relative errors of the problem defined by the manufactured solution (5.11) on the oscillating cosine surface (5.10), obtained with (4.64).

h	τ	$\max_t \Delta_t M$	$\max_t \delta_t M$
5.460569e-01	2.981782e-01	4.440892e-16	3.181535e-16
3.067358e-01	9.408683e-02	9.992007e-16	1.381521e-15
1.538629e-01	2.367379e-02	2.331468e-15	4.376747e-15
7.592024e-02	5.763882e-03	5.551115e-15	1.020051e-14

Table 5.10: Loss of mass of the numerical solution starting from the discontinuous initial datum (5.9) on the oscillating cosine surface (5.10), obtained with (4.64).

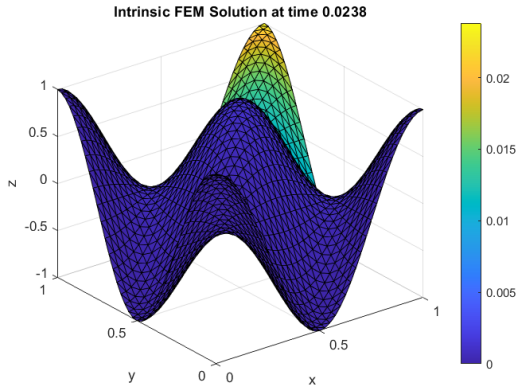

(a) Numerical solution at $t = 0.0238$.

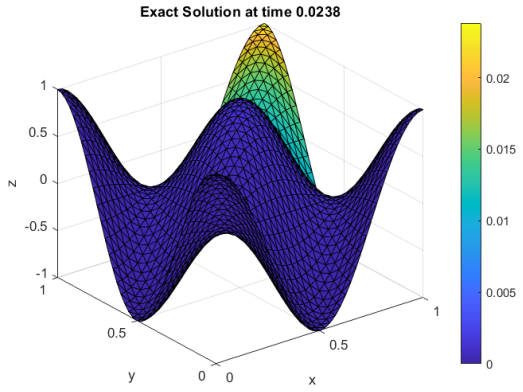

(b) Exact solution (5.11) at $t = 0.0238$.

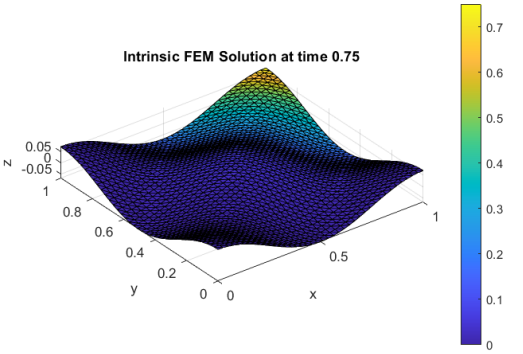

(c) Numerical solution at $t = 0.75$.

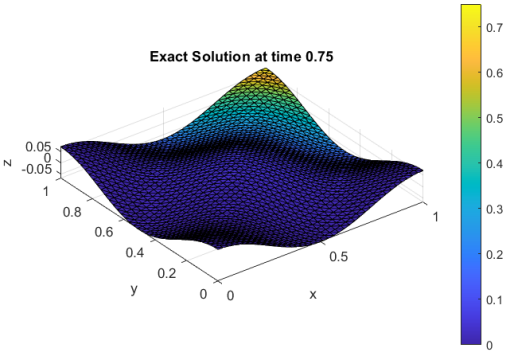

(d) Exact solution (5.11) at $t = 0.75$.

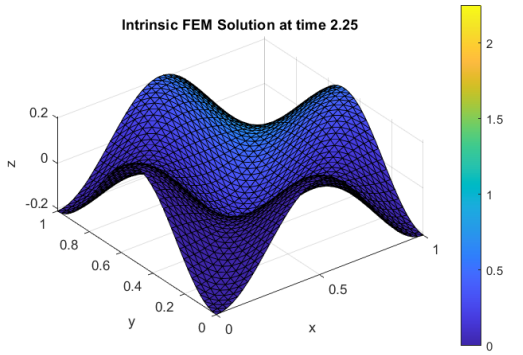

(e) Numerical solution at $t = 2.25$.

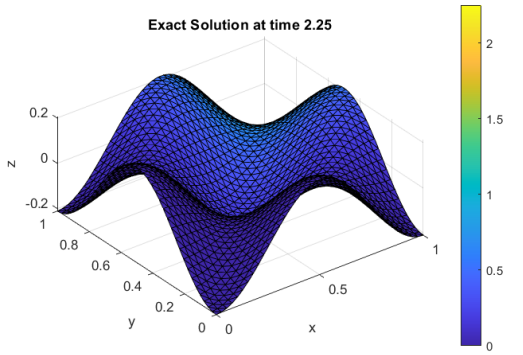

(f) Exact solution (5.11) at $t = 2.25$.

Figure 5.3: Comparison between the numerical solution of the problem on the oscillating cosine surface (5.10) and the exact solution (5.11).

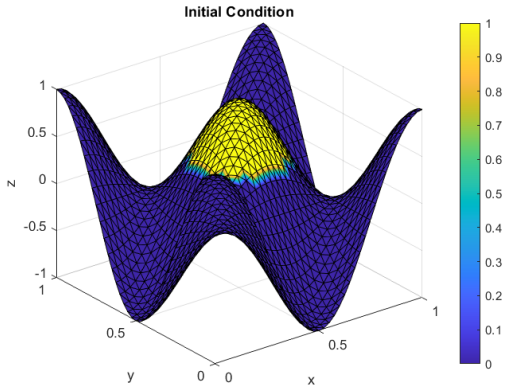

(a) Initial condition.

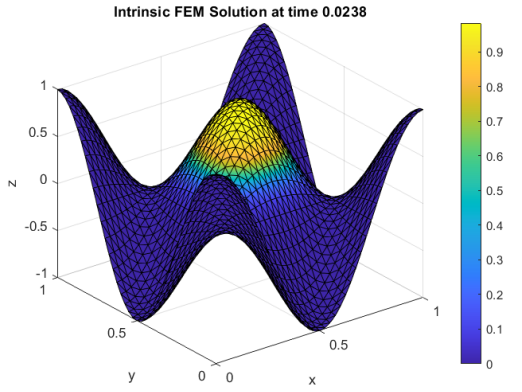

(b) Solution at time $t = 0.0238$.

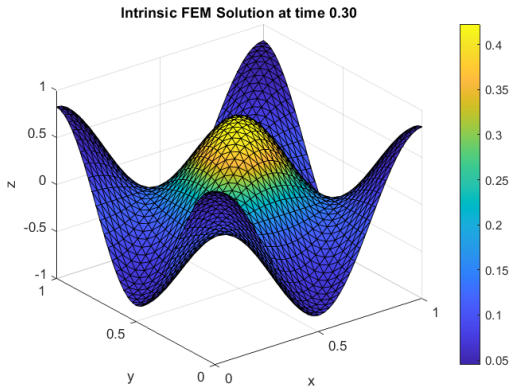

(c) Solution at time $t = 0.30$.

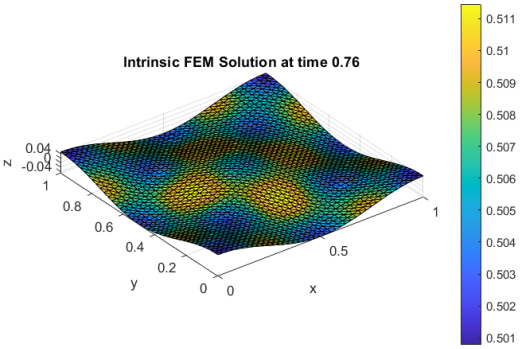

(d) Solution at time $t = 0.76$.

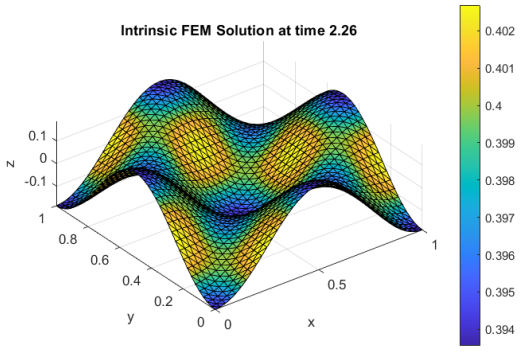

(e) Solution at time $t = 2.26$.

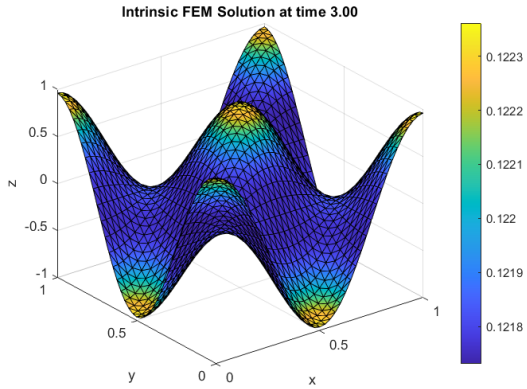

(f) Solution at time $t = 3.00$.

Figure 5.4: Evolution of the discotinuous initial datum (5.9) through the motion of the oscillating cosine surface (5.10).

5.2 General single-chart surfaces

Section 5.1.1 and Section 5.1.2 present simulations in which the surface can be represented as the graph of a function. This structure leads to simplified computations, particularly in the evaluation of the forcing term derived via the method of manufactured solutions. However, throughout this thesis no such assumption is imposed on the numerical scheme, which is therefore expected to remain valid in a much more general setting.

Another class of surfaces on which the solver can be tested consists of those admitting a single global parametrisation.

5.2.1 Enlarging paraboloid

In this section, the surface is the same paraboloid introduced in Section 5.1.1. However, in addition to collapsing onto a plane, it also expands in the x and y directions.

$$\begin{aligned} \phi_t : [0,1]^2 &\to \mathbb{R}^3 \\ (\xi_1, \xi_2) &\longmapsto \left((1+t)\xi_1, (1+t)\xi_2, e^{-t}\left(\xi_1(1-\xi_1) + \xi_2(1-\xi_2)\right)\right) \end{aligned} \tag{5.12}$$

The time window has been chosen to be $[0, 1]$.

Manufactured solution

It is interesting to consider a manufactured solution that depends explicitly on the spatial configuration of the surface. In this case, it coincides with (5.7), although in local coordinates it takes a different form due to the geometry of the underlying surface on which it is defined:

$$\begin{aligned} u(x, y, z, t) &= xyt \\ U(\xi_1, \xi_2, t) &= \xi_1\xi_2(1+t)^2 t \end{aligned} \tag{5.13}$$

Table 5.11, 5.12, 5.13 confirm the optimal convergence rate of the numerical schemes. Table 5.14 reports the relative errors with respect to the discretisation parameters h, τ. Figure 5.5 provides a graphical comparison between the numerical solution and the manufactured exact solution at three different time instants.

Conservation of mass

Again, the discontinuous initial datum defined in Section 5.1 (5.9) has been chosen. Table 5.15 shows that the total mass is conserved throughout the entire simulation, up to machine precision.

Figure 5.6 illustrates the evolution of the initial datum during the motion of the surface, at six different instants of time.

h	τ	$\max_k \lVert e_h \rVert_{L^2(\Gamma_k)}$	EOC	$\max_k \lVert e_h \rVert_{H^1(\Gamma_k)}$	EOC
4.270831e-01	4.560000e-02	4.959770e-02	-	6.632185e-01	-
2.289105e-01	1.310000e-02	1.697152e-02	1.72	3.279828e-01	1.13
1.244381e-01	3.871210e-03	4.543898e-03	2.16	1.721308e-01	1.06
6.022095e-02	9.066406e-04	9.230576e-04	2.20	8.173412e-02	1.03

Table 5.11: Errors and experimental order of accuracy of the problem defined by the manufactured solution (5.13) on the enlarging paraboloid (5.12), obtained with method (4.56).

h	τ	$\max_k \|e_h\|_{L^2(\Gamma_k)}$	EOC	$\max_k \|e_h\|_{H^1(\Gamma_k)}$	EOC
4.270831e-01	4.560000e-02	5.169412-e02	-	6.640568e-01	-
2.289105e-01	1.310000e-02	1.675612e-02	1.81	3.280860e-01	1.13
1.244381e-01	3.871210e-03	4.484145e-03	2.16	1.721479e-01	1.06
6.022095e-02	9.066406e-04	9.054602e-04	2.20	8.168542e-02	1.03

Table 5.12: Errors and experimental order of accuracy of the problem defined by the manufactured solution (5.13) on the enlarging paraboloid (5.12), obtained with method (4.64).

h	τ	$\max_k \|e_h\|_{L^2(\Gamma_k)}$	EOC	$\max_k \|e_h\|_{H^1(\Gamma_k)}$	EOC
4.270831e-01	4.560000e-02	5.041836e-02	-	6.635474e-01	-
2.289105e-01	1.310000e-02	1.687998e-02	1.75	3.280233e-01	1.13
1.244381e-01	3.871210e-03	4.518220e-03	2.16	1.721376e-01	1.06
6.022095e-02	9.066406e-04	9.163002e-04	2.20	8.347355e-02	1.00

Table 5.13: Errors and experimental order of accuracy of the problem defined by the manufactured solution (5.13) on the enlarging paraboloid (5.12), obtained with method (4.66).

h	τ	$\max_k \varepsilon_h^k(L^2)$	EOC	$\max_k \varepsilon_h^k(H^1)$	EOC
4.270831e-01	4.560000e-02	6.141285e-02	-	4.734995e-02	
2.289105e-01	1.310000e-02	2.687747e-02	1.32	1.201000e-02	2.20
1.244381e-01	3.871210e-03	9.781366e-03	1.66	3.195761e-03	2.17
6.022095e-02	9.066406e-04	2.580458e-03	1.84	8.853348e-04	1.77

Table 5.14: Relative errors of the problem defined by the manufactured solution (5.13) on the enlarging paraboloid (5.12), obtained with method (4.64).

h	τ	$\max_k \Delta_k M$	$\max_k \delta_k M$
5.153882e-01	2.656250e-01	6.938894e-17	9.868649e-16
2.524080e-01	6.370980e-02	2.498002e-16	1.580607e-15
1.244381e-01	1.548484e-02	9.159340e-16	7.203469e-15
6.173847e-02	3.811638e-03	1.554312e-15	1.183475e-14

Table 5.15: Loss of mass of the numerical solution starting from the discontinuous initial datum (5.9) on the enlarging paraboloid (5.12), obtained with method (4.64).

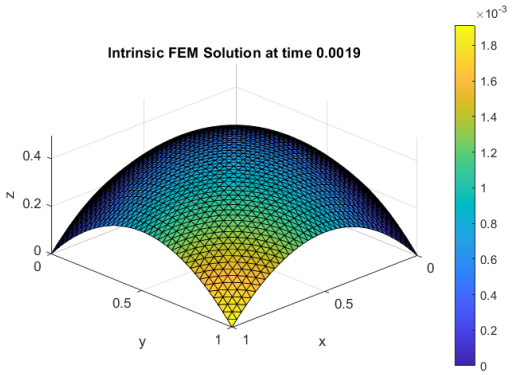

(a) Numerical solution at $t = 0.0019$.

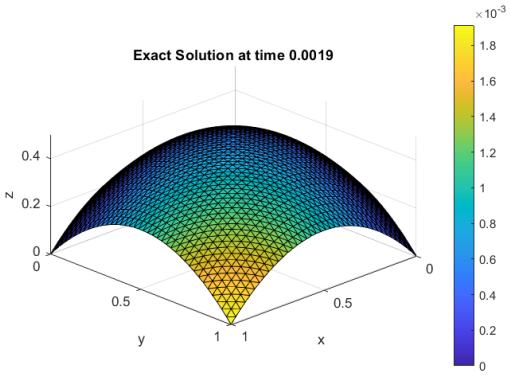

(b) Exact solution (5.13) at $t = 0.0019$.

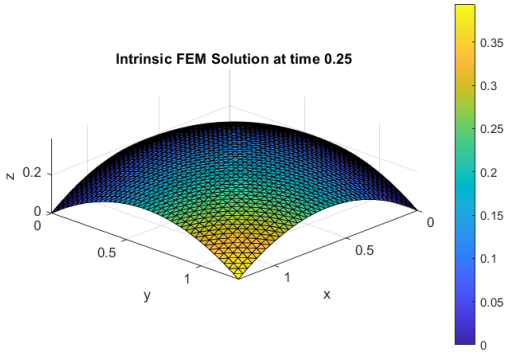

(c) Numerical solution at $t = 0.25$.

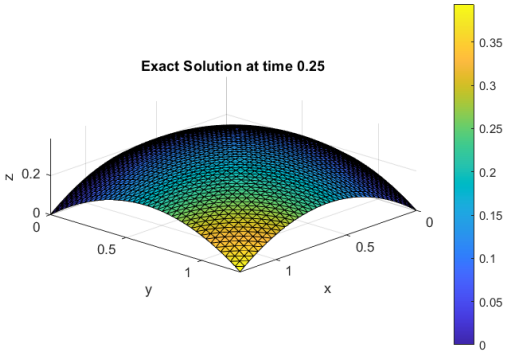

(d) Exact solution (5.13) at $t = 0.25$.

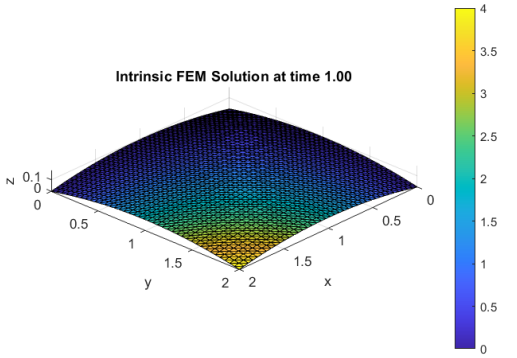

(e) Numerical solution at $t = 1.00$.

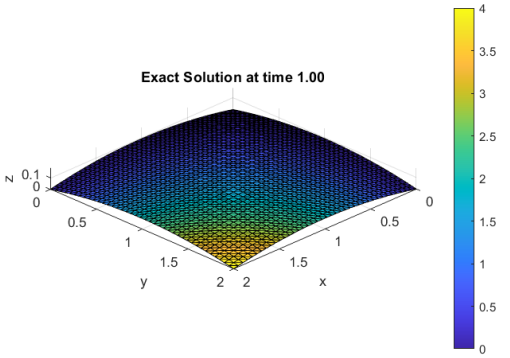

(f) Exact solution (5.13) at $t = 1.00$.

Figure 5.5: Comparison between the numerical solution of the problem on the enlarging paraboloid (5.12) and the exact solution (5.13).

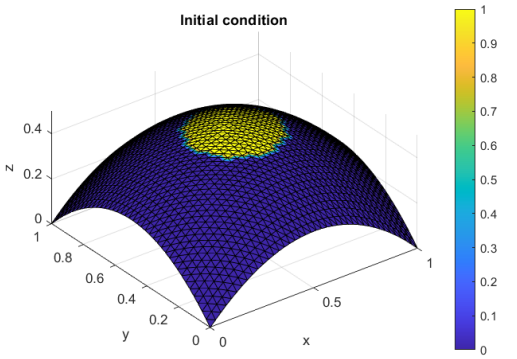

(a) Initial condition.

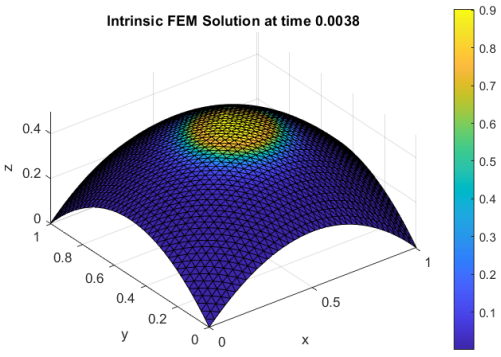

(b) Solution at time $t = 0.0038$.

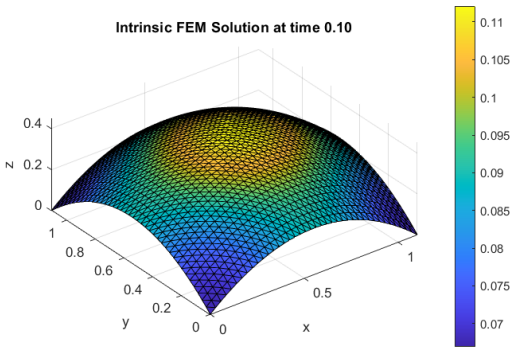

(c) Solution at time $t = 0.10$.

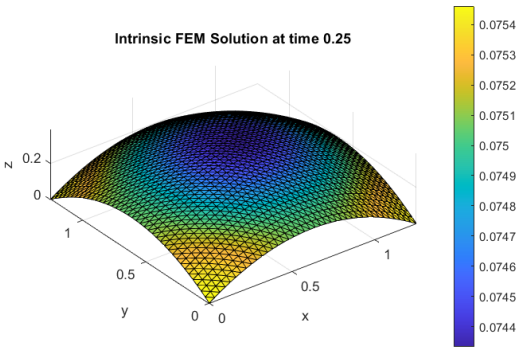

(d) Solution at time $t = 0.25$.

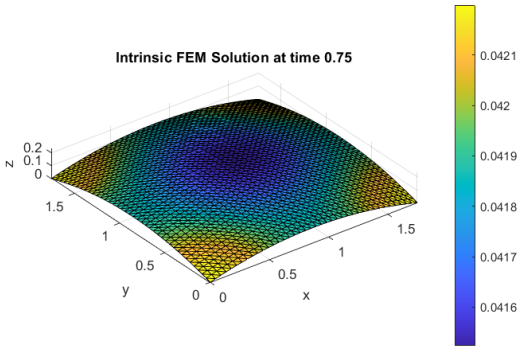

(e) Solution at time $t = 0.75$.

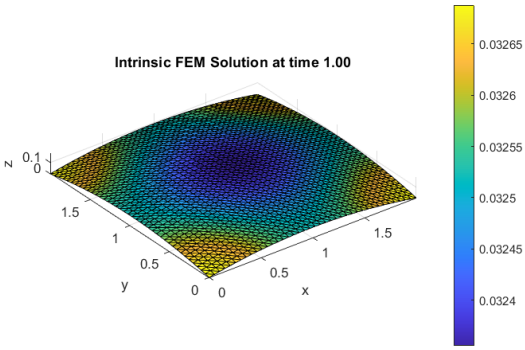

(f) Solution at time $t = 1.00$.

Figure 5.6: Evolution of the initial datum (5.9) through the motion of the enlarging paraboloid (5.12).

5.2.2 Enlarging perforated sphere

The previous example demonstrated the effectiveness of the solver for a surface that is not the graph of a function. However, the similarity between the chart and the xy plane may limit the generality of the benchmark. A more general example is given by the sphere parametrised in polar coordinates. Unfortunately, the sphere does not admit a single global regular parametrisation, since polar coordinates lead to a degenerate differential at the poles. Nevertheless, it is possible to consider a perforated sphere, obtained by removing small neighborhoods of the poles, which admits a regular parametrisation:

$$\begin{aligned} \phi_t : [0, 2\pi] \times \left[\frac{\pi}{12}, \frac{11\pi}{12}\right] &\to \mathbb{R}^3 \\ (\xi_1, \xi_2) &\longmapsto (1+t)\,(\cos(\xi_1)\sin(\xi_2), \sin(\xi_1)\sin(\xi_2), \cos(\xi_2)) \end{aligned} \tag{5.14}$$

Manufactured solution

Meshing the chart instead of the surface leads to a significant stretching of the surface elements. This is the main drawback of the proposed approach, with important consequences on the error behaviour, as reported in Table 5.16, 5.17, 5.18 and Table 5.19 . Nevertheless, the observed convergence rates remain satisfactory, since this effect is related to the mesh quality rather than to the numerical scheme itself. In other words, even if the triangles are highly distorted, halving the mesh size should still yield the expected reduction in the error.
The manufactured solution chosen for this simulation is general and non symmetric:

$$\begin{aligned} u(x, y, z, t) &= x + y - z \\ U(\xi_1, \xi_2, t) &= (1+t)\,(\cos(\xi_1)\sin(\xi_2) + \sin(\xi_1)\sin(\xi_2) - \cos(\xi_2)) \end{aligned} \tag{5.15}$$

Figure (5.7) compares graphically the numerical solution to the exact solution (5.15) at three different time instants.

Conservation of mass

Again, in order to better illustrate the diffusion of an initially concentrated mass during the simulation, a discontinuous initial datum has been chosen. For simplicity, it is defined directly on the chart:

$$U_0(\boldsymbol{\xi}) = \mathbf{1}_Q \tag{5.16}$$

with $Q = \{(\xi_1, \xi_2) : 0.75\pi \le \xi_1 \le 1.25\pi, 0.3\pi \le \xi_2 \le 0.7\pi\}$. Table 5.20 shows that the total mass is conserved throughout the entire simulation time. Figure 5.8 illustrates the evolution of the initial datum during the motion of the surface, at six different instants of time.

h	τ	$\max_k \|e_h\|_{L^2(\Gamma_k)}$	EOC	$\max_k \|e_h\|_{H^1(\Gamma_k)}$	EOC
4.360163e-01	9.505512e-02	8.363990e-01	-	2.448829e+00	-
2.115008e-01	2.236628e-02	1.678157e-01	2.22	1.040977e+00	1.18
1.040177e-01	5.409843e-03	3.565291e-02	2.18	4.969659e-01	1.04
5.156604e-02	1.329528e-03	5.993281e-03	2.54	2.516980e-01	0.97

Table 5.16: Errors and experimental order of accuracy of the problem defined by the manufactured solution (5.15) on the enlarging perforated sphere (5.14), obtained with method (4.56).

h	τ	$\max_k \|e_h\|_{L^2(\Gamma_k)}$	EOC	$\max_k \|e_h\|_{H^1(\Gamma_k)}$	EOC
4.360163e-01	9.505512e-02	8.126443e-01	-	2.422457e+00	-
2.115008e-01	2.236628e-02	1.620849e-01	2.23	1.037410e-00	1.17
1.040177e-01	5.409843e-03	3.423210e-02	2.19	4.964484e-01	1.04
5.156604e-02	1.329528e-03	5.853458e-03	2.52	2.445239e-01	1.01

Table 5.17: Errors and experimental order of accuracy of the problem defined by the manufactured solution (5.15) on the enlarging perforated sphere (5.14), obtained with method (4.64).

h	τ	$\max_k \|e_h\|_{L^2(\Gamma_k)}$	EOC	$\max_k \|e_h\|_{H^1(\Gamma_k)}$	EOC
4.360163e-01	9.505512e-02	7.420037e-01	-	2.376078e+00	-
2.115008e-01	2.236628e-02	1.463744e-01	2.24	1.032487e+00	1.15
1.040177e-01	5.409843e-03	3.046122e-02	2.21	4.959116e-01	1.03
5.156604e-02	1.329528e-03	5.956457e-03	2.32	2.480095e-01	0.99

Table 5.18: Errors and experimental order of accuracy of the problem defined by the manufactured solution (5.15) on the enlarging perforated sphere (5.14), obtained with method (4.66).

h	τ	$\max_k \varepsilon_h^k(L^2)$	EOC	$\max_k \varepsilon_h^k(H^1)$	EOC
4.360163e-01	9.505512e-02	5.851975e-02	-	3.737746e-02	-
2.115008e-01	2.236628e-02	1.163991e-02	2.23	7.758092e-03	2.17
1.040177e-01	5.409843e-03	2.489394e-03	2.17	1.824474e-03	2.04
5.156604e-02	1.329528e-03	4.746604e-04	2.36	4.452962e-04	2.01

Table 5.19: Relative errors of the problem defined by the manufactured solution (5.15) on the enlarging perforated sphere (5.14), obtained with method (4.64).

h	τ	$\max_t \Delta_t M$	$\max_t \delta_t M$
6.559183e-01	4.302289e-01	1.387779e-16	6.047797e-16
3.203396e-01	1.026175e-01	5.551115e-16	2.751477e-15
1.565816e-01	2.451779e-02	1.859624e-15	9.782706e-15
7.735167e-02	5.983281e-03	2.942091e-15	1.592451e-14

Table 5.20: Loss of mass of the numerical solution starting from the discontinuous initial datum (5.16) on the enlarging perforated sphere (5.14), obtained with method (4.64).

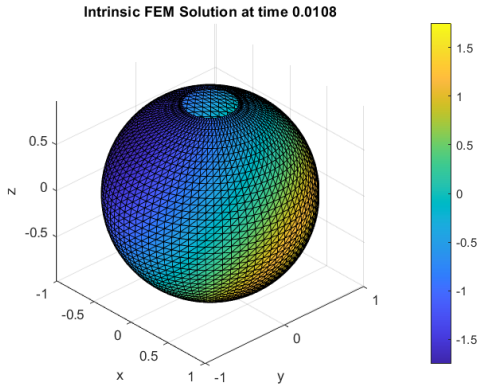

(a) Numerical solution at $t = 0.0108$.

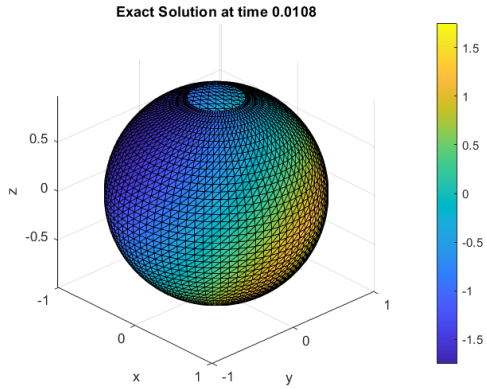

(b) Exact solution (5.15) at $t = 0.0108$.

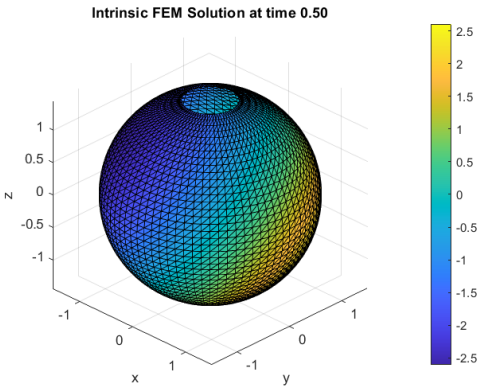

(c) Numerical solution at $t = 0.50$.

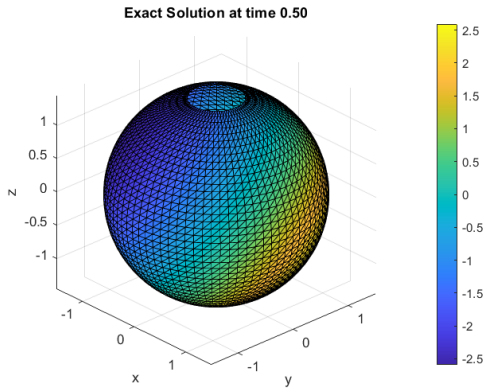

(d) Exact solution (5.15) at $t = 0.50$.

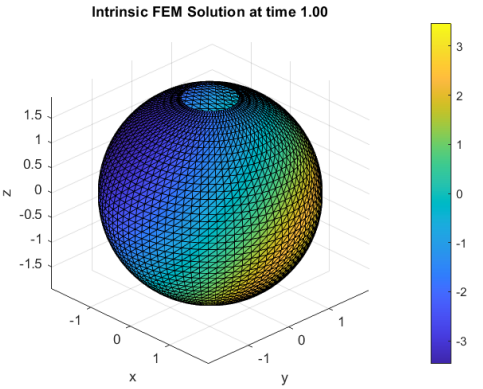

(e) Numerical solution at $t = 1.00$.

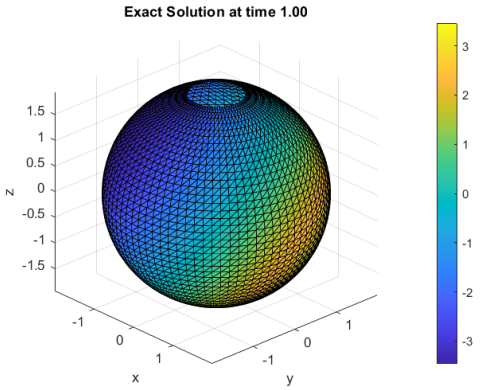

(f) Exact solution (5.15) at $t = 1.00$.

Figure 5.7: Comparison between the numerical solution of the problem on the enlarging perforated sphere (5.14) and the exact solution (5.15).

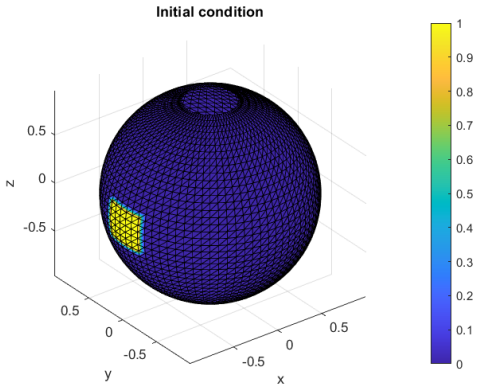

(a) Initial condition.

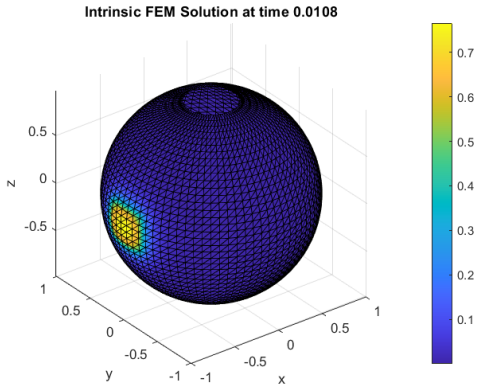

(b) Solution at time $t = 0.0108$.

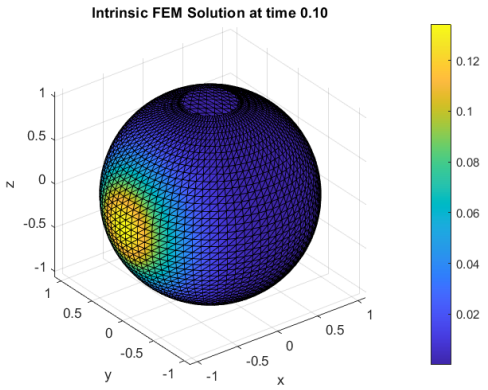

(c) Solution at time $t = 0.10$.

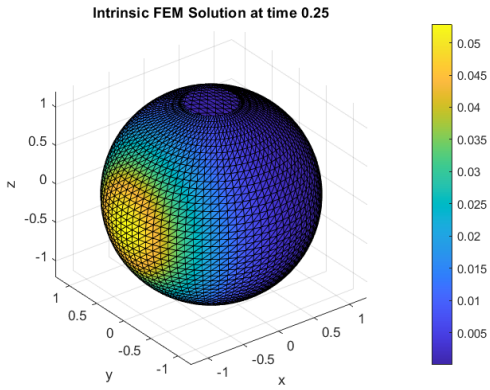

(d) Solution at time $t = 0.25$.

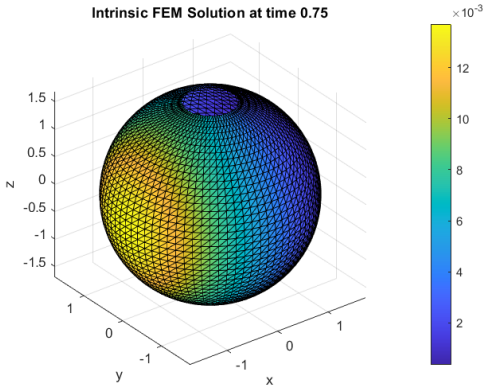

(e) Solution at time $t = 0.75$.

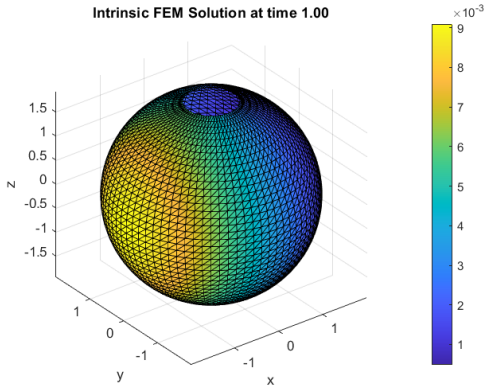

(f) Solution at time $t = 1.00$.

Figure 5.8: Evolution of the discontinuous initial datum (5.16) through the motion of the enlarging perforated sphere (5.14).

5.3 Multi-chart surfaces

The primary objective of the E-ISFEM formulation is to operate entirely in terms of intrinsic quantities, thereby avoiding any dependence on the particular embedding of the surface in the surrounding space. To accomplish this, the formulation is built upon local parametrisations of the surface, whose existence is ensured under suitable smoothness assumptions. These local descriptions provide the natural framework in which the intrinsic geometric and analytical quantities involved in the method can be defined and computed.

For the sake of simplicity and to streamline the presentation of the theoretical and numerical developments, the existence of a single global parametrisation has often been assumed throughout this thesis. This assumption significantly simplifies the notation and avoids the technicalities associated with handling multiple coordinate charts. Nevertheless, as has been repeatedly pointed out, this simplification does not represent a genuine restriction of the methodology and does not lead to any loss of generality. In particular, the extension of the construction to the case of multiple local parametrisations follows naturally from the framework developed in the previous chapters; see, for example, the discussion in Section 4.1.4.

The aim of this section is to provide further numerical evidence supporting these observations. To this end, we consider simulations on surfaces that cannot be represented by a single global parametrisation and therefore necessarily require the use of multiple local charts. These examples illustrate the applicability of the E-ISFEM framework in a more general setting and demonstrate that the method retains its effectiveness when the surface is described through an atlas of local parametrisations.

5.3.1 Enlarging sphere

This example considers a sphere whose radius increases linearly in time. An intrinsic description can be given using the following two local parametrisations:

$$\begin{aligned} &\phi_t^N : \mathbb{R}^2 \to S^2 \setminus \{N\} \\ &(\xi_1, \xi_2) \longmapsto (1+t)\left(\frac{2\xi_1}{\xi_1^2+\xi_2^2+1}, \frac{2\xi_2}{\xi_1^2+\xi_2^2+1}, \frac{\xi_1^2+\xi_2^2-1}{\xi_1^2+\xi_2^2+1}\right) \end{aligned} \tag{5.17}$$

$$\begin{aligned} &\phi_t^S : \mathbb{R}^2 \to S^2 \setminus \{S\} \\ &(\xi_1, \xi_2) \longmapsto (1+t)\left(\frac{2\xi_1}{\xi_1^2+\xi_2^2+1}, \frac{2\xi_2}{\xi_1^2+\xi_2^2+1}, \frac{1-\xi_1^2-\xi_2^2}{\xi_1^2+\xi_2^2+1}\right) \end{aligned} \tag{5.18}$$

These parametrisations are obtained as the inverse mappings of the classical stereographic projections of the sphere onto the plane $\mathbb{R}^2$. The use of stereographic coordinates provides a convenient local description of the surface while preserving its smooth geometric structure. It is important to observe that neither of the two parametrisations alone is sufficient to describe the entire sphere. However, the mappings defined in (5.17) and (5.18) complement each other and, taken together, provide a complete representation of the surface. More precisely, they form an atlas (Definition 2.2) for the sphere for every $t \in [0, T]$, thereby ensuring that the whole evolving surface can be covered by a collection of smooth local charts.

Manufactured solution

Another noteworthy difference with respect to the previous examples is that, in the present setting, no boundary conditions need to be imposed. This feature reflects the fact that the underlying surface is closed and therefore does not possess a boundary. Consequently, the verification of the method

through the use of manufactured solutions serves a dual purpose. On the one hand, it confirms the correctness and accuracy of the proposed numerical approach. On the other hand, it provides additional numerical evidence supporting the discussion on boundary conditions presented in Chapter 3, illustrating that the formulation remains consistent and effective even in the absence of boundary contributions. The chosen exact solution for this simulation reads:

$$\begin{aligned} u(x, y, z, t) &= xy \\ u \circ \phi_t^N(\xi_1, \xi_2, t) &= \frac{4\xi_1\xi_2(1+t)^2}{\xi_1^2 + \xi_2^2 + 1} \\ u \circ \phi_t^S(\xi_1, \xi_2, t) &= \frac{4\xi_1\xi_2(1+t)^2}{\xi_1^2 + \xi_2^2 + 1} \end{aligned} \tag{5.19}$$

Table 5.21, 5.22, 5.23 compare the experimental results obtained with the three different methods. Table 5.24 shows the relative errors of the E-ISFEM solution, while Figure 5.9 compares the numerical solution to the exact solution at three different time instants.

Conservation of mass

Again, the solver can be shown to be conservative by running simulation with a given initial condition and zero forcing term.

$$u_0(x, y, z) = \mathbf{1}_A \tag{5.20}$$

with $A = \{(x, y, z) \in S^2 : x < 0, y \in [-0.2, 0.2], z \in [-0.2, 0.2]\}$. Table 5.25 shows the conservative property of the method, while Figure 5.10 shows the evolution of the initial condition together with the evolution of the surface itself.

h	τ	$\max_k \|e_h\|_{L^2(\Gamma_k)}$	EOC	$\max_k \|e_h\|_{H^1(\Gamma_k)}$	EOC
6.180340e-01	3.819660e-02	8.766819e-01	-	4.774687e+00	-
3.249197e-01	1.055728e-02	3.315665e-01	1.51	2.555074e+00	0.97
1.646472e-01	2.710869e-03	7.108680e-02	2.27	1.235542e+00	1.07
8.260397e-02	6.823415e-04	1.634255e-03	2.13	6.223890e-01	0.99

Table 5.21: Errors and experimental order of accuracy of the problem defined by the manufactured solution (5.19) on the enlarging sphere, obtained with method (4.56).

h	τ	$\max_k \|e_h\|_{L^2(\Gamma_k)}$	EOC	$\max_k \|e_h\|_{H^1(\Gamma_k)}$	EOC
6.180340e-01	3.819660e-02	5.882342e-01	-	4.722172e+00	-
3.249197e-01	1.055728e-02	1.879289e-01	1.77	2.440042e+00	1.03
1.646472e-01	2.710869e-03	4.424189e-02	2.13	1.224430e+00	1.01
8.260397e-02	6.823415e-04	1.277260e-02	1.80	6.130450e-01	1.00

Table 5.22: Errors and experimental order of accuracy of the problem defined by the manufactured solution (5.19) on the enlarging sphere, obtained with method (4.64).

h	τ	$\max_k \|e_h\|_{L^2(\Gamma_k)}$	EOC	$\max_k \|e_h\|_{H^1(\Gamma_k)}$	EOC
6.180340e-01	3.819660e-02	3.966045e-01	-	4.635374e+00	-
3.249197e-01	1.055728e-02	1.370835e-01	1.65	2.426057e+00	1.01
1.646472e-01	2.710869e-03	3.142377e-02	2.17	1.222698e+00	1.01
8.260397e-02	6.823415e-04	9.804824e-03	1.69	6.148501e-01	1.00

Table 5.23: Errors and experimental order of accuracy of the problem defined by the manufactured solution (5.19) on the enlarging sphere, obtained with method (4.66).

h	τ	$\max_k \varepsilon_h^k(L^2)$	EOC	$\max_k \varepsilon_h^k(H^1)$	EOC
6.180340e-01	3.819660e-02	9.773257e-02	-	2.610081e-01	-
3.249197e-01	1.055728e-02	2.759408e-02	1.97	7.347989e-02	1.97
1.646472e-01	2.710869e-03	6.623080e-03	2.10	1.895030e-02	1.99
8.260397e-02	6.823415e-04	1.805450e-03	1.88	4.777715e-03	2.00

Table 5.24: Relative errors of the problem defined by the manufactured solution (5.19) on the enlarging sphere, obtained with method (4.64).

h	τ	$\max_t \Delta_t M$	$\max_t \delta_t M$
6.180340e-01	3.819660e-01	6.106227e-16	1.939191e-15
3.249197e-01	1.055728e-01	2.220446e-16	2.819462e-15
1.646472e-01	2.710869e-02	1.332268e-15	9.636331e-15
8.260397e-02	6.823415e-03	2.886580e-15	1.695688e-14

Table 5.25: Loss of mass of the numerical solution starting from the discontinuous initial datum (5.20) on the enlarging sphere, obtained with method (4.64).

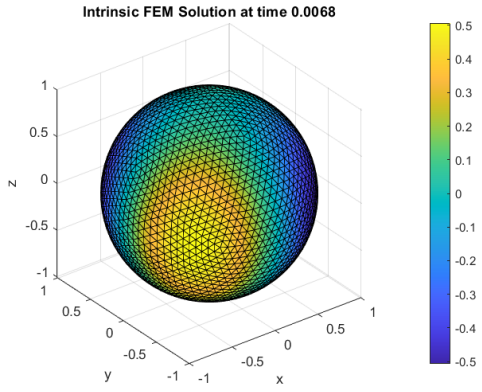

(a) Numerical solution at $t = 0.0068$.

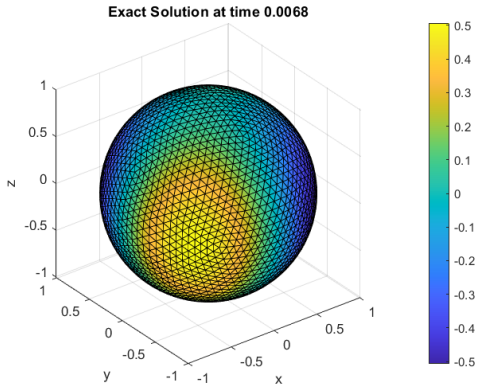

(b) Exact solution (5.19) at $t = 0.0068$.

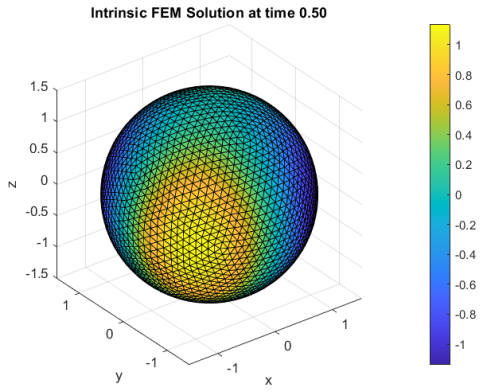

(c) Numerical solution at $t = 0.50$.

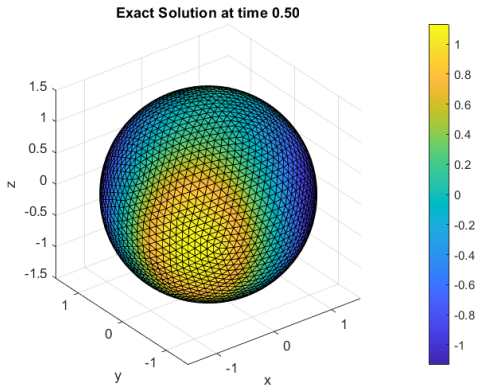

(d) Exact solution (5.19) at $t = 0.50$.

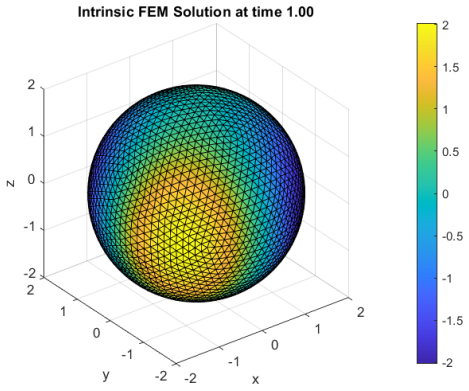

(e) Numerical solution at $t = 1.00$.

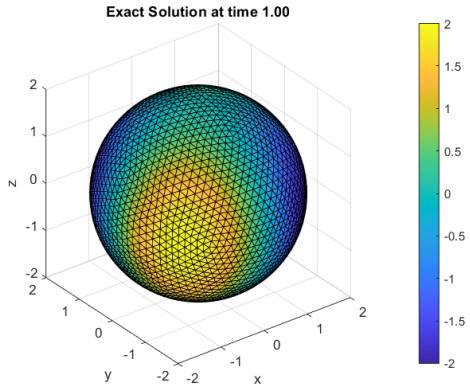

(f) Exact solution (5.19) at $t = 1.00$.

Figure 5.9: Comparison between the numerical solution and the exact solution (5.19) of the problem on the enlarging sphere.

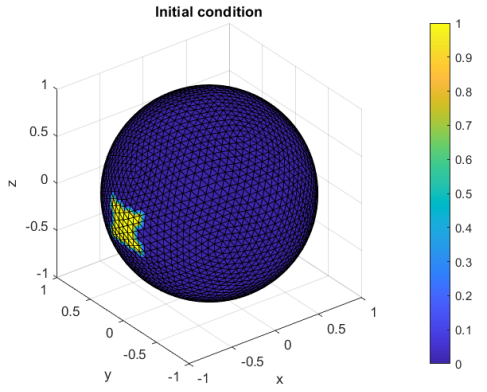

(a) Initial condition.

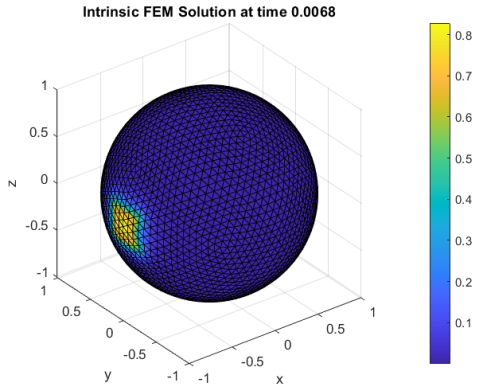

(b) Solution at time $t = 0.0068$.

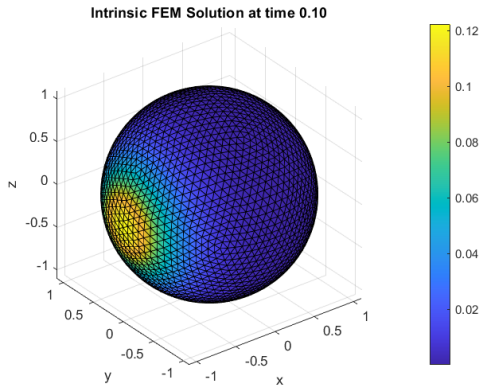

(c) Solution at time $t = 0.10$.

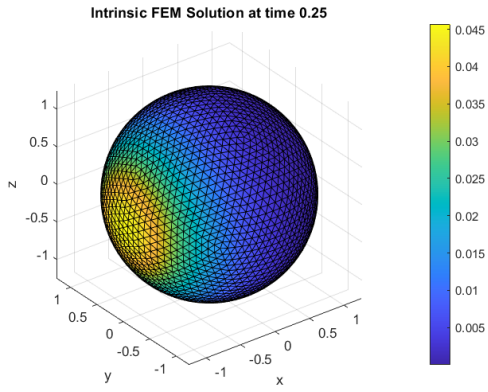

(d) Solution at time $t = 0.25$.

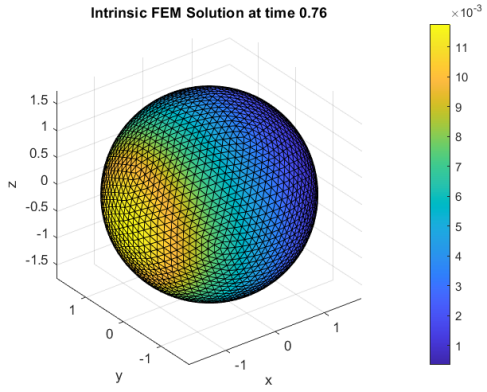

(e) Solution at time $t = 0.76$.

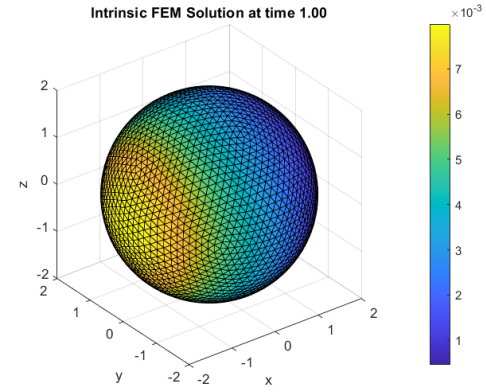

(f) Solution at time $t = 1.00$.

Figure 5.10: Evolution of the initial datum (5.20) through the motion of the enlarging sphere.

5.3.2 Ellipsoid

As a final validation of the numerical scheme, the same example considered in [18] is used. The purpose of this simulation is to compare the numerical results obtained with the E-ISFEM approach against those produced by the classical and well-established ESFEM method, in order to show that the intrinsic formulation presented in this thesis provides an effective alternative to the embedded framework.

The target surface is a unit sphere whose extension in the x-direction increases over time, causing the sphere to deform into an ellipsoid.

$$\Gamma_t = \left\{ \mathbf{x} \in \mathbb{R}^3 : \frac{x^2}{1 + 0.25\sin(t)} + y^2 + z^2 = 1 \right\} \tag{5.21}$$

The surface can be easily parametrised with a slight modification of what has been done in Section 5.3.1:

$$\begin{aligned} &\phi_t^N : \mathbb{R}^2 \to \Gamma_t \setminus \{N\} \\ &(\xi_1, \xi_2) \longmapsto \left(\frac{2\xi_1\sqrt{1 + 0.25\sin(t)}}{\xi_1^2 + \xi_2^2 + 1}, \frac{2\xi_2}{\xi_1^2 + \xi_2^2 + 1}, \frac{\xi_1^2 + \xi_2^2 - 1}{\xi_1^2 + \xi_2^2 + 1} \right) \end{aligned} \tag{5.22}$$

$$\begin{aligned} &\phi_t^S : \mathbb{R}^2 \to \Gamma_t \setminus \{S\} \\ &(\xi_1, \xi_2) \longmapsto \left(\frac{2\xi_1\sqrt{1 + 0.25\sin(t)}}{\xi_1^2 + \xi_2^2 + 1}, \frac{2\xi_2}{\xi_1^2 + \xi_2^2 + 1}, \frac{1 - \xi_1^2 - \xi_2^2}{\xi_1^2 + \xi_2^2 + 1} \right) \end{aligned} \tag{5.23}$$

The manufactured solution chosen in [18] is the following exponentially decaying function:

$$u(x, y, z, t) = e^{-6t} xy \tag{5.24}$$

In order to make a precise comparison with [18], it is necessary to introduce the following additional numerical errors:

$$\max_k \|e_h\|_{L^\infty(\Gamma_k)} = \max_k \sup_{\Gamma_k} |u - u_h| \tag{5.25}$$

$$\|e_h\|_{L^2([0,T], H^1(\Gamma_t))} = \sqrt{\int_0^T \left\| \nabla_{G_t} (u - u_h) \right\|^2_{L^2(\Gamma_t)} dt} \tag{5.26}$$

The time step is chosen accordingly as $\tau = h^2$, and the time interval is $[0, 2]$. Table 5.26 reports the numerical results obtained with the solver presented in this work, while Table 5.27 is taken directly from [18]. At first glance, the two tables are in good agreement: for coarse meshes, Table 5.26 exhibits larger errors, but due to a higher experimental order of convergence than that observed in Table 5.27, it achieves smaller errors for finer meshes.
Figure 5.11 shows the solution at the initial and final times of the simulation.

h	$\max_k \|e_h\|_{L^\infty(\Gamma_k)}$	EOC	$\max_k \|e_h\|_{L^2(\Gamma_k)}$	EOC	$\|e_h\|_{L^2([0,T],H^1(\Gamma_k))}$	EOC
6.846869e-01	9.740829e-02	-	2.024240e-01	-	2.688263e-01	-
3.599612e-01	4.765595e-02	1.11	8.959366e-02	1.27	1.631804e-01	0.77
1.824038e-01	1.375472e-02	1.83	2.572145e-02	1.84	8.506341e-02	0.96
9.151253e-02	3.444838e-03	2.01	6.622062e-03	1.97	4.393885e-02	0.96
4.579534e-02	5.767319e-04	2.58	1.245321e-03	2.41	2.218133e-02	1.01

Table 5.26: Errors and experimental order of accuracy of the problem defined by the manufactured solution (5.24) on the ellipsoid (5.21), solved with E-ISFEM numerical scheme (4.64).

h	$\max_k \|e_h\|_{L^\infty(\Gamma_k)}$	EOC	$\max_k \|e_h\|_{L^2(\Gamma_k)}$	EOC	$\|e_h\|_{L^2([0,T],H^1(\Gamma_k))}$	EOC
8.2737e-01	9.5488e-02	-	1.5424e-01	-	2.9287e-01	-
4.3422e-01	5.7944e-02	0.77	9.7788e-02	0.71	1.7507e-01	0.80
2.1939e-01	1.8764e-02	1.65	3.3083e-02	1.59	7.4327e-02	1.26
1.0994e-01	5.0819e-03	1.89	8.9784e-03	1.89	3.3367e-02	1.16
5.5007e-02	1.3038e-03	1.97	2.2950e-03	1.97	1.6053e-02	1.06

Table 5.27: Errors and experimental order of accuracy of the problem defined by the manufactured solution (5.24) on the ellipsoid (5.21), solved with ESFEM numerical scheme. This table is taken from [18].

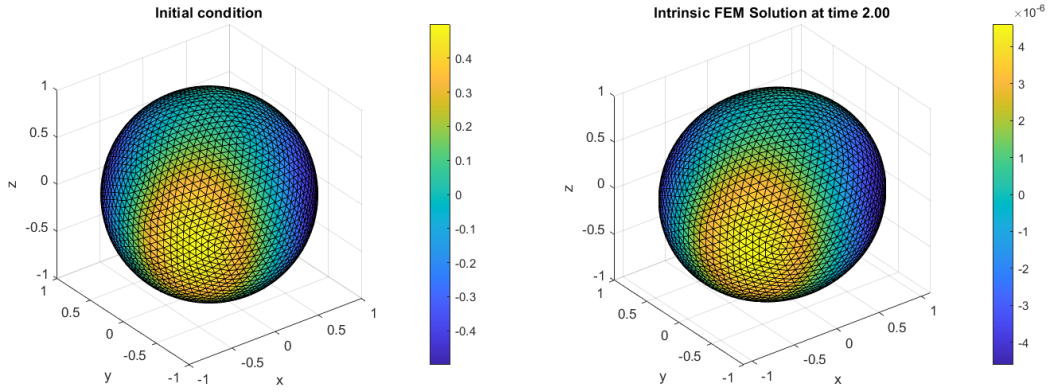

(a) Initial condition.

(b) Numerical solution at $t = 2.0$.

Figure 5.11: Graphical representation of the numerical solution of the problem defined by the manufactured solution (5.24) on the moving ellipsoid (5.21).

Chapter 6

Conclusions

This thesis has analysed an Evolving Intrinsic Surface Finite Element Method (E-ISFEM) for linear parabolic PDEs posed on moving surfaces. The work combines a differential geometric formulation of the problem with a rigorous Finite Element analysis and a series of numerical experiments that confirm the theoretical predictions.

On the analytical side, the governing conservation law was derived entirely in intrinsic terms. Stability and convergence of the semi-discrete and fully discrete formulations were established considering the abstract evolving space framework of [2], with explicit attention paid to the dependence of the stability constants on intrinsic geometric quantities such as the metric tensor G_t and the surface-measure factor λ. Optimal convergence rates of order $O(h^2)$ in the L^2 norm and $O(h)$ in the H^1 norm were proved for the spatial discretisation, while first-order accuracy in time was established for the backward Euler scheme.

On the computational side, the thesis presented a flexible strategy for computing the local FEM matrices based solely on the knowledge of the tangent planes at the mesh nodes. By introducing manufactured elements parametrisations, this approach preserves the exact surface geometry and introduces discretisation effects only through numerical quadrature. This is particularly relevant for applications in which the surface is known only through the mesh nodes and, possibly, the corresponding tangent planes. The procedure was shown to extend naturally to surfaces that require more than one parametrisation, broadening the applicability of the method well beyond graph-type surfaces.

The numerical experiments confirmed the expected optimal convergence rates on all test cases, ranging from smooth graph surfaces to closed surfaces such as the sphere and the ellipsoid. Mass conservation was verified to hold up to machine precision in every simulation. The direct comparison with the classical ESFEM results on the deforming ellipsoid showed that the E-ISFEM formulation achieves comparable accuracy.

Several directions remain open for future investigation. Despite of its experimental evidence, as discussed in Section 4.1.4, a rigorous analytical proof of the second-order accuracy of the quadrature rules is currently unavailable. Establishing such a result would enhance the theoretical foundation of the numerical method and constitutes a natural direction for future research aimed at complementing and strengthening the contributions of this dissertation. Finally, an extension to vector valued and tensor valued problems, for which the intrinsic framework is expected to offer the most significant advantages over embedded methods, represents a particularly promising direction.

Declaration of the Use of Artificial Intelligence Tools.

Artificial intelligence-based language assistance tools (ChatGPT, Gemini, and Claude) were used during the preparation of this thesis solely for language editing purposes, including the improvement of English grammar, clarity, and stylistic fluency. No scientific content, analyses, results, interpretations, or conclusions were generated by these tools. All text was critically reviewed by the author, who assumes full responsibility for the final content of the thesis.

References

[1] M. Abate and F. Tovena, *Curves and Surfaces*, Springer-Verlag , 2012.

[2] A. Alphonse, C. M. Elliott and B. Stinner, An abstract framework for parabolic PDEs on evolving spaces, *Portugaliae Mathematica*, 72(1): 1-46, 2015a.

[3] A. Alphonse, C. M. Elliott and B. Stinner, On some linear parabolic PDEs on moving hypersurfaces, *Interfaces and Free Boundaries*, 17:157-187, 2015b.

[4] E. Bachini, P. Brandner, T. Jankuhn, M. Nestler, S. Praetorius, A. Reusken and A. Voigt, Diffusion of tangential tensor fields: numerical issues and influence of geometric properties, *Journal of Numerical Mathematics*, 32(1):55-75, 2024.

[5] E. Bachini, M.W. Farthing and M. Putti, Intrinsic finite element method for advection-diffusion-reaction equations on surfaces, *Journal of Computational Physics*, 424:109827, 2021.

[6] E. Bachini, V. Krause, I. Nitschke and A. Voigt, Derivation and simulation of a two-phase fluid deformable surface model, *Journal of Fluid Mechanics*, 977:A41, 2023.

[7] E. Bachini, G. Manzini and M. Putti, Arbitrary-order intrinsic virtual element method for elliptic equations on surfaces, *Calcolo*, 58:30, 2021.

[8] E. Bachini and M. Putti, Geometrically Intrinsic Modeling of Shallow Water Flows, *Mathematical Modelling and Numerical Analysis*, 54(6):2125-2157, 2020.

[9] E. Bachini and M. Putti, Convergence analysis of the intrinsic surface finite element method, *arXiv:2203.073302v2*, 2024.

[10] G. D. Birkhoff and G. Rota, *Ordinary Differential Equations*, Ginn and Company, 1962.

[11] H. Brezis, *Functional Analysis, Sobolev Spaces and Partial Differential Equations*, Springer, 2011.

[12] R. L. Burden, J. D. Faires, *Numerical Analysis*, Cengage Learning, 1978.

[13] P. Cermelli, E. Fried and M.E. Gurtin, Transport relations for surface integrals arising in the formulation of balance laws for evolving fluid interfaces, *Journal of Fluid Mechanics*, 544:339-351, 2005.

[14] G. Dziuk, Finite elements for the Beltrami operator on arbitrary surfaces, *Partial Differential Equations and Calculus of Variations* (S. Hildebrandt and R. Leis, eds), Vol. 1357 of *Lecture Notes in Mathematics*, Springer, pp. 142-155, 1988.

[15] G. Dziuk and C.M. Elliott, Finite elements on evolving surfaces, *Journal of Numerical Analysis*, 27: 262-292, 2007.

[16] G. Dziuk and C.M. Elliott, A fully discrete evolving surface finite element method, *Journal of Numerical Analysis*, 50(5): 2677–2694, 2012.

[17] G. Dziuk and C.M. Elliott, L^2 estimates for evolving surface finite element method, *Mathematics of Computation*, 82(281): 1-24, 2013

[18] G. Dziuk and C.M. Elliott, Finite element methods for surface PDEs, *Acta Numerica*, 22:289-396, 2013.

[19] G. Dziuk, D. Kröner and T. Müller, Scalar conservation laws on moving surfaces, *Interfaces and Free Boundaries*, 15:203-236, 2013.

[20] C.M. Elliott and C. Venkataraman, Error analysis for an ALE evolving surface finite element method, *Numerical Methods for Partial Differential Equations*, 31(2):459-499, 2015.

[21] C.M. Elliott and T. Ranner, A unified theory for continuous in time evolving finite element space approximations to partial differential equations in evolving domains, *IMA Journal of Numerical Analysis*, 41(3):1696-1845, 2021.

[22] E. Emmrich, Discrete versions of Gronwall's lemma and their application to the numerical analysis of parabolic problems, *Preprint no.637*, 1999.

[23] L. C. Evans, *Partial Differential Equations*, American Mathematical Society, 1998.

[24] K. Georg and J. Tausch, Some error estimates for the numerical approximation of surface integrals, *Mathematics of Computation*, 62(206):755-763, 1994.

[25] J. M. Lee, *Integration on Manifolds*, Springer New York, 2012.

[26] D. Lengeler and T. Müller, Scalar conservation laws on constant and time-dependent Riemannian manifolds, *Journal of Differential Equations*, 254(4):1705-1727, 2013.

[27] B. Pigato, *Intrinsic Finite Element Method for Elliptic PDEs on Moving Surfaces*, MSc Thesis, University of Padua, 2025.

[28] A. Quarteroni, *Numerical Models for Differential Problems*, Springer, 2014.

[29] R. E. Showalter, *Monotone operators in Banach space and nonlinear partial differential equations*, American Mathematical Society (Mathematical Surveys and Monographs, vol.49), 1997.

[30] L. Zhang, T. Cui and H. Liu, A set of symmetric quadrature rules on triangles and tetrahedra, *Journal of Computational Mathematics*, 27(1):89-96, 2009.